FATIGUE CRACK & DELAMINATION GROWTH IN FIBRE METAL LAMINATES UNDER VARIABLE AMPLITUDE LOADING

SHARIFULLAH KHAN

Stellingen

behorende bij het proefschrift

**Fatigue Crack and Delamination Growth
in
Fibre Metal Laminates
under Variable Amplitude Loading**

Sharifullah Khan

Stellingen 1

In tegenstelling tot metalen profiteren vezelmetaallaminaten maar marginaal van de toepassing van overbelastingen. [dit proefschrift]

In contrast to metals, Fibre Metal Laminates benefit only marginally from the application of overloads. [this thesis]

Stellingen 2

In vezelmetaallaminaten wordt de vorming van afschuiflippen verhinderd door vezeloverbrugging.
[dit proefschrift]

In Fibre Metal Laminates, shear-lip formation is prevented by fibre bridging. [this thesis]

Stellingen 3

Om een gelijkwaardige nauwkeurigheid in de voorspelling van vermoeingsscheurgroei te verkrijgen, impliceert een toenemende materiaalcomplexiteit (van monlitisch metaal naar vezelmetaallaminaat) niet een toenemende complexiteit van het model. [Dit proefschrift]

To achieve similar accuracy in predicting fatigue crack growth, increasing material complexity (from monolithic metals to fibre metal laminates) does not imply increasing model complexity. [this thesis]

Stellingen 4

Belasting met variable amplitude benvloedt wel de vorm van de delaminatie, maar niet de delaminatiegroei. [Dit proefschrift]

Variable amplitude loading affects the delamination shape but not the delamination growth.
[this thesis]

Stellingen 5
Om incidenten in een industrie te vermijden kunnen procedures worden gedefinieerd, maar alles komt neer op de mens die de vereiste handeling uitvoert.

Procedures can be defined to avoid incidents in an industry but everything funnels down to the human taking the required action.

Stellingen 6
In de olie en gas industrie is roestvast staal niet de optimale oplossing voor het aanpakken van corrosieproblemen.

In oil & gas industry, stainless steel is not the optimum solution to tackle corrosion issues.

Stellingen 7
Een goed wetenschapper is een goed *communicator*.

Good scientist should be good communicator .

Stellingen 8
Een individu kan geen CO_2-neutraliteit bereiken.

[Naar een toespraak van Michael Braungart bij de Shell Ecomarathon 2012, Rotterdam]

An individual cannot achieve carbon neutrality.

[After Michael Braungart speech at Shell Ecomarathon 2012, Rotterdam.]

Stellingen 9
De wetenschap zou sneller vooruitgang boeken als alle goed gedocumenteerde experimenten, die in tegenspraak zijn met de geteste hypothese, gepubliceerd zouden worden.

Science would progress faster if all well-documented experiments that are in disagreement to tested hypothesis are published.

Stellingen 10
Het geld dat een land uitgeeft aan onderwijs, onderzoek en ontwikkeling moet worden beschouwd als een investering en niet als een kostenpost.

The money spent by a country on education, research, and development should be considered investment and not expenditure.

Deze stellingen worden opponeerbaar en verdedigbaar geacht en zijn als zodanig goedgekeurd door de promotor, Prof. dr. ir. Rinze Benedictus.

These propositions are regarded as opposable and defendable, and have been approved as such by the supervisor, Prof. dr. ir. Rinze Benedictus.

FATIGUE CRACK & DELAMINATION GROWTH
IN
FIBRE METAL LAMINATES

under Variable Amplitude Loading

FATIGUE CRACK & DELAMINATION GROWTH
IN
FIBRE METAL LAMINATES

under Variable Amplitude Loading

Proefschrift

ter verkrijging van de graad van doctor
aan de Technische Universiteit Delft,
op gezag van de Rector Magnificus Prof. ir. K.C.A.M. Luyben,
voorzitter van het College voor Promoties,
in het openbaar te verdedigen op maandag 7 januari 2013 om
10:00 uur

door

Sharifullah KHAN

Master of Science in Aeronautical Engineering,
École Nationale Supérieure de l'Aéronautique et de l'Espace,
Toulouse, France
geboren te Bannu, Pakistan

Dit proefschrift is goedgekeurd door de promotor:

Prof. dr. ir. R. Benedictus

Copromotor Dr. ir. R. C. Alderliesten,

Samenstelling promotiecommissie:

Rector Magnificus   voorzitter
Prof. dr. ir. R. Benedictus   Technische Universiteit Delft, promotor
Dr. ir. R. C. Alderliesten   Technische Universiteit Delft, copromotor
Dr.- Ing. T. Beumler   Airbus Deutschland GmbH
Prof. dr. ir. R. Marissen   Technische Universiteit Delft
Prof. dr. ir. A. de Boer   University of Twente
Prof. dr. W. Van Paepegem   Ghent University
Prof. dr. P. Horst   Technische Universität Braunschweig
Prof. dr. Z. Gurdal   Technische Universiteit Delft (reservelid)

TUDelft

The greatest weakness of most humans is their
hesitancy to tell others how much they love them
while they are alive

-Optimus Prime

Dedicated to my Beloved Wife Uzma

Contents

List of Figures

List of Tables

Nomenclature

$\frac{da}{dN}$	Crack growth rate	mm/cycle
$\frac{db}{dN}$	Delamination growth rate	mm/cycle
A_{ij}	Extensional stiffness matrix of a laminate	-
b	Delamination length	mm
B_{ij}	Coupling stiffness matrix of a laminate	-
C_d, n_d	Paris constants for delamination growth relation	-
C_{cg}, n_{cg}	Paris constants for crack growth relation	-
D_{ij}	Bending stiffness matrix of a laminate	-
E	Young's Modulus	MPa
G	Shear Modulus	MPa
G_d	Strain energy release rate	MPa mm
j	Number of fibre/metal interfaces	-
k	Surface curvature of a laminate	-
n	Number of layers	-
N_i	External load acting on the laminate	N
P	External load per unit length	N/mm
Q_{ij}	Reduced stiffness matrix of a laminate	-

S_{Ti}	Deviator stress	MPa
T	Temperature	°C
t	Material thickness	mm
U	Elber's crack closure coefficient	–
α_i	Coefficient of thermal expansion	C^{-1}
δ	Displacement	mm
γ	Shear strain	mm/mm
ν	Crack tip opening	mm
σ	Applied stress	MPa
σ_e	Effective stress (Von Mises)	MPa
$\sigma_{0.2}$	Yield stress	MPa
θ	Angle from the x-axis to the 1-axis	°
υ	Poisson's ratio	
$\varepsilon_{i,pl}$	Post stretching strain	mm/mm
ε	Strain	mm/mm
$\varepsilon_{0.2}$	Plastic strain	mm/mm

Indices

∞	Far-field
0	Middle surface properties
$1,2,..,6$	Principle material coordinates
al	Aluminium
al,P	Aluminium layer (Delaminated)
br	Bridging
cr	Cracked metallic layers
$cure$	As cured conditions
D	Delayed

eff	Effective
f	Fibre
$f,0$	0° fibres related
$f,0,P$	0° delaminated fibres
$f,90$	90° fibres related
$f,90,P$	90° delaminated fibres
f,r	Fibre/Resin
k	k^{th} layer
lam	Laminate ($ARALL$, $GLARE$)
max	Maximum value
$mean$	Mean value
min	Minimum value
OL	Overload
p	Corrected plastic zone size
pl	Plastic strain due to yield
$postr$	Post stretched conditions
pp	Prepreg related
$residual$	Component due to residual stress
T	Due to thermal expansion
TR	Transition
use	Room temperature conditions
x,y,z	Laminate coordinates
y	Irwin plastic zone size

Abbreviation

$ARALL$	Aramid Reinforced Aluminium Laminate
CA	Constant Amplitude
$CCLS$	Centre-Crack Lap Shear

CCT	Centre-Crack Tension
DCLS	Double-Crack Lap Shear
FMLs	Fibre Metal Laminates
GLARE	GLAss-REinforced
LDA	Linear Damage Accumulation
OL	Overload
VA	Variable Amplitude
WFS	Wide-Body Fuselage Spectrum

Chapter **1**

INTRODUCTION

A goal without a plan
is just a wish.

Antoine de Saint Exupery
(1900-1944)

Fibre Metal laminates consist of alternating layers of unidirectional impregnated fibre lamina and thin metallic sheets adhesively bonded together, as shown in Figure 1.1. *FMLs* are hybrid materials having better mechanical and damage tolerance properties than the individual constituents. *FMLs* have been developed primarily for aircraft structures as a substitute to high strength aluminium alloys. To manufacture *FMLs*, a stack of plies is cured at elevated temperature and pressure. This curing process results in residual tensile stress in metal layers and compressive stresses in fibre layer. Post-stretching is sometimes used to reverse this un-favourable residual stress distribution by plastically deforming the metallic layers. This technique improves the fatigue crack growth properties but can only be applied to uni-directional *FMLs*. Uni-directional *FMLs* are mainly used in stringers and straps [1].

In the past, *FMLs* have been thoroughly investigated especially in the area

of fatigue crack growth and related mechanisms [1]. Major part of these investigations [2] concern Constant Amplitude *(CA)* loading in order to understand the basic phenomena followed by limited work dealing with Variable Amplitude *(VA)* loading [3–6]. This suggests that the behaviour of *FMLs* under *VA* loading needs to be further investigated.

At Delft University of Technology, intensive research has been done in order to study the different fatigue related phenomena of *FMLs*. In 1988 a fatigue crack growth prediction model for *ARALL* was developed [7] followed by another more accurate and generic model in 2005 [8]. The second model is capable of predicting fatigue crack growth, bridging stress distribution and delamination shape (profile) under *CA* loading.
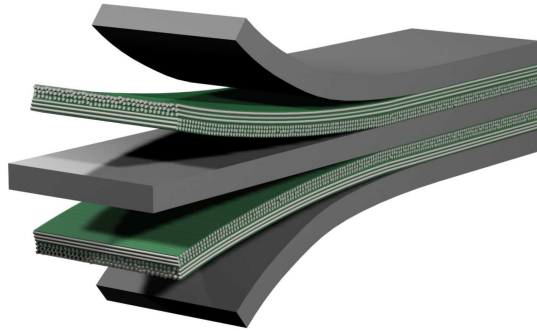
Figure 1.1: A typical Fibre Metal Laminate Lay-up [8]

1.1 Scientific Research Motivation

FMLs are developed mainly for aerospace applications [9–12]. In service they will be subjected to variable amplitude *(VA)* loading ranging from simple overloads to more complex loadings (e.g. take-off/landing, gust, etc.).

Constant amplitude *(CA)* prediction methods can be used to predict the fatigue crack growth of a structural component under *VA* loading. Beumler [13] has discussed spectrum factors to translate the full spectrum into a *CA* load sequence using equivalent stress. But there are some issues:

1. Predicting the crack growth for *VA* case with *CA* test using spectrum

factors [13] remains an intelligent guess. The confidence level of these *VA* predictions can be covered by increasing the safety factor. This safety factor may solve the issue but at the cost of weight, due to over-designed components.

2. In addition, crack growth retardation due to crack-tip plasticity and other *VA* loading related phenomena will not be addressed in the *CA* case. If crack-tip plasticity is not considered, spectrum factors can only be determined for each *VA* separately by tests. No generic factor can be determined without understanding the *VA* sequence effects.

In order to develop a generic prediction model, addressing the above mentioned issues, it becomes necessary to develop the understanding about the fatigue and crack growth phenomena existing in *FMLs* under *VA* loading.

After acquiring detailed understanding of phenomena in *FMLs* under *VA* loading, the next step is the development of an analytical prediction model. However, it is necessary to think about the *OEMs'* concern in the prediction model. *OEMs'* need an effective and efficient prediction model requiring less processor time.

1.2   Initial Research Problem & Framework

To come to a prediction model for *VA* loading in *FMLs*, all related aspects need to be investigated.

The main question addressed in this thesis is: Which aspects related to arbitrary load sequences have an additional effect on the currently identified fracture mechanisms? How should these influences be described, with practical constraints of an effective, efficient and simple prediction model.

The research is detailed into specific questions

1. When only delamination growth is considered, can any additional influence be observed attributed to arbitrary loading? If so, how can it be accounted for in the prediction method?

2. When considering the combination of crack-delamination growth, can the information acquired in step-1 explain observations on delamination. If not, what are additional influences?

3. How does the methodology for *VA* fatigue in the end, relate to *CA* fatigue? Does it require reconsidering the knowledge on *CA*?

4. Considering crack growth, will metal in *FMLs* behave similar to mono-lithic metal under *VA* fatigue? Can the contribution of hybrid lay-up be quantified in the methodology?

To answer all these questions, a combined experimental-analytical approach has been adopted. Fatigue crack growth and delamination growth tests have been performed to understand the mechanisms or the interaction of different mechanisms in *FMLs* under *VA* loading. For delamination study, delamination growth *(db/dN)* and delamination shape have been investigated. In order to investigate delamination growth independent of fatigue crack growth, double-crack lap shear specimens have been used. While for delamination shape, centre crack tension specimens have been used. In addition, digital image correlation *(DIC)* has been used as strain measurement technique to observe the delamination shapes in-situ testing. For fatigue crack growth, centre crack tension specimens have been tested under selective *VA* loading and flight spectrum loading. This delamination and fatigue crack growth observations and understanding is used in the development of an analytical prediction model for *VA* loading.

1.3 Structure of this Dissertation

Chapter 2 briefly introduces *FMLs* and relevant fatigue mechanisms. In addition the significance of *VA* loading is also explained in this chapter.

Details about the delamination growth specimen, procedure and setup as well as discussion of the results are given in chapter 3.

Detailed investigation of the effect of *VA* loading on the delamination shape is given in chapter 4.

Chapter 5 presents the investigation of the behaviour of metal layers in *FMLs*. The comparison is performed based on crack tip plasticity analysis.

The development of an Analytical prediction model for *FMLs* under *VA* loading, using all the above research is given in chapter 6. Followed by the development of a sub-routine to predict the fatigue and delamination in post-stretched *FMLs*, given in chapter 7.

The final chapter outlines the conclusions and recommendations for research in the future.

References

[1] A. Vlot, J. Gunnink, Fiber Metal Laminates - An introduction, Kluwer Academic Publishers, Dordrecht, The Netherlands, 2001.

[2] R. C. Alderliesten, On the available relevant approaches for fatigue crack propagation prediction in glare, International Journal of Fatigue 29 (2007) 289–304.

[3] R. C. Alderliesten, H. J. M. Woerden, Load history effects during fatigue crack propagation in GLARE, in: M. Guillaume (Ed.), Fatigue of Aeronautical structures as an Engineering Challenge, Vol. I, 2003, pp. 509–530.

[4] H. M. Plokker, R. C. Alderliesten, R. Benedictus, Crack closure in fiber metal laminates, Fatigue and Fracture of Engineering Materials and Structures 30 (2007) 608–620.

[5] J. Schijve, F. J. Wiltink, V. J. W. Van Bodegom, Flight-simulation fatigue tests on notched specimens of fiber-metal laminates, Tech. Rep. Report No. LRV-10, Delft University of Technology, The Netherlands (1994).

[6] G. H. J. J. Roebroeks, Fibre-metal laminates recent developments and applications, International Journal of Fatigue 16 (1) (1994) 33–42.

[7] R. Marissen, Fatigue crack growth in arall - a hybrid aluminium-aramid composite material, Tech. rep., Delft University of Technology, Delft,LR-574 (1988).

[8] R. C. Alderliesten, Fatigue crack propagation and delamination growth in glare, Ph.D. thesis, Delft University of Technology, Delft (2005).

[9] C. A. J. R. Vermeeren, An historic overview of the development of fibre metal laminate, Applied Composite Materials 10 (2003) 189–205.

[10] A. Vlot, L. B. Vogelesang, T. F. Vries, Toward application of fibre metal laminates in large aircraft, Aircraft Engineering & Aerospace Technology 71 (1999) 558–570.

[11] S. Karishnakumar, Fiber metal laminates - the synthesis of metals and composites, Material and Manufacturing process. 9 (2) (1994) 295–354.

[12] L. B. Vogelesang, A. Vlot, Development of fibre metal laminates for advanced aerospace structures, Journal of Materials Processing Technology 103 (2000) 1–5.

[13] T. Beumler, Flying glare – a contribution to aircraft certification issues on strengths properties in non-damaged and fatigue damaged glare structures., Ph.D. thesis, Delft University of Technology, Delft (2004).

FIBRE METAL LAMINATES

The most difficult part was deciding where to begin read.
The bookshelves extended out of sight, their information
stretching as if to eternity.

by Brandon Sanderson
(1975-)

This chapter provides the a brief introduction on Fibre Metal Laminates, their main characteristics, manufacturing and inspection process. In addition, the major phenomena observed in the fatigue mechanisms of Fibre Metal laminates are discussed. Finally, Variable Amplitude loading and its effect on the crack growth is discussed.

Looking at the history of *FML* development, it seems that the main driver of the development is the available expertise and knowledge on metal combined with the identified benefits of composite materials. Research on application of fibres to the bond line has been started in seventies at Fokker facilities, Netherlands [1]. At the same time, the favourable behaviour of laminated aluminium sheets has been identified at Delft University under CA loading [2]. In 1978, *FMLs* having carbon and aramid fibres have been tested under flight spectrum loading, to study the effects of different fibres [3]. These tests showed quite promising results. During the development phase different fibre types were used to find the optimal solution for the aircraft industry. Table 2.1 high-

Table 2.1: Identified advantages of various fibres for FMLs

Fibre	Advantage	Disadvantage	Available laminates
Aramid	low weight	low strength	ARALL [5]
Glass	high strength	high weight	GLARE [6]
	high failure strain	low stiffness	
Carbon	low weight	low failure strain	TIGr [7]
,	high stiffness	corrosion issue	CARALL [8]
	high strength	expensive	

Table 2.2: Commercially available fibre metal laminates

	Grade	Metal type	Metal thickness (mm)	Fibre layer (mm)	Fibre direction (°)	Stretched %	Characteristics
ARALL	1	7075-T6	0.3	0.22	0/0	0.4	Fatigue, strength
	2	2024-T3	0.3	0.22	0/0	0.0	Fatigue, formability
	3	7475-T76	0.3	0.22	0/0	0.4	Fatigue, strength, exfoliation
	4	2024-T8	0.3	0.22	0/0	0.0	Fatigue, elevated temperature
GLARE	1	7475-T61	0.3-0.4	0.266	0/0	0.4	Fatigue, strength, yield stress
	2	2024-T3	0.2-0.5	0.266	0/0,90/90	0.0	Fatigue, strength
	3	2024-T3	0.2-0.5	0.266	0/90	0.0	Fatigue, impact
	4	2024-T3	0.2-0.5	0.266	0/90/0,90/0/90	0.0	Fatigue, strength in 0/90 direction
	5	2024-T3	0.2-0.5	0.266	0/90/90/0	0.0	Impact
	6	2024-T3	0.2-0.5	0.266	+45/-45,-45/+45	0.0	Shear, off-axis properties

lights the advantages and disadvantages of various fibres. While the activities regarding the optimization of this new material concept were terminated at Fokker, Delft University continued its research. Details about the development of *FMLs* are well documented in [4].

ARALL (Aramid Reinforced Aluminium Laminate) was the first *FML* commercially available for the aircraft industry [9]. In 1983, two grades of *ARALL* were commercialized, but later in 1987 two more grades were released (details about these grades are shown in table 2.2). Despite the advantages, the McDonald-Douglas C-17 aft cargo door was the only major application for *ARALL* [10]. Major drawbacks of *ARALL* were fibre microbuckling, premature failure when subjected to compressive loads and moisture absorption [11].

In 1987, on-going research for the development of an optimal *FML* resulted

in a successor of *ARALL*, named *GLARE* (GLAss-REinforced). In *GLARE* high-strength glass fibres are either present in 0°, 90°, 45° or in a combination (detailed in table 2.2). Instead of *ARALL*, *GLARE* is currently applied in the aircraft industry [12, 13] because of the better mechanical and damage tolerance properties, especially under flight (spectrum) loading.

2.1   Nomenclature of FMLs

Similar to a traditional composite, different *FML* lay-ups are possible and to identify or categorize these laminates, a coding system is preferred. This coding system is important for design, production and material qualification. The code for an arbitrary laminate is

GLARE Ax – B/C – t

where

A defines the grade of the laminate as defined in Table 2.2
x gives information on the prepreg ply orientation with respect to loading direction
B indicates the number of aluminium alloy plies
C indicates the number of glass fibre prepreg plies
t indicates the thickness of the aluminium alloy layers

For example, *GLARE 3– %5/4 – 0.3 is Glare 3 with 5 metal and 4 prepreg layers. The metal layers are 0.3 mm thick.*

2.2   Properties of FMLs

FMLs have a number of advantages when compared with conventional aluminium alloys or even fibre reinforced plastics. *FMLs* have a superior crack growth rates and fatigue performance which allow long inspection intervals. In comparison to composites, they offer simple maintenance methods, easy inspection during service, higher impact resistance and less environmental degradation.

Unlike *ARALL*, *GLARE* has good fatigue properties in combination with compressive loading [5]. Beside the excellent fatigue characteristics, *GLARE* also has good impact and damage tolerance characteristics [14]. In addition, the fibre/epoxy layers act as barriers against corrosion of the inner metallic sheets, whereas the metal layers protect the fibre/epoxy layers from picking up moisture. The laminate has an inherent high burn-through resistance as

well as good thermal insulation properties. Some of the advantages of fibres used in *FMLs* are shown in Table 2.1.
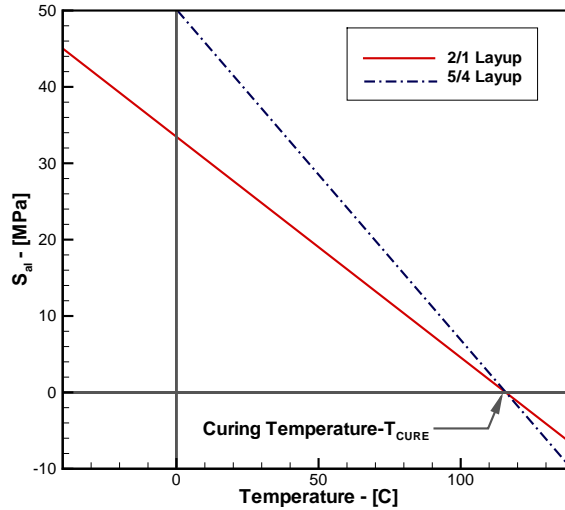
Figure 2.1: Residual stresses in aluminium layers as function of temperature [15].

2.3   Manufacturing Process

The aluminium layers in *GLARE* have a thickness of 0.3 – 0.5 mm and are pretreated before being laminated into a panel. This pre-treatment consists of chromic acid or phosphoric acid anodizing and subsequent priming with *BR-127* adhesive systems [17]. The fibres are delivered as a prepreg including the *FM94* adhesive system from Cytec [18].

The aluminium and prepreg layers are bonded together in an autoclave curing process at an elevated temperature of 120°C at a maximum pressure of 6 to 11 bar. This implies that the layers are bonded together at a high temperature and are cooled down in bonded condition. As a result of the difference in coefficients of thermal expansion, given in Table 2.3, the aluminium layers want to shrink more than the prepreg layers. Assuming a rigid bond between the aluminium and prepreg layers during cooling, this results in tensile residual stress in the aluminum layers and compressive residual stress in the prepreg layers.

Table 2.3: Mechanical properties of Aluminium 2024-T3 and Prepreg S2/FM94 [16]

| | Unit | 2024-T3 | S2-glass, FM-94 | |
			∥ Fibre axis	⊥ Fibre axis
Thickness of single layer	mm	0.3	0.133	
Young's Modulus	MPa	72,400	48,900	5,500
Shear Modulus	MPa	27,600	5,550	
Poisson's ratio ν_{xy}	-	0.33		
Poisson's ratio ν_{yx}	-	0.33	0.0371	
Thermal expansion coefficient	$10^{-6}C^{-1}$	22	6.1	26.2
Curing temperature	$°C$	-	120	

2.4   Post Stretching

Figure 2.1 shows that cooling down results in a tensile stress in the aluminium layers, of which the magnitude depends on the lay-up. This residual stress is unfavorable for fatigue loading. The stress allows an increased crack opening and so enlarges the stress intensity factor at the crack tip.

Post-stretching of cured fibre-metal laminates is sometimes performed to overcome potential negative effects of these residual tensile stresses in the metal layers. The residual tensile stress in the aluminium layers can be reversed into a compressive stress by yielding the laminate to a small (positive) strain percentage. It has been proven to have a beneficial effect on the fatigue properties [15, 19]. Post-stretching can be seen as a means to alter the internal stress distribution in the laminates to obtain desirable properties. The post-stretching mechanism is illustrated in figure 2.2. Further detail has been provided in the Chapter 7.

2.5   Inspection & Quality Control

The ultrasonic C-scan method can be applied to inspect and verify the quality of manufactured *GLARE* panels. This method is a non-destructive inspection method and it can detect disbonds and porosities within a laminates [18].
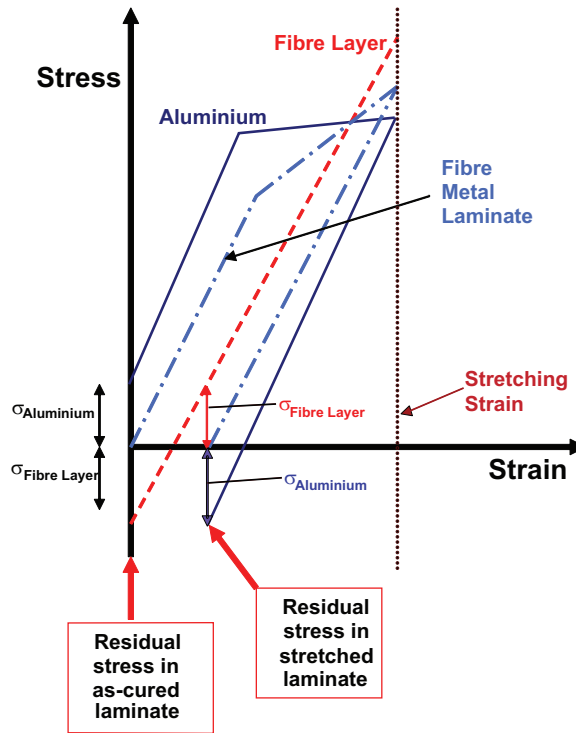
Figure 2.2: Illustration of post-stretching process with stress and strain curves

The objective of non-destructive inspection method is to determine whether the scanned panel can be accepted or should be rejected.

The defects in *GLARE* panels can be due to foreign material contamination, like wrapping foils, raw material contamination, such as glass splinters, or porosities or delaminations due to air inclusions. This C-scan method is also used to detect any positioning error in case of splices or doublers or even the fibre orientation.

To accept or reject a *GLARE* panel based on C-scan evaluation, it is necessary to establish certain criteria. As mentioned by Van Meer and Coenen [18], effect of defects, static and fatigue tests should be done to investigated the effects of any defect.

Part of the load is "BRIDGED" over the crack

METAL
FIBRE
METAL

D   D

Crack

D

D=Delamination Boundary
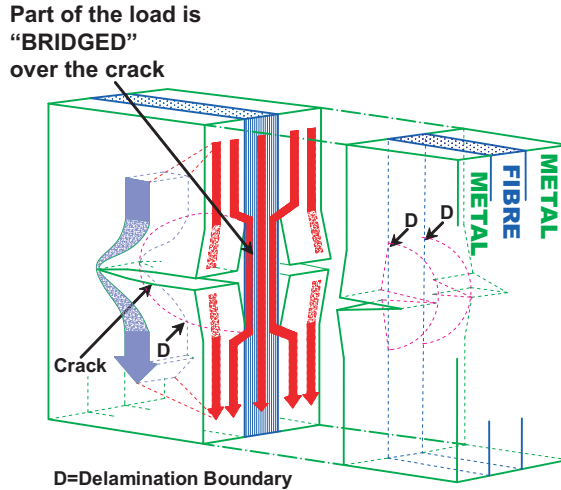
Figure 2.3: Crack bridging of the fibres and delamination of the layers

2.6   Fatigue in Fibre Metal Laminates

2.6.1   Fatigue Crack Propagation

In *FMLs*, fatigue crack propagation can be divided into two main mechanisms: crack propagation in metal layers and delamination at the metal-fibre interface. In reality, both of these mechanisms form a balanced and so-called coupled process. These mechanisms are shown in figure 2.3.

The fatigue crack growth behaviour in *FMLs* can be described with Linear Elastic Fracture Mechanics *(LEFM)*. This implies that, like monolithic metals, the crack growth rate in *FMLs* is related to a crack-tip stress intensity factor. But it is not that simple, because in *FMLs* the crack-tip stress intensity factor is influenced by the contribution of bridging fibres, which is effected by the delamination at the fibre-metal interface.

When the cracks in the metal layers start growing, the fibres remain intact in the wake of the crack. These fibres provide a path of the load transfer over the crack and restrain the crack from opening. As a consequence, less load needs to be transfered around the crack-tip in the metal layers, resulting in a lower crack-tip stress intensity factor.

During fatigue crack growth in the metal layers, a continuous stress distribution around the crack in each layer and shear stresses at the interface occurs.

This redistribution, results in an almost constant crack-tip stress intensity factor during major part of the crack growth life. The fibre bridging mechanism depends on a number of factors, such as the stiffness and thickness of each individual layer, the number of metal-fibre interfaces, the direction of each fibre-adhesive layer with respect to the loading direction, the applied loading, the crack configuration (surface of part through cracks) and the environmental conditions (temperature) [20].

Delamination growth is a process in which the layers adjacent to the cracked metallic layers delaminate due to the cyclic shear stresses that occur, because of load transfer at the fibre-metal interface [21]. No stresses occur between the layers in the delaminated area. But the stress relaxation will occur in the fibre layers itself [22]. The advantage of delamination growth is the fact that the increase in the length of the bridging fibres reduces the strains and stresses in the fibres, preventing fibre failure.

In the following sections, these mechanisms will be discussed in detail.

2.6.2   Crack Bridging and Restraint on Crack Opening

The fibres in *FMLs* are insensitive to fatigue. They transfer a significant part of the load over the crack and restrain the crack opening, as shown in figure 2.3. Due to this restraining, the crack opening in *GLARE* is smaller as compared to monolithic metal. The amount of load that is transferred around the crack in the metal layers is smaller due to the transfer of the major part through the fibres, over the crack. This mechanism results in smaller crack-tip stress intensity factor as compared to monolithic metal, for equal crack length and applied load. Moreover, the crack-tip stress intensity factor is not significantly influenced by the increase of the crack length which is contrary to what is observed in monolithic metals.

Crack bridging becomes maximumly effective after a certain crack length is reached, which means, after the crack opening displacement reached a certain magnitude. A small crack opening means low strain in the fibres and as a consequence low bridging stress. Therefore, the fibre bridging and the restraint on crack opening will be small for small crack lengths, but will become effective after the crack length reaches a certain size [21, 22].

2.6.3   Delamination at the Interface

Marissen [21] has reported that crack opening during the crack propagation phase is due to the two main factors:

- Fibre elongation in the delamination area (Figure. 2.4(a)).
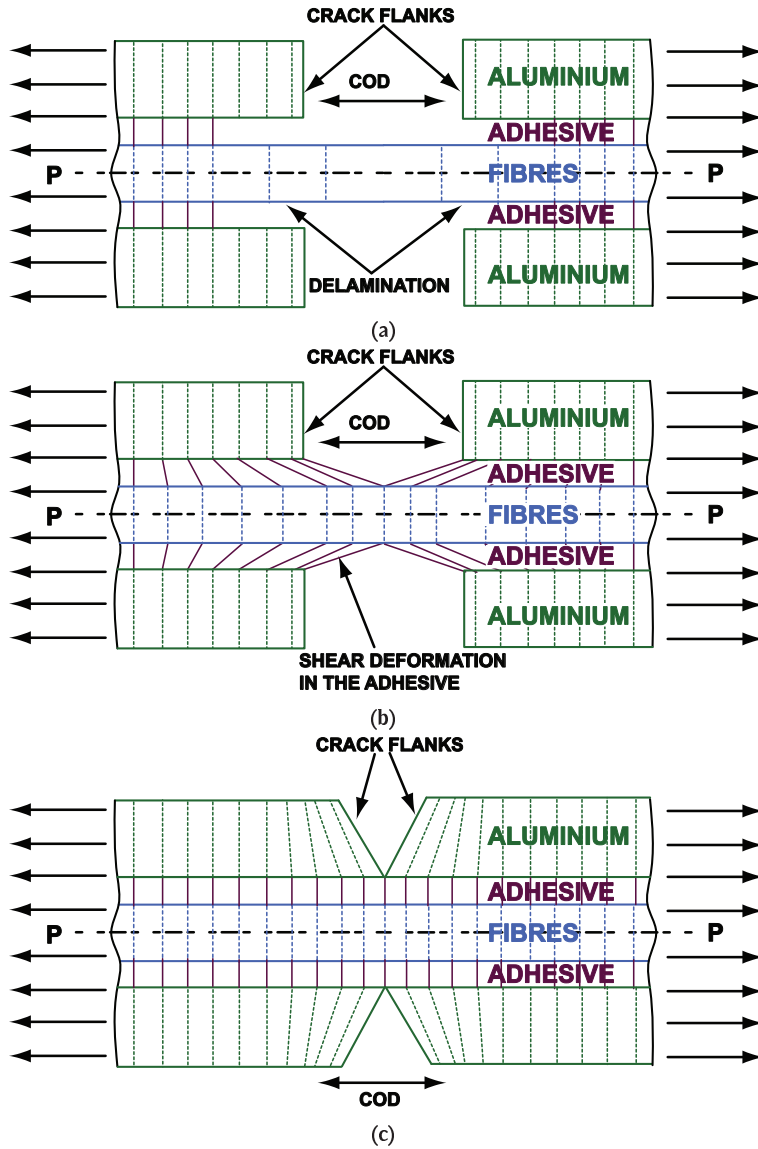
Figure 2.4: Crack opening displacement due to delamination (a), adhesive shear deformation (b), and metal layer deformation (c) [20]

- Adhesive shear deformation (Figure. 2.4(b)).

In addition, Guo and Wu [23], mentioned the deformation of metal layer (Figure. 2.4(c)), but assumed it to be insignificant in comparison with the other two factors.

The cyclic shear stresses at the metal-fibre interface due to the load transfer from the metal to fibre layers are causing this delamination growth. The magnitude of cyclic shear stress is determined by the material and loading parameters, such as the thickness and stiffness of the individual layers, the lay-up, the fibre orientation in the prepreg, and the minimum and maximum applied stress.

In addition to the level of these cyclic shear stresses, the delamination growth rate depends on the delamination resistance of the prepreg. Increasing the delamination resistance provides better fibre bridging [21].

During loading, when the crack-flanks are opened in aluminium layer, the intact fibres are elongated over the delamination length. This means for a given crack opening, that the delamination length determines the strain and thus the stress in the fibre layers. Large delamination lengths result in small bridging stresses, with small cyclic shear stresses at the interface inducing small delamination growth rates. In other words, the delamination growth rate and the bridging stress are in balance, continuously influencing each other.

The bridging stress also contributes to the stress intensity factor at the crack tip in the aluminium layers, which determines the crack growth rate. High bridging stresses along the crack result in low stress intensities at the crack tip and thus small crack growth rates.

This means that the fatigue crack growth mechanism in Glare is characterised by the processes of crack growth in the aluminium layers and delamination growth at the interfaces, which continuously influence each other. The ratio between crack length and delamination length depends on the laminate lay-up and on the crack growth characteristics of the aluminium and the delamination resistance of the interface.

2.6.4   Adhesive Shear Deformation

Besides the elongation of fibres, Marissen attributes a part of the crack opening to the deformation of the adhesive rich layers in the prepreg in Arall. Due to fibre bridging, the load has to be transferred from the aluminium layers to the fibre layers through the interface. This results in shear stresses at the interface, inducing shear deformation of the adhesive rich layer.

Marissen concluded that in the ideal situation of an infinitely stiff adhesive between the layers, the crack opening and the stress intensity factor would be zero for a laminate without a starter notch and without delamination. However, in the actual situation due to local shear deformation of the adhesive, some crack opening will occur. This is schematically represented in Figure 2.4(b). As result of the slightly opened crack, the stress intensity factor in the aluminium layers is no longer zero.

In the above discussion, the effect of delamination was neglected. If delamination of the layers occurs, the length over which the fibres will elongate increases, resulting in lower fibre stresses. The situation, however, will be qualitatively the same.
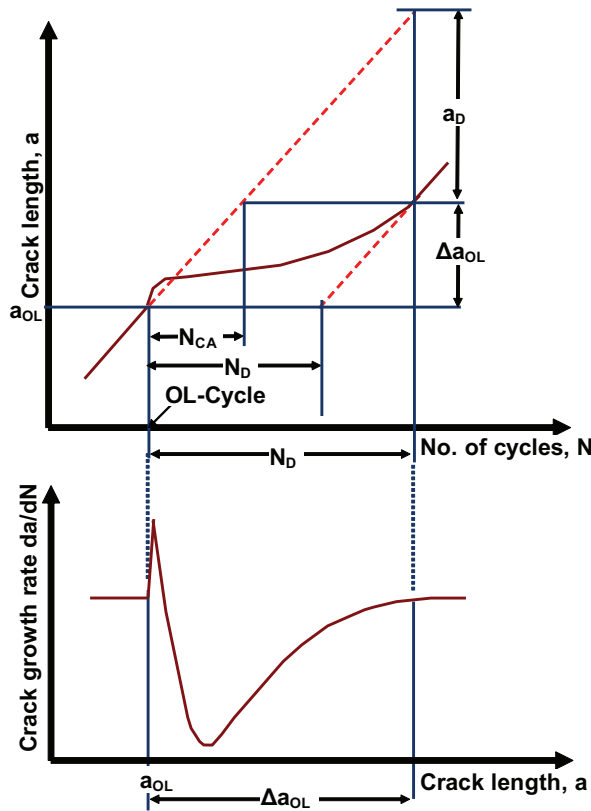
Figure 2.5: Schematic of crack growth retardation following an overload in metals [24]

2.6.5   Effect on Fatigue Performance of *FMLs*

The fatigue crack growth behaviour of Glare was described with the stress intensity factor approach in a qualitative way. The argument of this thesis is that the stress intensity factor at the crack tip determines the crack growth rate in the aluminium layers. Control of the stress intensity factor means control of the crack growth rates in the Glare material. The stress intensity factor at the crack tip can be reduced by [21]

- Increasing the stiffness of the fibre layers. This can be obtained by applying fibres with a higher Young's modulus, or by increasing the fibre layer thickness or by increasing the fibre volume fraction within the prepreg. The bridging stresses in these cases will be higher at the same crack opening displacement.

- Decreasing the stiffness of the aluminium layers by decreasing the thickness of the aluminium layers.

- Increasing the delamination resistance. The delamination areas will be smaller, resulting in higher bridging stresses and thus lower stress intensities.

- Increasing the adhesive or prepreg shear stiffness, which restrains the crack opening more and lowers the stress intensity at the crack tip. In general, the fatigue characteristics of Glare can be enhanced by optimization of the laminate with respect to fibres and adhesives in combination with the laminate lay-up.

2.7   Variable Amplitude Loading

The retardation effects on crack growth resulting from a single overload cycle is illustrated in Figure 2.5. During the overload cycle, yielding of the material near the crack tip occurs, creating a large plastic zone [25–31]. Due to the presence of this plastic zone in front of the crack-tip, surrounded in an elastically deformed region, the crack-tip experiences a squeezing effect, which results in the development of residual compressive stresses at and around the crack-tip. The compressive stress field reduces the available crack-tip driving force and causes a significant reduction in fatigue crack growth rate [26, 28, 32]. The crack retardation zone, i.e. the crack extent over which retardation of crack growth is experienced, may be characterized by parameters, a_D (overload affected total crack length) and N_D (delay cycles), and is schematically represented in figure 2.5. After the crack has grown beyond this region, the crack growth rate returns to its original rate

in the absence of other retardation effects. This is the typical phenomenon observed in metals, however, *FMLs* having metal as a constituent show the same retardation phenomenon but presence of fibre reduce this effect.

2.8   Fatigue Crack Growth Retardation Model

2.8.1   For metals

Fatigue crack growth retardation models can be divided into two main categories: those based on crack growth through a plastic zone ahead of the crack tip and those based on crack closure in the wake of the crack (see Figure 2.6). Early interaction models were based on crack-tip plasticity which was assumed to be the major cause of fatigue crack growth retardation. A well-known and simple model of this category is the Wheeler Model [33–47]. These crack-tip plasticity models were followed by the advance and complex fatigue crack growth prediction models based on the crack closure in the wake of the crack as the major cause of fatigue crack growth retardation. These models are categorized in semi-empirical models (such as *ONERA, PREFFAS and CORPUS*) and Strip-yield models. Details on these models are given in [48]
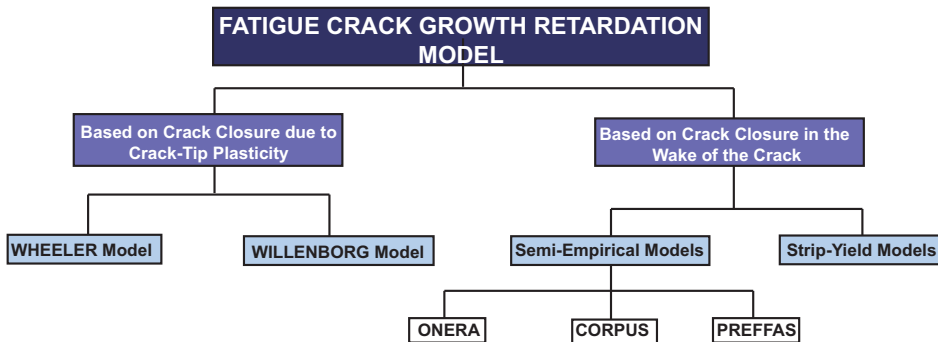
Figure 2.6: Classification of Fatigue crack growth retardation models

2.8.2   For FMLs

In *FMLs*, all the metal related phenomena are to some extent reduced due to intact fibres. Because of this fact, a simple crack growth prediction model may be sufficient to predict the fatigue crack growth in *FMLs* under *VA*

loading. This highlights that complex and advance models may not be requi-red in case of complex materials like *FMLs* under *VA* loading. A simplified interaction model (crack-tip plasticity) is used for fatigue crack growth pre-dictions under *VA* loading in *FMLs*. The details about the crack-tip plasticity model are discussed in this section.

2.8.3   Crack-Tip Plasticity

According to the theory of elasticity, the stress at the tip of the crack becomes infinite when a structure is loaded. In reality, the crack-tip becomes blunted upon loading. Additionally, for a ductile material, the theoretical crack-tip stresses exceed the yield strength of the material, $\sigma_{0.2}$, resulting in yielding in front of the crack-tip. As a result, a zone of plastically deformed material of theoretical size r_p is formed ahead of the crack tip, as illustrated in figure 2.7.

When the cracked structure is loaded in tension the total elastic and plastic strain within the plastic zone becomes larger than the elastic strain of the surrounding material. During the subsequent unloading stage, the surroun-ding elastic material acts like a spring that clamps the residual strain within the plastic zone and exerts compressive forces on to the zone. As a result, a zone of compressive residual stress ahead of the crack-tip is created after unloading (from tensile applied stress).
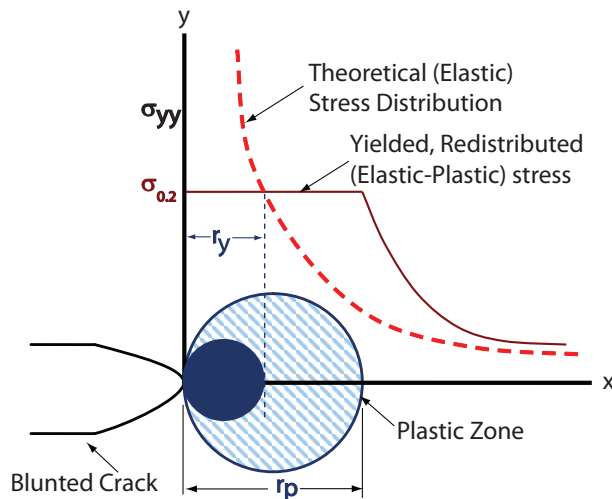
Figure 2.7: Schematic stress distribution at the crack-tip under tensile loading

The crack-tip plastic zone can also be viewed as the load interaction zone

since the residual stress interferes with the applied stress to the crack-tip. The interference of the residual stress with the applied stress is known to have a significant effect on the fatigue crack growth rates of the structure under *VA* loading. In the event of a tensile overload, a more extensive and larger zone of compressive residual stress is created ahead of the crack-tip. As the crack advances through the zone during subsequent fatigue cycles, the compressive residual stress contributes to the well-known fatigue crack growth retardation in the subsequent cycles following a tensile overload.

2.8.4   The Irwin Approach

Irwin made a simple estimation of the plastic zone along the crack plane for elastic, perfectly-plastic materials. The simplest estimate can be made by substituting $\theta = 0$ in

$$\sigma_{0.2} = \frac{K_I}{\sqrt{2\pi r}} \cos\frac{\theta}{2}\left(1 + \sin\frac{\theta}{2}\sin\frac{3\theta}{2}\right) \tag{2.1}$$

and solving for a distance, r_y, at which $\sigma_y = \sigma_{0.2}$, details about this equation are given in [49–51]. This leads to the equation:

$$r_y = \frac{1}{2\pi}\left(\frac{K}{\sigma_{0.2}}\right)^2 \tag{2.2}$$

The distance r_y is schematically illustrated in figure 2.7. This estimate of plastic zone is incorrect, because it is based on an elastic stress distribution [49–51]. Figure 2.7 also shows the elastic-plastic stress distribution with plastic zone size r_p. The areas under elastic and elastic-plastic stress distribution must be the same in order to satisfy force equilibrium in y-direction. This condition can be met by making r_p such that the following equation is satisfied:

$$\int_0^{r_p} \frac{K_I}{\sqrt{2\pi r}}dx - \sigma_{0.2}r_y = \sigma_{0.2}(r_p - r_y) \tag{2.3}$$

Solving for r_p gives:

$$r_p = 2r_y = \frac{1}{\pi}\left(\frac{K}{\sigma_{0.2}}\right)^2 \tag{2.4}$$

Equation 2.4 is derived for plane stress condition. For plane strain condition it can be modified as

$$r_{p,plstrain} = \frac{1}{3}r_p = \frac{1}{3\pi}\left(\frac{K}{\sigma_{0.2}}\right)^2 \tag{2.5}$$

2.8.5   Description of Wheeler Yield Zone Model

According to Gallagher [52] and Schijve [53], the models that try to explain the interaction effect by considering the condition in front of crack tip (plastic zone) are labelled as Yield Zone Models. Wheeler [54] started this generation of prediction models involving interaction effects in the prediction of crack growth.

The Wheeler prediction model uses the modified linear damage accumulation relation,

$$a = a_0 + \sum_{i=1}^{n} f(\Delta K, r, ..) = a_0 + \sum_{i=1}^{n} \Delta a_i \tag{2.6}$$

using a simple retardation parameter C_P,

$$a = a_0 + \sum_{i=1}^{n} C_P f(\Delta K, r, ..) \tag{2.7}$$

The linear damage accumulation provides a prediction of *VA* fatigue life by adding cycle-by-cycle crack growth increments Δa_i, mathematically represented in equation 2.7. The modified crack length and crack growth rate equations can be written as:

$$\frac{da}{dn} = C_P \cdot C_{cg} \Delta K^{n_{cg}} \tag{2.8}$$

where C_P varies from 0 to 1 depending on the location of the crack tip in a previously created larger zone ($r_{p,OL}$ in figure 2.1) and the plastic zone size of the current load cycle $r_{p,i}$. The C_P is calculated using:

$$C_P = \left[\frac{r_{p,i}}{(a_{OL} + r_{p,OL}) - a_i}\right]^m \quad when \quad a_i + r_{p,i} < a_{OL} + r_{p,OL} \tag{2.9}$$

or

$$C_P = 1 \quad when \quad a_{OL} + r_{p,OL} \leq a_i + r_{p,i} \tag{2.10}$$

where $r_{p,i}$ is the current plastic zone size, $r_{p,OL}$ is the overload plastic zone size, a_{OL} is the crack length at overloading, illustrated in figure 2.8. m is the experimentally calculated exponent which depends on the stress level, the crack shape as well as the load spectrum.

Wheeler assumed that m, once calibrated, can be used for other spectra. But later it was shown that the accuracy of predictions will suffer if different loading spectra are used with the same m value [33, 55]. For metallic structures, the Wheeler model is unable to predict the phenomenon of crack arrest after a high overload, because the predicted retardation factor immediately after the overload will not be zero [35]. Secondly, the Wheeler model did not recognize the occurrence of delayed retardation. Actually, the model assumes very simple crack growth behavior; whereas immediately after application of peak loads the real phenomena are very complex.
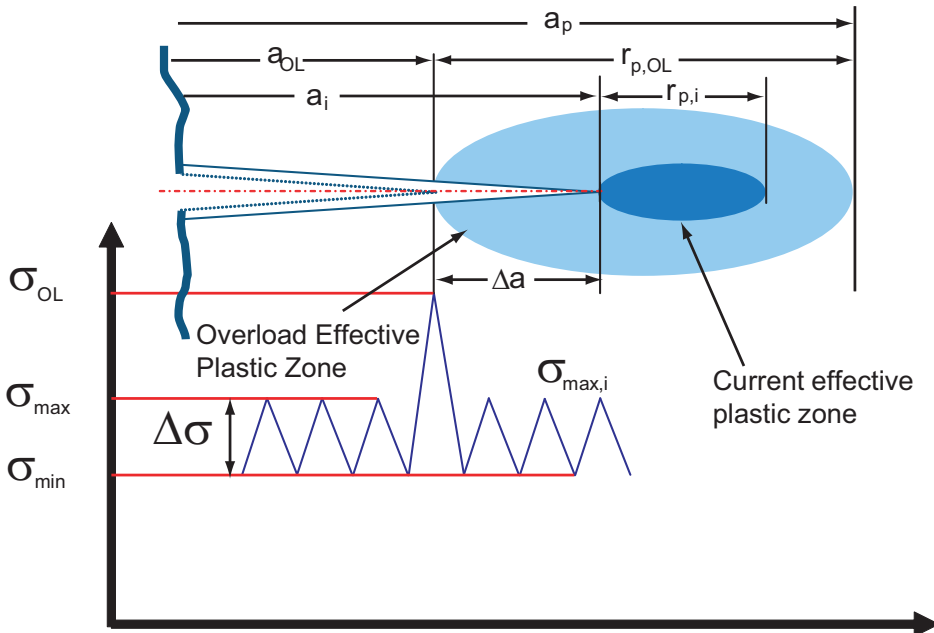
Figure 2.8: Relative sizes of plastic zones in the Yield Zone Models. [56]

2.8.6   Modified Wheeler Model

In the original Wheeler model, the Paris equation is used for crack growth calculation. A problem of the Paris equation is its dependency on the stress ratio. To include the stress ratio effect in the *CA* crack growth prediction, a number of equations have been proposed in the literature [57]. Gallagher [52] used the Walker [58] crack growth relation, while Pereira et al. [59] and Finney [33] used the Forman relation [60]. Here the Schijve relation [61] (Equation 2.11) is used for the *CA* baseline stress ratio correction.

$$\Delta K_{eff} = (0.55 + 0.33R + 0.12R^2) \cdot \Delta K \qquad (2.11)$$

The original Wheeler's crack growth relation (Equation 2.8) is modified as

$$\frac{da}{dn} = C_P \cdot C_{cg} \Delta K_{eff}{}^{n_{cg}} \qquad (2.12)$$

2.8.7   Crack closure models
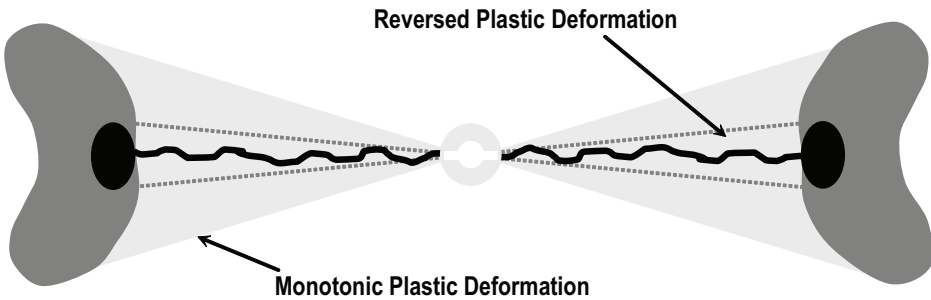
Figure 2.9: Plastic Zone

The occurrence of crack closure of a fatigue at a positive tensile stress level after removing the load on the specimen is a physical reality [62]. In order to be accurate, this phenomenon should be an essential element of a crack growth prediction model. During crack growth, the plastic zone is moving with the tip of the crack as well as increasing in size, figure 2.9. The same will be true for the reversed plastic zone. This deformation involves elongation in the y-direction. As a result of this elongation the crack will close (at least partly) during unloading, and after full unloading ($P = 0$) compressive residual stresses will be present in the wake of the crack. As the fractured

surfaces are pressed together by plastic deformation left in the wake of the crack, the residual compressive stresses are transmitted through the crack. This phenomenon in literature is referred to as "Crack Closure". It was first observed by Elber [62]. and it is sometimes referred to as the Elber Mechanism. The presence of this phenomenon can be justified either by stiffness measurement [61], which is not an accurate way of measurement, or by the effect on fatigue crack growth.

Elber suggested that only that part of the load cycle will contribute to crack extension where the crack is fully open until the crack tip, because crack tip singularity does not exist during the part of the load cycle when the crack tip is closed. This leads to the definition of an effective stress range and stress intensity factor.

$$\Delta S_{eff} = S_{\max} - S_{op}; \Delta K_{eff} = K_{\max} - K_{op} \qquad (2.13)$$

Elber devised the famous crack closure relation involving the stress intensity factor and stress ratio.

$$U = \frac{\Delta K_{eff}}{\Delta K} = \frac{\Delta S_{eff}}{\Delta S} = 0.5 + 0.4R \qquad (2.14)$$

Figure 2.10 compares the different crack closure relations as a function of R. Elber's relation indicate that S_{op} is increasing again for a negative R-value which is physically unrealistic. Analytical work of Newman [63] has shown that it should be a decreasing function for $R- > -1$. For this reason, Schijve [64] proposed a new relation between U and R based on the trends as predicted by Newman.

$$U = 0.55 + 0.35R + 0.1R^2 \qquad (2.15)$$

This relation shows a continuously decreasing S_{op} for a decreasing R-value. This trend should be expected because for a certain S_{max} value, a lower R-value implied a lower S_{min} value. The weakness of this approach is the implicit and unproven assumptions that crack closure is responsible for all load ratio effects and that these can be correlated by an equation. But this relation is proved to be the only crack closure estimation method due to unavailability of accurate direct crack closure measuring techniques [3].

After the introduction of the crack closure concept by Elber [62], a lot of effort was put in understanding the phenomenon to predict crack growth. These efforts include the early phase work which were mainly numerical techniques (finite element analysis) as detailed by Newman [65] and Ohiji et al. [66]. Numerical techniques were shown to be very accurate but are more complicated for modeling and meshing aspects. The major issues were
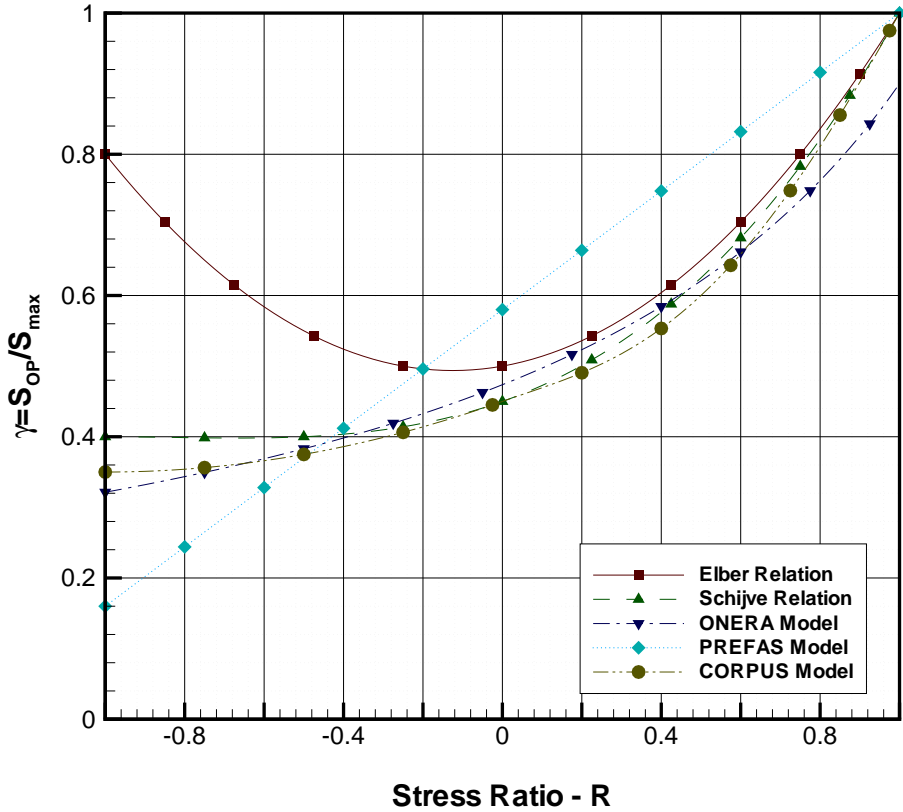
Figure 2.10: The crack opening stress level according to different relations

the calculation costs and time, which made scientists developing simple analytical crack closure models [67–69]. Crack closure models for VA-loading require cycle-by-cycle calculation of the crack opening stress, Sop and the corresponding K_{op}. The three main models which are based on Elbers crack closure assumption were primary developed to predict fatigue crack growth under flight simulation loading [70]. These models are:

1. ONERA Model

2. CORPUS Model

3. PREFFAS Model

In this thesis CORPUS model is discussed and later implemented for predicting fatigue crack growth in FMLs.

The CORPUS Model
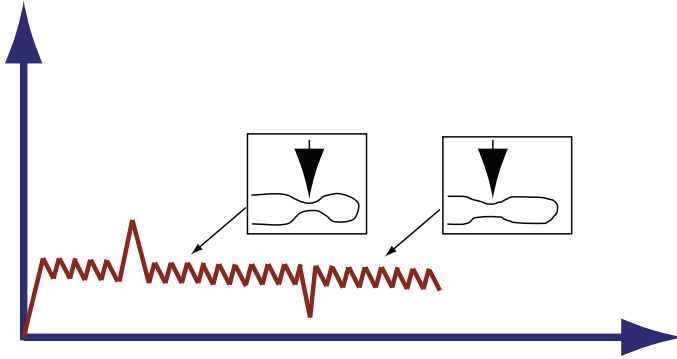
Figure 2.11: A hump created by an overload and flattened by an underload

The CORPUS model (Computation Of Retarded Propagation Under Spectrum loading) was proposed by De Koning [71] in 1981. This model developed used for crack growth prediction under flight simulation load sequences. The CORPUS model was based on the hump mechanism, i.e. crack closure is visualized by the hump formation (figure 2.11) on crack surfaces. There is no evidence supporting the formation of the humps on the crack surface presented in literature. However, only schematics are available to understand the hump creation and flattening. In case of an overload, a larger hump will be created and will be flattened by a later compressive load in the spectrum. In every cycle, a hump is created with associated S_{op} level, and for the estimation of S_{op} a cycle-by-cycle calculation is required, since S_{op} is an essential part of CORPUS model for crack extension.

De Koning [71] was able to introduce a few new concepts in the crack growth models. These were related to the concept of primary and secondary plastic zones, the consideration of plane strain/plane stress for plastic zone estimation and the multiple overload effect. Although the concept behind the model is quite simple, the mathematical interpretation of the model appears to be fairly complex. Padmadinata [72] and Putra [73] explained the CORPUS model very systematically in their thesis. The description in this paper is mainly attributed to both authors and is based on their analyses.

In order to describe the hump behaviour after application of an overload-underload combination, a form similar to Elber's function was determined empirically for 7075-T6 and 2024-T3 material:

$$U = (-0.4R^4 + 0.9R^3 - 0.15R^2 + 0.2R + 0.45); R > 0 \qquad (2.16)$$

$$U = (-0.1R^2 + 0.2R + 0.45); -0.5 < R < 0 \qquad (2.17)$$

Using Finite Element Analysis, Newman [74] demonstrated that S_{op} depends on $S_{max,n}$, $S_{min,n}$ and on the level of σ_{max} in comparison to the yield stress, which Newman assumed as an average yield stress. In order to incorporate the influence of high load levels, De Koning defined a correction factor h for the S_{op} values. The correction function was obtained by a curve fitting procedure to Newman's results.

An overload is playing a major rule in creating the hump while an underload will reduce the hump and hump opening stresses. A lower underload decreases the Sop level of the previous cycles while an overload higher than the previous overload cycles increases the Sop level.

An important feature of the CORPUS model is that it also differentiates between a plastic zone developing into virgin (elastic) material and a plastic zone extending in already plastically deformed material. The first ones are called Primary Plastic Zone *(PPZ)* and the latter ones are called Secondary Plastic Zone *(SPZ)*.

De Koning formulated a special equation by modifying the Irwin [75] equation as well as the Dixon finite width correction for centrally cracked specimen, in order to account for a large zone if S_{max} approaches the net section yield-limit. This resulted in a fairly complicated equation for calculating a PPZ involving a variable for the stress state assumption. The plastic zone size has an important role in the delay switch and the material memory consideration.

Interactions between an overload with an overlapping PPZ causes an increase of the crack opening levels, which will give more crack growth retardation. This effect plays an important role in the CORPUS model. The hump opening stress given by the equations 2.16 and 2.17 is valid for a single overload $S_{max,n}$ combined with an underload $S_{min,n}$. If a series of overloads is applied, de Koning assumes that $S_{op,n}$ will reach an upper bound stationary level defined by

$$1 + m_{st,n} \left[\frac{1}{U} - 1 \right] \qquad (2.18)$$

Where $m_{st,n}$ is a stationary parameter which depends on the crack growth increment Δa between the overloads and the plastic zone size D_n of the overload. For the CA case $\Delta a/D_n$ goes to zero and gives a value of $m_{st} = 0.1$. Finally, if the crack has grown through the overload plastic zone ($\Delta a/D_n$¿1), the overload interaction is ignored and equation 2.13 is used to calculate the ΔK_{eff} values for Paris relation. If a series of overloads is applied, the hump opening stress will reach the stationary value given by equation 2.13.

After the application of the overload, the value of $S_{op,n}$ is increased step by step. To compute the load interaction effect, a relaxation factor δ was taken into consideration (0.28 for 2024-T3). This value is valid for the interaction effects of overloads of the same level in plane stress condition. For a general case, where overload of different levels interact at different states of stress, two correction factors were introduced. The corrected relaxation factor is

$$\delta = 0.28\delta_1\delta_2 \qquad (2.19)$$

δ_1 accounts for interaction of different overload levels and δ_2 accounts for the effect of reduced interaction in plane strain condition. It should be kept in mind that only interaction between the recent overload and the overload associated with dominant hump is considered.

Concepts adopted in the CORPUS model are related to crack closure (Elber mechanism), plastic zone size, location of crack tip in plastic zone, hump and retardation mechanism.

After comparing the predicted and tested results, Padmadinata stated the following conclusions:

1. Crack growth in most severe flights was under estimated.

2. The CORPUS model gives much importance to a rarely occurring negative load if that load is more compressive (gust load) than the frequently occurring ground stress level. The prediction is inaccurate but conservative in that case.

3. Some improvements have to be done on the load sequence, as in some cases with simple load sequences, a sequence effect was predicted but it was not observed in the test series and sometimes it occurred in tests but CORPUS model did not predict it.

4. The CORPUS model predicts a higher crack growth rate for a lower yield stress if the other material constants are not changed. The latter condition is not realistic, but it indicates that relevant CA crack growth rates are essential for good predictions.

5. The CORPUS model does not consider the multiple overload effects on the 7075 alloy.

2.9   Summary

This chapter has briefly introduced the concept of *FMLs* with their nomenclature and benefits over monolithic metals. In addition, different types of

crack growth prediction models used for the monolithic metals are discussed. These models are mainly for variable amplitude loading. These models are modified for the fatigue crack growth prediction in *FMLs* under variable amplitude loading and discussed in Chapter 6.

References

[1] A. Vlot, Glare - History of the development of a new aircraft material, Kluwer Academic Press, Inc., 2001.

[2] R. C. Alderliesten, H. J. M. Woerden, Load history effects during fatigue crack propagation in glare, in: M. Guillaume (Ed.), Fatigue of Aeronautical structures as an Engineering Challenge, Vol. I, 2003, pp. 509–530.

[3] C. A. J. R. Vermeeren, An historic overview of the development of fibre metal laminate, Applied Composite Materials 10 (2003) 189–205.

[4] S. Mall, S. Johnson, R. A. Everett Jr., Cyclic debonding of adhesively bonded composite, in: K. L. Mittal (Ed.), Adhesive joints: Formation, Characteristics, and Testing, American Chemical Society,, Plenum Press, 1982, pp. 639–658.

[5] K. Ohiji, K. Ogura, Y. Ohkubo, Cyclic analysis of a propagating crack and its correlation with fatigue crack growth, Engineering Fracture Mechanics 7 (1975) 457–464.

[6] A. Vlot, J. W. Gunnink, Fibre Metal Laminates-An introduction, Kluwer Academic Publishers, Dordrecht, The Netherlands, 2001.

[7] D. A. Buianek, S. M. Spearing, Fatigue damage in titanium-graphite hybrid laminate, Composite Science and Technolgy 62 (2002) 607–617.

[8] C. T. Lin, P. W. Kao, Fatigue delamination growth in carbon fiber-reinforced aluminium laminate, Composites Part A 27A (1) (1996) 9–15.

[9] L. B. Vogelesang, R. Marissen, J. Schijve, A new fatigue resistant material: Aramid aluminum laminate, in: J. B. de Jonge, H. H. van der Linden (Eds.), Aircraft fatigue in the eighties, Vol. 3.4, 1981, pp. 1–39.

[10] R. Fredell, The development of inspection and repair methods for the c-17 aft cargo door., Tech. Rep. LR-704, Faculty of Aerospace Engineering, Delft. (November 1992).

[11] J. Cook, Processing and properties of high temperature metal/fiber-reinforced-thermoplastic laminates, Tech. Rep. AD-A278 791, Air Vehicle and Crew Systems Technology Department, Warminster, PA. (October 1993).

[12] A. Vlot, L. B. Vogelesang, T. F. Vries, Toward application of fibre metal laminates in large aircraft, Aircraft Engineering & Aerospace Technology 71 (1999) 558–570.

[13] L. Schwarmann, N. Ohrloff, T. Beumler, On the application of glare for airbus fuselage structures, in: A. Beuker, T. de Jong, J. Sinke, L. B. Vogelesang (Eds.), Fatigue of Aircraft Materials, Delft University Press., 1992, pp. 191–198.

[14] A. Vlot, J. W. Gunnink, Fibre Metal Laminates-An introduction, Kluwer Academic Publishers, Dordrecht, The Netherlands, 2001.

[15] C. S. Pegels, A study on the residual stress of glare1 (1995).

[16] R. C. Alderliesten, J. Schijve, S. van der Zwaag, Application of the energy release rate approach for delamination growth in glare, Engineering Fracture Mechanics 73 (2006) 697–709.

[17] Cytec Industries Inc., BR (R) Corrosion Inhibiting Primer, Datasheet (2003).

[18] A. Vlot, J. Gunnink, Fiber Metal Laminates - An introduction, Kluwer Academic Publishers, Dordrecht, The Netherlands, 2001.

[19] G. H. J. J. Roebroeks, Towards glare, the development of a fatigue insensitive and damage tolerant aircraft material, Ph.D. thesis, Delft University of Technology, Delft (1991).

[20] R. C. Alderliesten, Fatigue crack propagation and delamination growth in glare, Ph.D. thesis, Delft University of Technology, Delft (2005).

[21] R. Marissen, Fatigue crack growth in arall - a hybrid aluminium-aramid composite material, Tech. rep., Delft University of Technology, Delft,LR-574 (1988).

[22] R. Alderliesten, Fatigue crack propagation and delamination growth in glare, Ph.D. thesis, Delft University of Technology, Delft (2005).

[23] Y. J. Guo, X. R. Wu, Bridging stress distribution in center-cracked fiber reinforced metal laminates: modelling and experiment, Engineering Fracture Mechanics 63 (1999) 147–163.

[24] M. Skorupa, Load interaction effects during fatigue crack growth under variable amplitude loading-a literature review. part *i*: Empirical trends, Fatigue & Fracture of Engineering Materials and Structures, 21 (1998) 987–1006.

[25] C. Robin, M. Louah, G. Pluvinage, Influence of an overload on the fatigue crack growth in steels, Fatigue of engineering materials and structures 6 (1) (1983) 1–3, cited By (since 1996) 17.

[26] R. K. Pandey, B. B. Verma, Overload induced fatigue crack growth and significance of retardation zone, in: Proceedings of ICF IX, 1997, pp. 1285–1297.

[27] R. Kumar, Investigation of yield strength and single cycle overload on crack closure, International Journal of Pressure Vessels and Piping 51 (3) (1992) 329–348, cited By (since 1996) 3.

[28] G. S. Wang, B. Palmberg, A. F. Blom, Stress state-related fatigue crack growth under spectrum loading, Fatigue and Fracture of Engineering Materials and Structures 15 (7) (1992) 695–712, cited By (since 1996) 8.

[29] M. Darvish, S. Johansson, Fatigue crack growth studies under combination of single overload and cyclic condensation environment, Engineering Fracture Mechanics 52 (2) (1995) 295–297,299–319, cited By (since 1996) 8.

[30] X. L. Zheng, Overload effects on fatigue behaviour and life prediction of low-carbon steels, International Journal of Fatigue 17 (5) (1995) 331–337, cited By (since 1996) 8.

[31] B. B. Verma, R. K. Pandey, Effects of loading variables on overload induced fatigue crack growth retardation parameters, Journal of Materials Science 34 (19) (1999) 4867–4871, cited By (since 1996) 4.

[32] D. Shuter, W. Geary, The influence of specimen thickness on fatigue crack growth retardation following an overload, International Journal of Fatigue 17 (2) (1995) 111–119, cited By (since 1996) 15.

[33] M. Finney, Sensitivity of fatigue crack growth prediction (using wheeler retardation) to data representation, Journal of Testing and Evaluation 17 (1989) 74–81.

[34] B. K. C. Yuen, F. Taheri, Proposed modification to the wheeler retardation model for multiple overloading fatigue cycles, International Journal of Fatigue 28 (2006) 1803–1819.

[35] D. M. Corlby, P. F. Packman, On the influence of single and multiple peak overloads on fatigue crack propagation in 7075-t6511 aluminum, Engineering Fracture Mechanics 5 (1973) 479–497.

[36] K. S. Kim, S. C. Kim, C. S. Shim, P. J. Y., A study on the effect of overload ratio on fatigue crack growth, Key Engineering Material 261-263 (2004) 1159–1168.

[37] H. Alawi, Designing reliably for fatigue crack growth under random loading, Engineering Fracture Mechanics 37 (1990) 75–85.

[38] F. Taheri, D. Trask, N. Pegg, Experimental and analytical investigation of fatigue characteristics of 350wt steel under constant and variable amplitude loadings, Journal of Marine Structures 16 (2001) 69–91.

[39] P. A. Rushton, F. Taheri, Prediction of variable amplitude crack growth in 350wt steel using a modified wheeler approach, Journal of Marine Structures 16 (2003) 517–539.

[40] J. M. Finney, Modelling for fatigue crack growth prediction in aircraft, Fatigue Fracture Engineering Materials & Structures 8 (1985) 205–222.

[41] H. Alawi, Designing reliably for fatigue crack growth under random loading, Engineering Fracture Mechanics 37 (1990) 75–85.

[42] K. Dolinski, Fatigue crack growth with retardation under stationary stochastic loading, Engineering Fracture Mechanics 27 (1987) 279–290.

[43] B. Sheu, P. S. Song, S. Hwang, Shaping exponent in wheeler model under a single overload, Engineering Fracture Mechanics 51 (1995) 135–143.

[44] Z. Khan, A. Rauf, M. Younas, Prediction of fatigue crack propagation life in notched members under variable amplitude loading, Journal of Material Engineering Performance 6 (1997) 365–373.

[45] M. Hawkayard, B. E. Pawell, J. M. Stephenson, Fatigue crack growth from simulation flight cycles involving superimposed vibrations, International Journal of Fatigue 21 (1999) 559–568.

[46] P. S. Song, B. C. Sheu, L. Chang, A modified wheeler model to improve predictions of crack growth following a single overload, JSME Internation Journal Series A 44 (2001) 117–22.

[47] M. A. Wahab, R. G. R., J. H. Park, Experimental study on the influence of overload induced residual stress field on fatigue crack growth in aluminium alloy, Journal of Material and Processing Technology 153-154 (2004) 945–951.

[48] S. U. Khan, R. C. Alderliesten, J. Schijve, R. Benedictus, On the fatigue crack growth prediction under variable amplitude loading, in: D. G. Pavlou (Ed.), Computational and experimental analysis of damaged materials 2007, Transworld Research Network, Kerala, India., 2007, Ch. 4, pp. 77–105.

[49] A. Saxena, Nonlinear fracture mechanics for engineers, CRC Press, Florida., 1998.

[50] N. Perez, Fracture Mechanics, Kluwer Academic Publishers, Boston., 2004.

[51] T. L. Anderson, Fracture Mechanics : Fundamentals and applications, CRC Press, Florida., 1995.

[52] J. P. Gallagher, A generalized development of yield zone models, Tech. rep., AFFDL-TM-74-28-FBR (1974).

[53] J. Schijve, Fatigue of Structures and Materials, Kluwer, 2001.

[54] O. Wheeler, Spectrum loading and crack growth., Tech. rep., ASMR 72 MetX also G.D. Report FZM 5602 (1970).

[55] M. A. Meggiolaro, J. T. Pinho de Castro, Comparison of load interaction models in fatigue crack propagation., in: Proceedings of the XVI Brazilian Congress in Mechanical Engineering (COBEM), ABCM, Vol. 12, 2001, pp. 247–256.

[56] F. A. Veer, The effect of shear lips, loading transitions and test frequency on constant delta-k and constant load amplitude fatigue tests, Ph.D. thesis, Delft University of Technology (1993).

[57] D. M. Corlby, P. F. Packman, On the influence of single and multiple peak overloads on fatigue crack propagation in 7075-t6511 aluminum, Engineering Fracture Mechanics 5 (1973) 479–497.

[58] K. Walker, The effect of stress ratio during crack propagation and fatigue for 2024-T3 and 7075-T6 aluminum, Astm stp 462, American Society of Testing and Materials (1970).

[59] M. V. S. Pereira, F. A. I. Darwish, A. F. Camarao, S. H. Motta, On the prediction of fatigue crack retardation using wheeler and willenborg models, Materials Research 10 (2) (2007) 101–107.

[60] R. G. Forman, V. E. Kearney, R. M. Engle, Numerical analysis of crack propagation in cyclic-loaded structures, Journal of Basic Engineering 89 (1967) 459–463.

[61] J. Schijve, Some formulas for the crack opening stress level, Engineering Fracture Mechanics 14 (1981) 461–465.

[62] W. Elber, Fatigue crack closure under cyclic tension, Engineering Fracture Mechanics 2 (1970) 37–45.

[63] J. C. J. Newman, A finite-element analysis of fatigue crack closure. mechanics of crack growth, STP 590, ASTM (1976).

[64] J. Schijve, Some formulas for the crack opening stress level, Engineering Fracture Mechanics 14 (1981) 461–465.

[65] J. C. J. Newman, Finite element analysis of fatigue crack propagation – including the effects of crack closure, Ph.D. thesis, Virginia Polytechnic Institute and State University, Blacksburg, VA (1974).

[66] G. H. J. J. Roebroeks, Towards glare, the development of a fatigue insensitive and damage tolerant aircraft material, Ph.D. thesis, Delft University of Technology, Delft (1991).

[67] C. R. Dill, H. D.and Saff, Spectrum crack growth prediction method based on crack surface displacement and contact analyses, STP 595, ASTM (1976).

[68] B. Budiansky, H. J. W., Analysis of closure fatigue crack growth, Journal of Applied Mechanics 45 (1978) 267–278.

[69] H. Fuehring, T. Seeger, Dugdale crack closure analysis of fatigue cracks under constant amplitude loading, Engineering Fracture Mechanics 11 (1979) 99–122.

[70] J. Schijve, Observations on the prediction of fatigue crack growth propagation under variable amplitude loading, in: Fatigue Crack Growth Under Spectrum Loads, no. 595 in ASTM STP, American Society for Testing and Materials, 1976, pp. 3–23.

[71] A. U. de Koning, H. H. van der Linden, Prediction of fatigue crack growth rates under variable amplitude loading, Tech. Rep. NLR MP 81023U, NLR, Amsterdam (1981).

[72] U. H. Padmadinata, Investigation of crack-closure prediction models for fatigue in aluminum alloy sheet under flight simulation loading, Ph.D. thesis, Delft University of Technology. (1990).

[73] I. S. Putra, Fatigue crack growth predictions of surface cracks under constant amplitude and variable amplitude loading, Ph.D. thesis, Delft University of Technology (1994).

[74] J. Newman, J. C., A crack closure model for predicting fatigue crack growth under aircraft spectrum loading, Tech. Rep. ASTM STP 748, ASTM (1981).

[75] G. R. Irwin, Linear fracture mechanics, fracture transition, and fracture control, Engineering Fracture Mechanics 1 (1968) 241–257.

Chapter 3

DELAMINATION GROWTH

To raise new questions, new possibilities, to regard old problems from a new angle, requires creative imagination and marks real advance in science.

Albert Einstein
(1879-1955)

Experimental and analytical investigation of the effect of variable amplitude (VA) load sequences on delamination behavior in Fibre metal laminates FMLs is presented in this chapter. Delamination tests are performed and results are compared with linear damage accumulation prediction. The correlation between the test results and predictions highlighted the absence of load sequence and interaction effects in delamination growth rate under VA loading.

The fatigue crack growth behavior of Fibre Metal Laminates has been extensively investigated in the past decades. The majority of papers published on this topic report fatigue and fracture experiments on various coupon specimens, analysis of observations and development of understanding by means of empirical or theoretical models [1–14]. The main advantage of *FMLs* is the very slow and approximately constant crack growth under even full spectrum loading as a result of crack bridging by intact fibers. The crack growth is accompanied

37

by delamination growth in the wake of the crack, which to some extent is considered to be favorable for these materials, in contrast to fibre reinforced polymer composites.
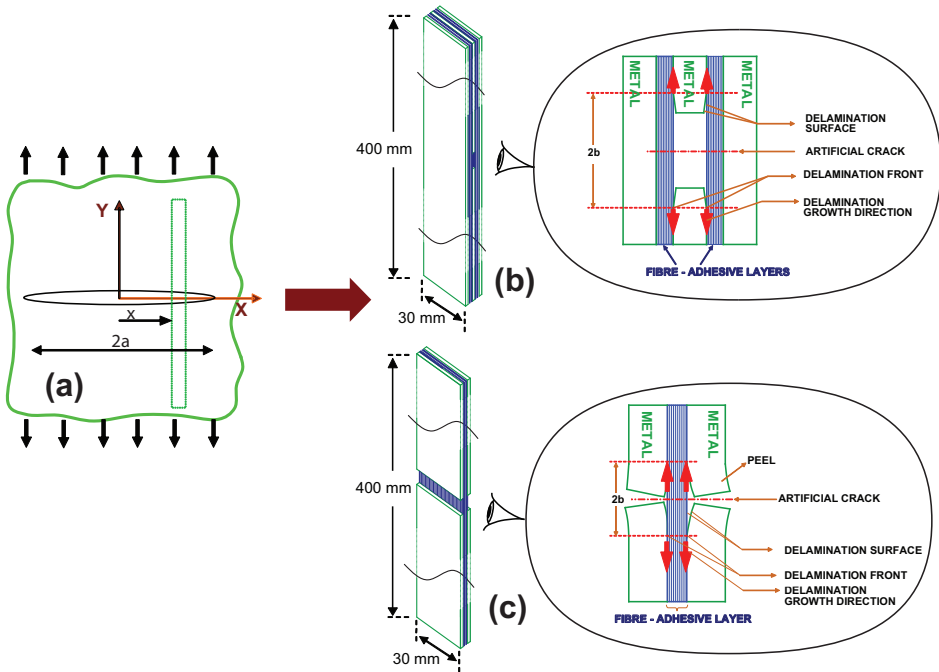
Figure 3.1: a. Illustration of typical delamination and *CCT* specimens, b. Center-cracked lap shear *CCLS*specimen geometry [15], c. Double cracked lap shear *DCLS* specimen geometry [21]

Although various crack growth experiments on *FMLs* have been reported where simple *VA* load sequences or actual flight simulation spectra were applied [8–11], a detailed understanding of the interaction effects in *FMLs* is not yet at hand. At least not to the same level of understanding as for crack growth under constant amplitude *(CA)* loading.

Alderliesten and Woerden [14], for example, studied delamination shapes created during *CA* loading with and without overloads. A major question following from their discussion is whether the delamination growth is affected solely by the behavior of the metals (plasticity) or whether additional sequence effects (retardation, acceleration) influence the growth. This question becomes especially important when looking at the study by Alderliesten et al. [15], where delamination observations were made during testing of a single specimen at subsequently different load levels. The presence of in-

teraction effects in the delamination growth rate might have an effect on the results obtained.

To enable the development of an analytical model describing the physical fracture behavior under arbitrary fatigue loading in *FMLs*, this question concerning interaction effects in delamination growth must be addressed. This chapter reports on additional delamination growth tests on similar *FML* specimens with various block load sequences and *VA* load spectra. The results are compared and analyzed with current fracture mechanics based descriptions for delamination growth [15–20] to answer the question, whether or not interaction effects are present in the delamination growth.

3.1   Delamination Growth Rate Calculations

The energy release rate for delamination is calculated based on energy balance in the centered-cracked lap shear *(CCLS)* as well as double-cracked lap shear *(DCLS)* specimen delamination specimen as shown in figure 3.1 [1, 15, 16]. The details about these types of specimen is given in the next section.

Delamination growth is described using a Paris type relation with two experimentally determined constants C_d, n_d and the difference of strain energy release rates $G_{d,max}$ and $G_{d,min}$ using equation 3.1 and stress ratio R. The detailed derivation of equation 3.1 is given in Appendix A.

$$G_d = \frac{\sigma_{lam}^2}{2jE_{al}}\left[\frac{\lambda^2}{E_{al}}(n_{al}-n_{cr})t_{al} - \lambda^2 n_{al}t_{al} + \frac{E_{f,0}}{E_{al}}n_{f,0}t_{f,0}(\gamma^2-\lambda^2)+ \right.$$
$$\left. \frac{E_{f,90}}{E_{al}}n_{f,90}t_{f,90}(\gamma^2-\lambda^2) \right] \tag{3.1}$$

$$\frac{db}{dN} = C_d(\Delta G)^{n_d} \tag{3.2}$$

Rans and Alderliesten [22], used $\Delta G = (\sqrt{G_{d,\text{max}}} - \sqrt{G_{d,\text{min}}})^2$ to investigate the influence of residual stress on the delamination growth. According to them the residual component of the strain energy rate is removed by using the rule of super-positioning, which is mathematically explained as

$$\Delta G = \left(\sqrt{G_{\text{max}}} - \sqrt{G_{\text{min}}}\right)^2$$

$$= \left[\left(\sqrt{G_{d,\text{max}}} + \sqrt{G_{residual}}\right) - \left(\sqrt{G_{d,\text{min}}} + \sqrt{G_{residual}}\right)\right]^2$$

$$= \left[\left(\sqrt{G_{d,\text{max}}}\right) - \left(\sqrt{G_{d,\text{min}}}\right)\right]^2$$
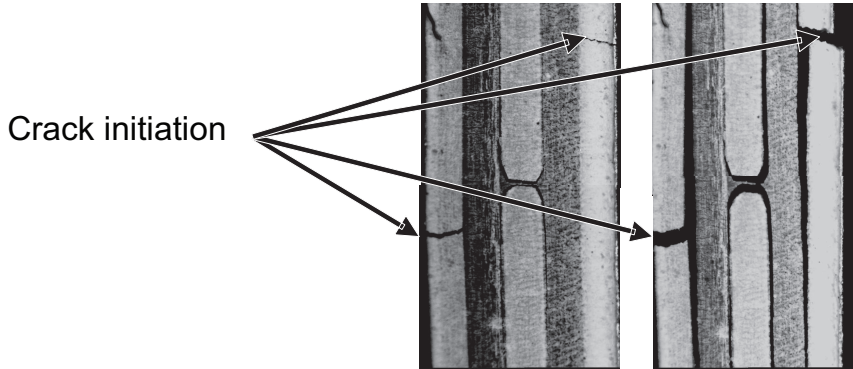
Figure 3.2: Early failure of intact metal layers in center-cracked lap shear specimen

The linear damage accumulation *(LDA)* rule is based on a cycle-by-cycle analysis independent of preceding load cycles. It is an integration of calculated delamination growth increments Δb_i using equation 3.2 to obtain a prediction for the full load spectrum or one block of load sequences. As a result, it is the simplest method to predict the delamination growth under VA loading. The advantage of the *LDA* rule is computational efficiency. In the present research, *LDA* is used to prove the absence of any interaction effects. In the other words, interaction effects will be absent in delamination growth under *VA* loading if the delamination growth rate predicted using *LDA* correlates well with the experimentally obtained growth rate.

In general, the *LDA* rule can be presented mathematically as:

$$b = b_0 + \sum_{i=1}^{N} \Delta b_i \qquad (3.3)$$

3.2 Experimental Program

3.2.1 Test Specimen

To investigate delamination growth, a specimen should be selected that will not induce interaction with other fracture phenomena. In center-cracked tension *(CCT)* specimen for example, delaminations coexists with metal crack growth, which cannot be excluded when analyzing the delaminations. Better specimens are *CCLS* and double-cracked lap shear *(DCLS)*, see figure 3.1, which can be related to *CCT* afterwards as illustrated in the same figure.

Initially, a *CCLS* specimen (configuration illustrated figure 3.1-b) has been selected, which is believed to represent a pure mode II configuration [16]. These specimens have been manufactured using the standard *GLARE 2-3/2-0.3* configuration. Due to the early failure of the intact aluminium layers as shown in figure 3.2, the range in delamination lengths that could be used in the analysis was very limited. In order to avoid this problem, *DCLS* specimen (illustrated in figure 3.1-c) has been used. These specimens have been manufactured using standard *GLARE 2-2/1-0.3* layup with two 0.3 mm thick cracked outer layers of aluminium *2024-T3* with in-between two unidirectional glass fibres epoxy layers with a nominal thickness after curing of 0.26 mm. Although this configuration mathematically seems to have a mode I contribution to the delamination mechanisms [16], it was shown by Alderliesten et al. [15] that this mode has no effect on the observed delamination growth. The mechanical properties of the constituents of the tested specimens are summarized in Table 2.3.

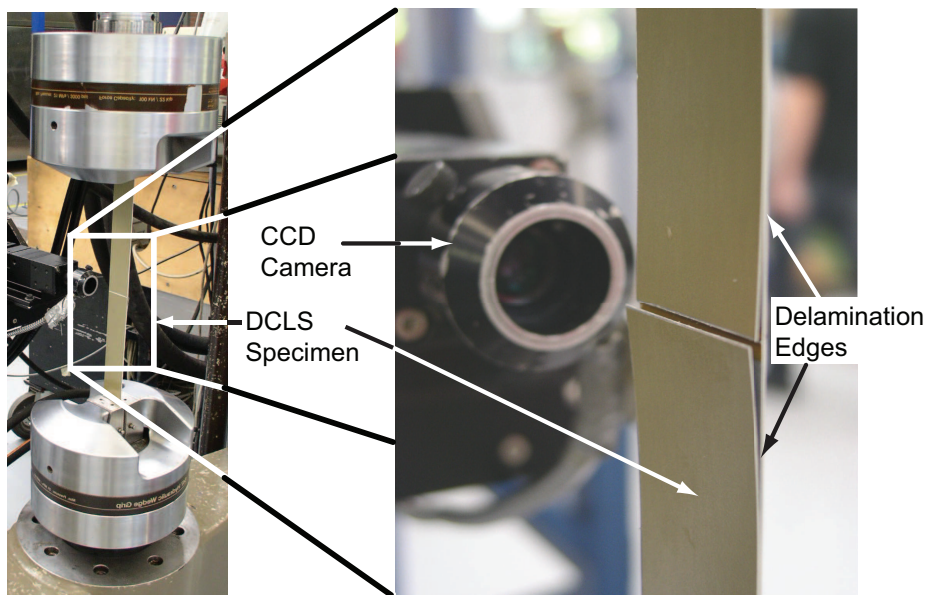### 3.2.2 Test Equipment & Procedure

Figure 3.3: Testing setup

The tests were conducted in lab air at room temperature in a closed loop mechanical and computer controlled servo-hydraulic testing system with a

load capacity of 10 metric tons. The delamination lengths were measured from one side of specimen at the four locations near the artificial cracks in the aluminium layers and subsequently averaged. The delamination measurements were performed at intervals, while the test was on hold at its maximum applied stress level. The measurements were performed with a *CCD* camera using in-house developed imaging software "Impress". The full test setup is shown in figure 3.3.

3.2.3   Test Matrix

The experiments were conducted with *HI-LO* and *LO-HI* block load sequences, with programmed block loading, multiple block loading and flight spectrum loading. The test matrix is given in table 3.1, showing the load sequence and the applied stress levels.

3.3   Results & Discussion
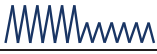
3.3.1   Block Load Sequences

Delamination test results for block and multiple block load sequences are shown in figure 3.4-(a), (b) and 3.5-(a). Delamination lengths measured from the four edges are plotted against the number of cycles in figure 3.4-(a). A straight line through the delamination data represents the average delamination growth rate (Figure 3.4-(a)).

In all tests performed, the delamination growth was initially non-linear, but it became linear after the delamination progressed a short distance. The length of this distance appeared to depend on the applied stress levels. There are two aspects that might have an effect on this initial non-linear behaviour. The application of Teflon inserts and the deburring of the metal layer edges (as shown in figure 3.6). During fabrication of specimens, a thin Teflon tape was placed at the delamination initiation location in order to accelerate delamination initiation. In addition, the metal layer edges were deburred to avoid any unwanted damage to the neighboring prepreg layer as a result of sharp edges/burs. As a consequence, the delamination initially has to grow along the deburred surface, during which delamination will be having a significant contribution of Mode I to the Mode II delamination growth. This start-up effect was also observed by Mall et al. [23] in case of a composite-to-composite bonded joint tested under *CA* fatigue.

The block and multiple block load cases show that the delamination growth rate mainly depends on the applied stress levels. The same observation is

Table 3.1: Delamination test matrix

	Load Sequence		Stress Values [MPa]	Stress Ratio [R]
Block loading		LO-HI	150-169	0.05
		HI-LO	169-150	0.05
Block loading		LO-HI	150-187.5	0.05
		HI-LO	187.5-150	0.05
Multiple Block Loading		HI-LO	200-187.5-150-125	0.05
		LO-HI	125-150-187.5-200	0.05
Periodic LO-HI-LO		Large period	105 to 195 in 285 cycles	0.86 to 0.03
		Short period	105 to 195 in 100 cycles	0.86 to 0.03
Periodic Over-loads		Increasing step	80 to 220 to 80	
		Decreasing step	80 to 220 to 80	
Programmed Block Loading		$N_{LARGE}=1$ $N_{SMALL}=100$	$\sigma_{max_{LARGE}}=187.5$ $\sigma_{max_{SMALL}}=150$	0.04 0.05
		$N_{LARGE}=1$ $N_{SMALL}=20$	$\sigma_{max_{LARGE}}=187.5$ $\sigma_{max_{SMALL}}=150$	0.04 0.05
		$N_{LARGE}=1$ $N_{SMALL}=4$	$\sigma_{max_{LARGE}}=187.5$ $\sigma_{max_{SMALL}}=150$	0.04 0.05
Mini-TWIST	$\sigma_{mean}=100$ MPa, Truncation level=IV, Ground-air-ground stress=$0.02 \times \sigma_{mean}$			
WFS	Typical wide-body fuselage spectrum			
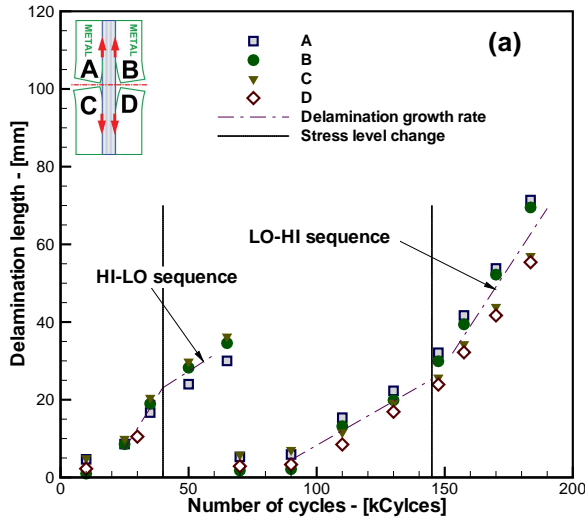
(a)
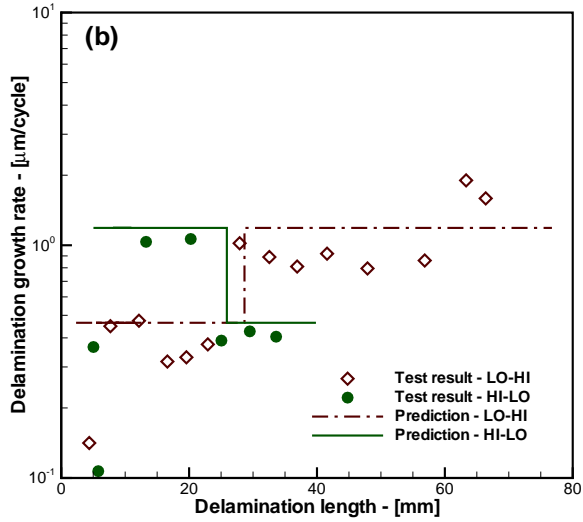
(b)

Figure 3.4: Delamination growth tests results: (a). Two block loading (B Vs. N); (b). Two block loading (db/dN Vs. b)

reported by Alderliesten et al. [15] and Mall et al. [23]. In the correlation between test and *LDA* predictions (using equations 3.1 and 3.2) for two blocks (Figure 3.4-(a) and (b)), multiple block (Figure 3.5-(a)) and program-
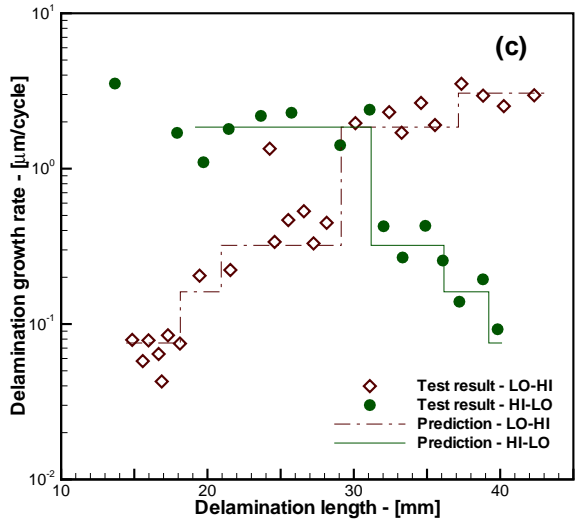
(a)
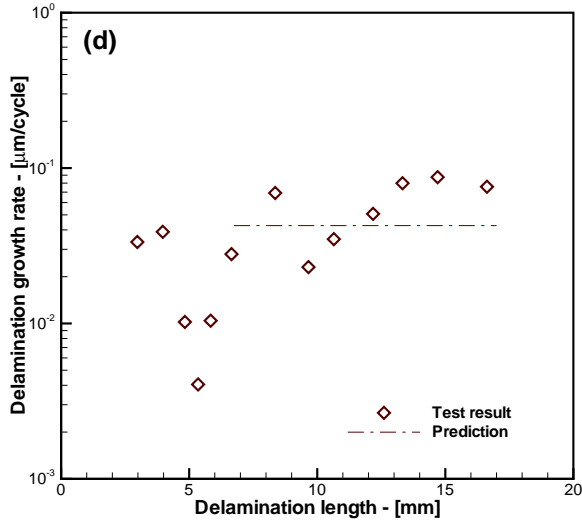
(b)

Figure 3.5: Delamination growth tests results: (a). Multiple block load (db/dN Vs. b); (b). Mini-Twist (db/dN Vs. b)

med block (Figure 3.7) load cases, an obvious interaction effect can not be observed.
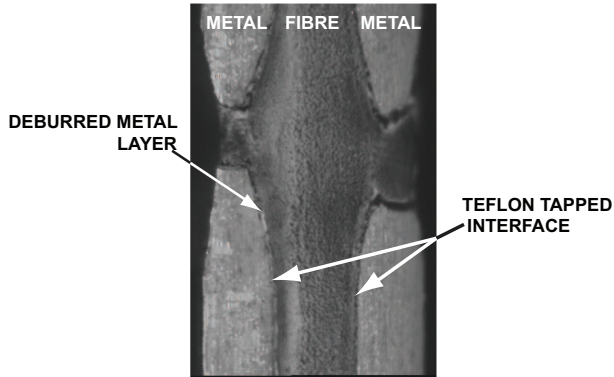
Figure 3.6: Deburred metal layers and Teflon tape location
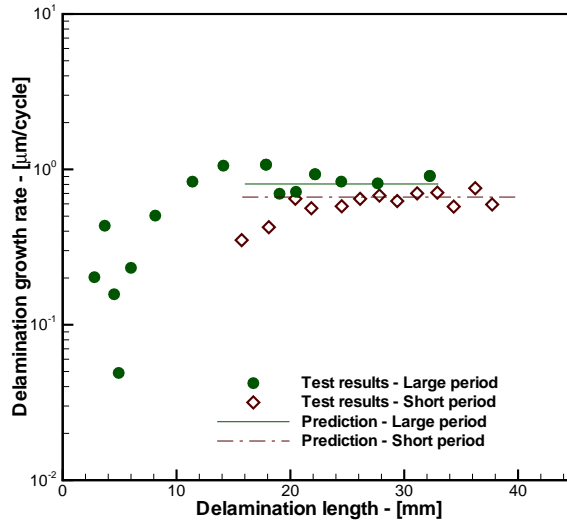
Figure 3.7: Delamination growth tests results for Periodic LO-HI-LO spectra – Large and short period

3.3.2   Flight Load Sequences

The questions arise, Whether any interaction effect (if present) can be captured by block load test. If it only has a small effect (order of magnitude μm or few cycles) average da/dN does not reveal anything. The second question is, what test should be performed to capture any interaction if present. To answer these questions, single OL may be to tricky because of measurement techniques. That's why flight spectra test were preferred to compare LDA.
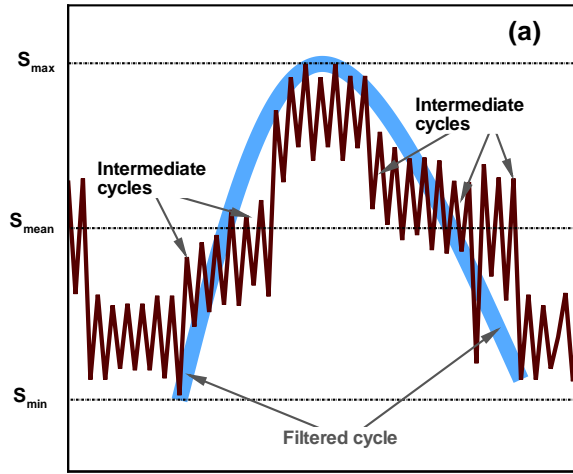
(a)
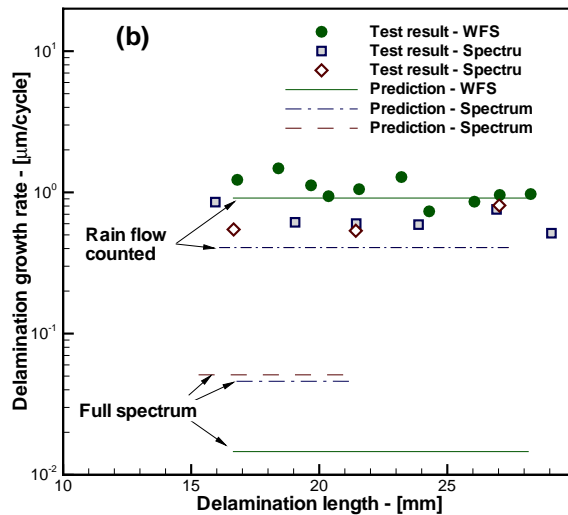
(b)

Figure 3.8: a. Rain flow counting technique; b. Delamination growth tests results for *WFS* and programmed block load (Increasing and decreasing steps spectra)

These flight spectra were: 1. Mini-Twist, 2. Typical wide body fuselage spectrum *(WFS)*. In case of Mini-Twist spectrum the correlation between the test results and prediction does not indicate a presence of interaction

effects(Figure 3.5-(b)).
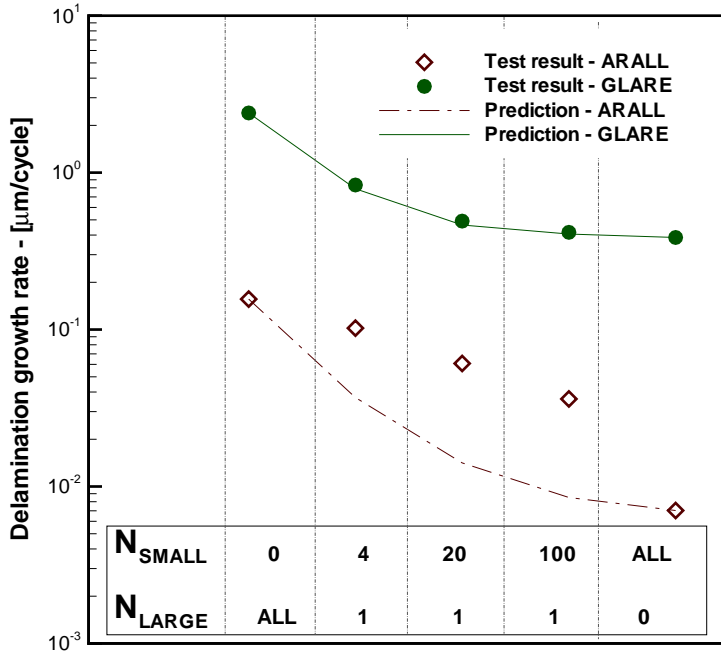
Figure 3.9: Delamination growth tests results comparison of *ARALL* and *GLARE*

On the other hand, between the test result and prediction for *WFS* a correlation is absent. The difference between the Mini-Twist and *WFS* spectrum is the presence of a number of intermediate cycles that break up the large cycles into smaller cycles in *WFS* spectrum, as shown in figure 3.8-(a). The rain-flow counting technique [24–26], mentioned in literature as a cycle counting and filtering technique for crack growth in metal structures, is used here to account for these intermediate cycles. As a result, in the filtered situation the large cycles are considered only, schematically shown in figure 3.8-(a). As shown in figure 3.8-(b), the rain-flow counting technique combined with *LDA* predictions resulted in a close match between the test result and prediction for *WFS* and program block load test. The correlation of test data and rain-flow counted spectrum prediction highlighted that the delamination growth rate depends on the large cycles and the delamination is not affected by the intermediate cycles within large cycles.

3.3.3   Delamination Behaviour of *ARALL* & *GLARE*

Marissen [1] tested *ARALL* delamination specimens under repetitive block loads, mentioned as 'Programmed Block Loading' in table 3.1. In this load spectrum, single *OL* cycles N_{LARGE} were applied with varying the number of preceding small cycles, N_{SMALL}. He reported some interaction effects, which are different in nature than the ones known to exist in metal crack growth. In his tests, increase in delamination growth rate, calculated using Miner's *LDA* rule, was observed by increasing the number of small cycles between *OL* cycles (Figure 3.9).

To compare the current research with Marissen's findings, a similar spectrum has been applied to *GLARE*. No interaction was observed, as can be illustrated by comparing the results with *LDA* predictions, which is based on non-interaction (Figure 3.9). This observation does not agree with the Marissen's observation. Then the question arises what can be different in *ARALL* from *GLARE* which caused interaction effects? Further evaluation is done to study the possible causes of different delamination behaviour of *ARALL* and *GLARE*.
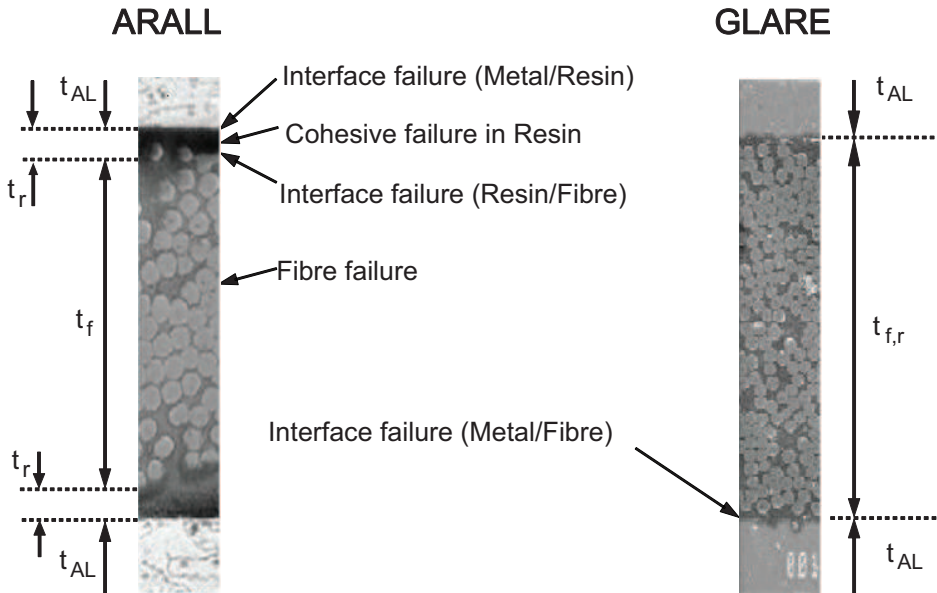
Figure 3.10: Delamination paths (t_{al} = Aluminium layer thickness, t_f = Fibre layer Thickness, t_r = Resin-rich layer thickness, $t_{f,r}$ = Fibre/Resin thickness (*GLARE*))

First, the question is whether the experimental techniques may cause such difference in observation? Marissen used a photo-elastic technique to mea-

sure the delamination length, while a *CCD* camera was used in the current research. In principle, there should not be any error due to the measurement technique because in the correlation (Fig. 3.9) the delamination growth rate - db/dN is used instead of delamination length - b. A systematic difference in capturing the length would only provide a difference in delamination length, not in rates. In addition, Mall et al. [23] compared three different measurement techniques to measure the debond length. They concluded that measurements using different techniques are quite close to each other and any of the method can be adopted.

Second, the metal/fibre interface may be the cause of difference in *ARALL* and *GLARE*. In *ARALL*, BSL-312-UL is used as the adhesive system, whereas FM-94 is used in *GLARE*. Verbruggen [27] has compared the fibre-epoxy bonding for glass fibres and aramid fibres. Aramid-epoxy has shown poor adhesion compared to glass-epoxy. Similarly, Roebroeks [28] has stated that *GLARE* has a high peel strength in comparison with *ARALL*. In view of possible delaminations during manufacturing processes or later in-service, he considered high peel strength being advantageous.
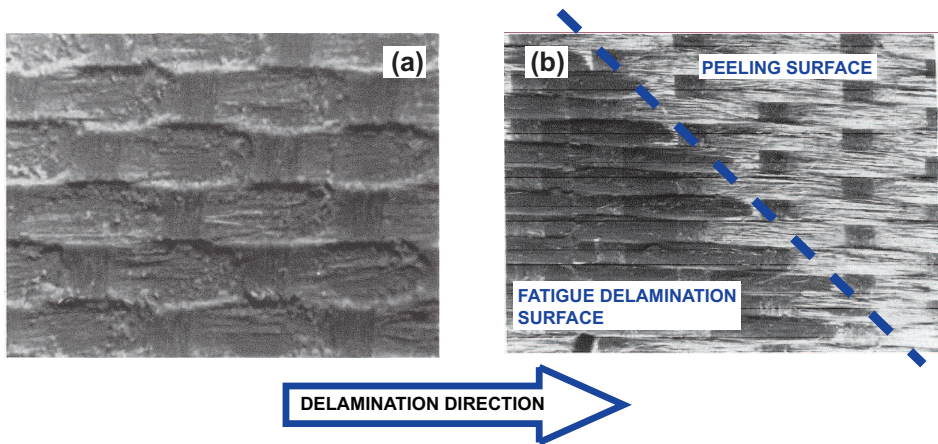
Figure 3.11: Fatigue delamination surface in *ARALL*: a. Imprint of the fabric in the adhesive, b. Delamination front at the fibre side. [1]

The number of possible fracture paths in *ARALL* is larger because of its inhomogeneous composition. Microscopic examination of a cross-section of the *ARALL* specimen showed that it consists of a resin-rich layer (1/10 of prepreg thickness) near the adherends and a fibre-rich layer (8/10 of prepreg thickness) in the center of the prepreg layer. The delamination paths are shown in figure 3.10. On the other hand, the delamination in *GLARE* exists at the metal/fibre interface. That is the only path of delamination observed in *GLARE* (as shown in figure 3.10).

Despite the poor aramid-epoxy adhesion, low peel strength and multiple delamination paths, Alderliesten [21] has shown that *ARALL* (BSL-312-UL) has almost similar delamination resistance as *GLARE* (FM-94). This means that all of these differences have insignificant effect on the *CA* delamination resistance and hence cannot contribute to the difference between the delamination behaviour of *ARALL* and *GLARE*.

In *ARALL*, Twaron HM fabric in combination with BSL-312-UL adhesive is used. Delaminated surfaces show an irregular pattern (surface), as shown in figure 3.11. Due to twaron weaved fabric, the delamination front always stops at the roving perpendicular to the loading direction. These rovings apparently act as 'delamination stoppers', and the overall delamination growth is reduced [1]. It can be stated about Marissen's tests that for *CA* loading, either high or low, the delamination grows with a constant rate even entangling at the rovings. Whenever, an *OL* is applied during *CA* loading, a certain jump over the roving or increase in delamination length can be expected which leads to the higher delamination growth rate observed by Marissen. This increase in delamination growth rate is more pronounced when the number of *OLs* were increased in the *CA* cycles. On the other hand, in *GLARE*, S2 Glass uni-directional prepreg in combination of FM-94 is used. The delaminated surfaces in *GLARE* show a straight (smooth) profile along the metal-fibre interface, as shown in figure 3.12. Phenomenon like delamination stoppers was not observed because there are no fibres present perpendicular to the delamination growth direction. There is not a big difference between the test results and *LDA* predictions.

The major differences in *GLARE* and *ARALL* are briefly given in table 3.2

Table 3.2: Possible causes of different delamination behaviour of *ARALL* and *GLARE*

	ARALL	GLARE	Reference
Metal type	7075-T6	2024-T3	[1, 21]
Metal layer thickness [mm]	0.45	0.3	[1, 21]
	Tawaron	Glass	[1, 21]
Fibre type	Fabric	Prepreg	[1, 21]
	woven	Uni-directional	[1, 21]
Fibre layer thickness [mm]	0.3	2×0.133	[1, 21]
Adhesive Type	BSL-312-UL	FM-94	[1, 21]
Resin rich layer	Present	Absent	[29]
Fibre volume fraction	54%	60%	
Fibre/Epoxy bonding	Weak bonding	Strong interfacial bonding	[27]
Peel-strength	2.5 N/mm	7.5 N/mm	[28]
Possible delamination path	1: Interface failure at the resin rich layer-adherend interface 2: Cohesive failure in resin rich layer 3: Interface failure at resin-fibre interface 4: Fibre failure	1: Interfacial failure at adhesive-adherend interface	Figure 3.10
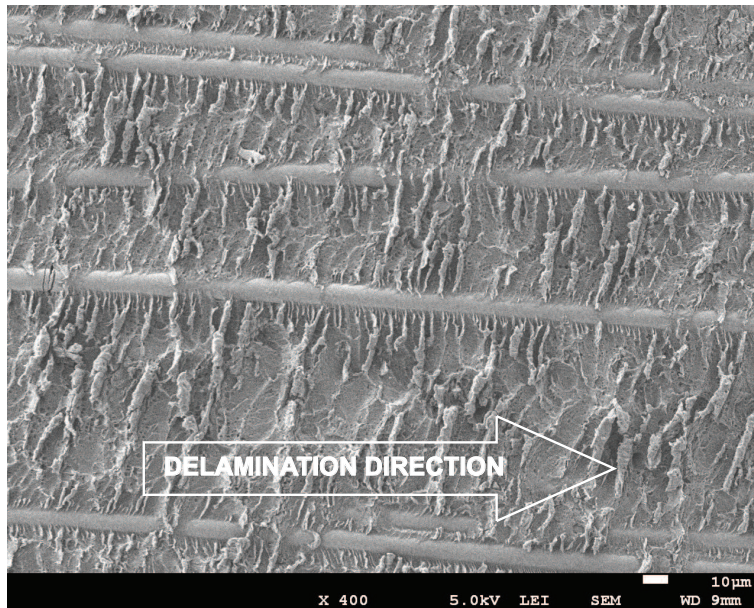
Figure 3.12: Delamination surface of fibre side

3.3.4   SEM Analysis of Delaminated Surfaces

Several specimens have been analyzed using Scanning Electronic Microscopy
(SEM) to investigate the delamination surfaces at both metal and the fibre
side. Previously, Verbruggen [23] performed *SEM* to compare the adhe-
sive properties of three different types of fibres, namely Aramid, Glass and
Carbon. In addition, Marissen [1] has shown the presence of striations
on the delaminated surface at the metal side. However, he was unable to
relate these striations to the delamination growth data and thus to draw
conclusions on the presence of interaction effects (i.e. delamination growth
acceleration). Nonetheless, Marissen reported that *SEM* might be helpful
if striations could be related to applied stress values. In the present re-
search, *SEM* has also been performed in order to acquire information about
the presence or absence of interaction effects in delamination growth. At
the fibre side, no striations or delamination growth markings could be ob-
served, but the important observation here is that the delamination front is
quite regular without fibres pullout or delamination front moving almost in
a straight manner, as shown in figure 3.12. Figure 3.12 also shows that the
fibres are covered with resin, which highlights the good adhesion between
resin and fibres. Because all fibres are covered with adhesive residue, the
delamination evidently occurs as a cohesive failure in the adhesive.
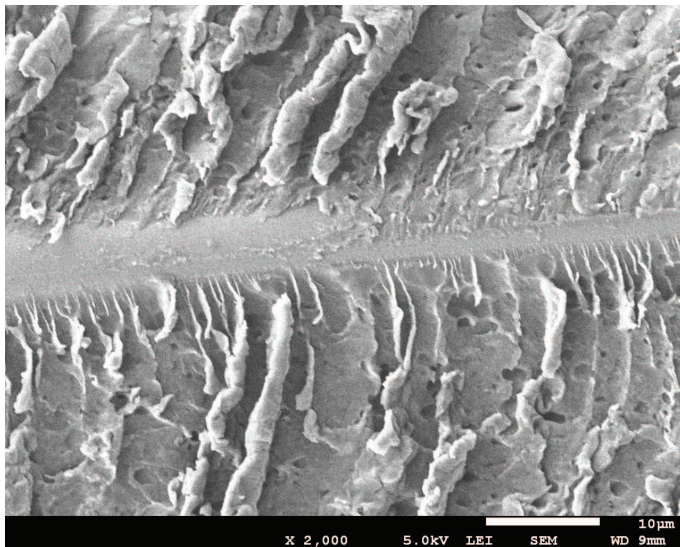
(a)
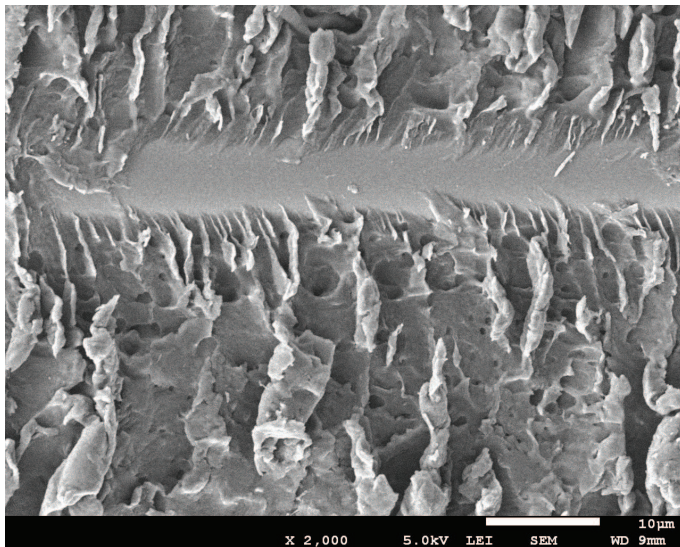
(b)

Figure 3.13: Illustration of the fibre/matrix adhesion; a. at LO stress amplitude (150MPa), b.at HI stress amplitude (169MPa)

Figure 3.13 illustrates the fibre/matrix adhesion at the delamination surface; cusps can be observed that according to Purslow [30] indicate shear failure.
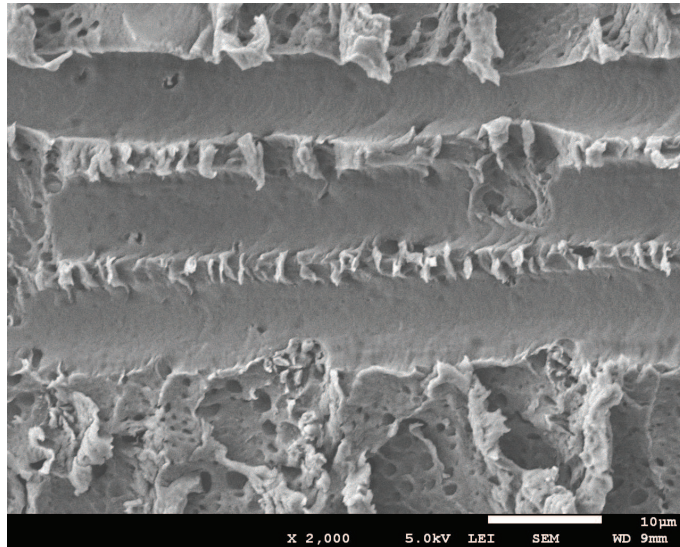
Figure 3.14: Delamination markings (striation) observed in the fibre imprints at the metal side of the delaminated specimens.

Markings that may be considered delamination growth striations were observed in the fibre imprints at the metal side of the delaminated specimen, as shown in figure 3.14.

A closer observation of these marking revealed that they can be related to the stress amplitude. For example, when the striations for *LO-HI* load sequence are counted, twice as much markings were observed over the same distance in the *LO* cycle, as compared to the *HI* cycle. This factor *2* difference between both spacings, shown in Figure 3.15, corresponds with the observed macroscopic delamination growth rates (i.e., delamination growth rate during the *LO* cycles is $db/dN = 3.9 \times 10^{-4}$ mm/cycle, while at *HI* cycles, $db/dN = 8.5 \times 10^{-4}$ mm/cycle). The spacing/cycle may not be exactly related to db/dN but a relative comparison is justified.

In case of flight spectrum and periodic block load sequence, similar striations are observed. The spacing between these striations can be related to the S_{max}, as shown in figure 3.16 for periodic block load sequence. Delamination striations (figure 3.16 and 3.17) observed in fibre imprints are not continuous like fatigue crack growth striation observed in metals, which is also observed by Roebroeks [31] in case of *ARALL*. This discontinuity is due to the either low S_{max} or missing fibre imprints.
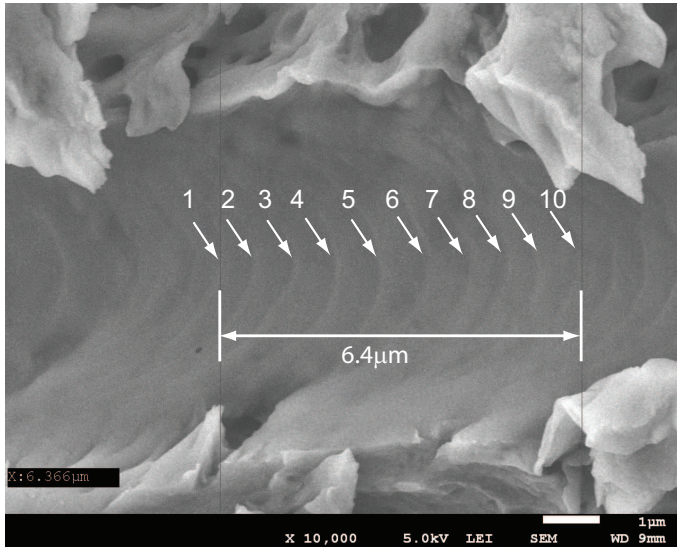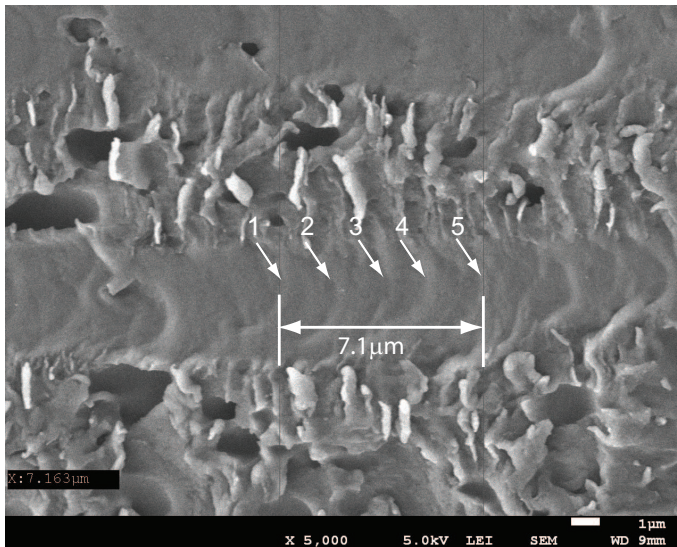
Figure 3.15: Delamination growth markings (striation) at LO stress amplitude (169MPa) a.. and at HI stress amplitude (150MPa) b.

(a)

(b)
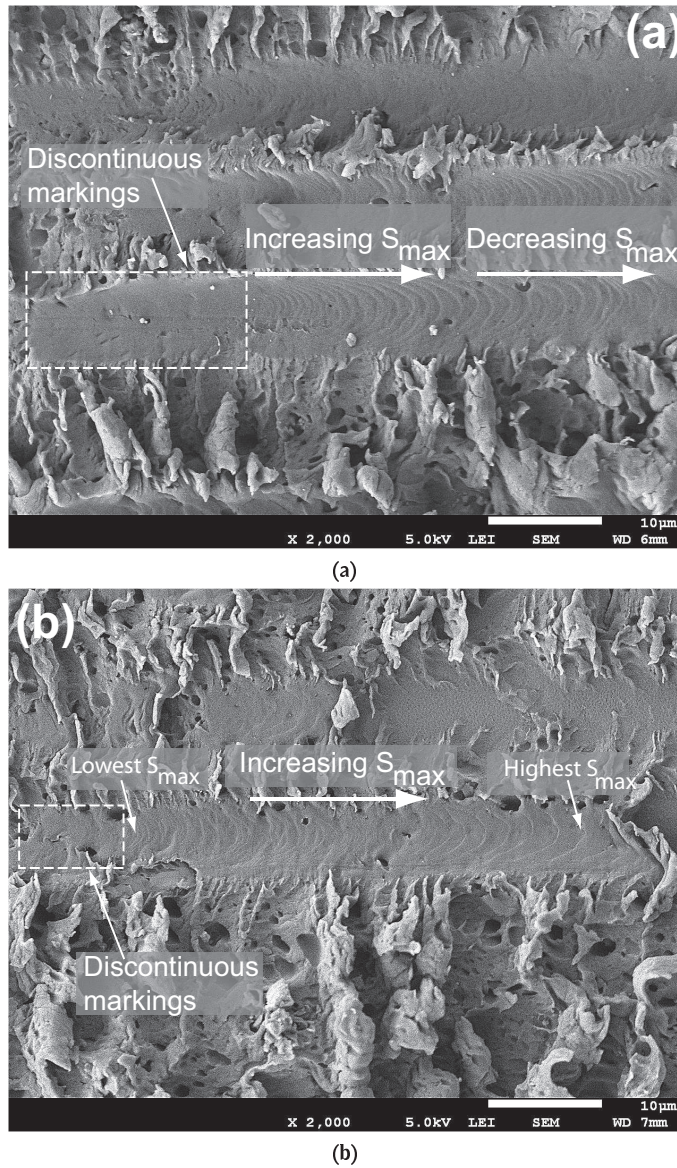
Figure 3.16: Delamination growth markings (striation) of Periodic LO–HI–LO load sequence: a. Long Period. b. Short Period

3.3.5   Delamination Prediction Aspects

Delamination growth at the interfaces in *GLARE* under *VA* loading is independent of interaction effects, which enables the use of *CA* delamination
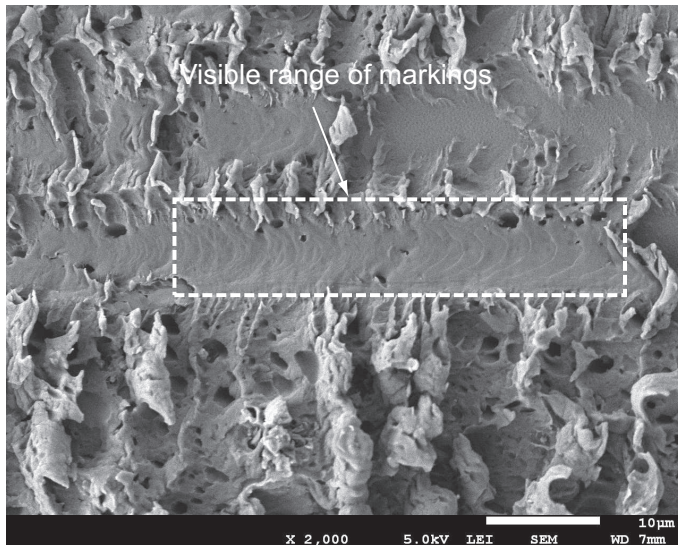
Figure 3.17: Discontinuity observed in Delamination markings (striation).

growth prediction as formulated by Alderliesten et al. [15] for prediction under *VA* loading. However, for *ARALL* and *FMLs* with similar interface characteristics, further investigation is required to formulate the conclusions about the potential interaction effects.

In *FMLs* the fatigue delamination is always localized around the crack and is coupled with the crack growth in metal layers. In case of *ARALL*, as reported by Marissen, if on one hand the *OL* increases the delamination growth rate, but on the other hand, it decreases the crack growth rate (crack growth retardation). The crack growth retardation subsides the increase in the delamination growth rate. This can be seen in the fatigue crack growth predictions for *ARALL* and *GLARE*, under *OL* cases, when compared with the test data, presented in 6 and C.

3.4   Summary

The delamination growth behaviour in *GLARE* has been investigated with delamination experiments using different load sequences and load spectra. It has been observed in the block load sequence test that the average delamination growth rate is independent of the applied load sequence. In addition, with the applied measurement technique no influence on the growth rate could be observed related to the transition from one load level to other

level.

Full flight spectrum tests have been performed because the block load sequence tests might not be sufficiently accurate to capture interaction effects. Correlation of the observed growth with linear damage accumulation prediction clearly showed that interaction effects under mode II delamination growth in *FMLs* are absent.

The Rain-flow counting technique must be used to load spectra with intermediate small cycles in the large cycles to calculate the delamination growth rate. Predictions correlated very well with the test results for the flight spectrum as well as the programmed block loading spectra, after applying this technique.

ARALL and *GLARE* laminates have different delamination characteristics. Interaction effects were reported by Marissen in case of *ARALL*. On the other hand, *GLARE* specimens, when tested using similar load spectra, do not show any interaction effect. Further investigation on *ARALL* and *GLARE* showed that fibre-adhesive bonding, peel strength and multiple delamination paths have insignificant effect on delamination growth rate. However, typography of fibre can be a major reason to cause different delamination behaviour of *ARALL* as compared to *GLARE*.

While looking at the delaminated surfaces using *SEM*, no markings were observed at the fibre side, but at the resin/metal side striations (markings) due to delamination growth were observed. In case of block load sequences (LO-HI and HI-LO), no interaction effects were observed using the striations and their spacing. For the periodic load sequences striations were observed and their spacings could be related to the maximum applied stress S_{max}.

For the development of a crack growth prediction model for *FMLs* under *VA* loading this means that the delamination extension can be calculated based on cycle-by-cycle analysis excluding any interaction effect due to the load variations after applying rain flow counting.

References

[1] R. Marissen, Fatigue crack growth in arall - a hybrid aluminium-aramid composite material, Tech. rep., Delft University of Technology, Delft,LR-574 (1988).

[2] T. Takamatsu, T. Matsumura, N. Ogura, T. Shimokawa, Y. Kakuta, Fatigue crack growth properties of a glare3-5/4 fiber/metal laminate, Engineering Fracture Mechanics 63 (1999) 253–272.

[3] T. Takamatsu, T. Matsumura, N. Ogura, T. Shimokawa, Y. Kakuta, Evaluation of fatigue crack growth behaviour of glare3 fiber/metal laminates using compliance method, Engineering Fracture Mechanics 70 (2003) 2603–2616.

[4] Y. J. Guo, X. R. Wu, A theoretical model for predicting fatigue crack growth rates in fibre-reinforced metal laminates, Fatigue & Fracture of Engineering Materials and Structures 21 (1998) 1133–1145.

[5] Y. J. Guo, X. R. Wu, Bridging stress distribution in center-cracked fiber reinforced metal laminates: modelling and experiment, Engineering Fracture Mechanics 63 (1999) 147–163.

[6] R. C. Alderliesten, Analytical prediction model for fatigue crack propagation and delamination growth in glare, International Journal of Fatigue 29 (2007) 628–646.

[7] Y. J. Guo, X. R. Wu, A phenomenological model for predicting crack growth in fiber-reinforced metal laminates under constant-amplitude loading, Composite Science and Technology 59 (1999) 1825–1831.

[8] J. Schijve, F. J. Wiltink, V. J. W. Van Bodegom, Flight-simulation fatigue tests on notched specimens of fiber-metal laminates, Tech. Rep. Report No. LRV-10, Delft University of Technology, The Netherlands (1994).

[9] Y. J. Guo, X. R. Wu, Fatigue behaviour and life prediction of frml under ca and va loading, Fatigue & Fracture of Engineering Materials and Structures 25 (2002) 417–432.

[10] R. Marissen, Flight simulation behavior of arall, Engineering Fracture Mechanics 19 (1984) 261–277.

[11] M. Kawai, A. Hachinohe, Two stress level fatigue of unidirectional fml hybrid composites: Glare2,, International Journal of Fatigue 24 (2002) 567–580.

[12] H. M. Plokker, Crack closure in glare, Master's thesis, Delft University of Technology, The Netherlands (2005).

[13] H. J. M. Woerden, Variable amplitude fatigue of glare 3, Preliminary master thesis, Delft University of Technology, The Netherlands (1998).

[14] R. C. Alderliesten, H. J. M. Woerden, Load history effects during fatigue crack propagation in glare, in: M. Guillaume (Ed.), Fatigue of Aeronautical structures as an Engineering Challenge, Vol. I, 2003, pp. 509–530.

[15] R. C. Alderliesten, J. Schijve, S. van der Zwaag, Application of the energy release rate approach for delamination growth in glare, Engineering Fracture Mechanics 73 (2006) 697–709.

[16] A. Suiker, N. Fleck, Crack tunnelling and plane-strain delamination in layered solids., International Journal of Fracture 125 (2004) 1–20.

[17] A. C. Carg, Delamination - a damage mode in composite structures, Engineering Fracture Mechanics 29 (1988) 557–584.

[18] C. G. Gustafson, H. Masaki, Delamination fatigue crack growth in unidirectional graphite/epoxy laminates, Journal of Reinforced Plastics and Composites 6 (1987) 36–52.

[19] J. Schon, A model of fatigue delamination in composites, Composite Science and Technology 60 (2000) 553–558.

[20] Y. J. Guo, X. R. Wu, Z. L. Zhang, Characterization of delamination growth behaviour of hybrid bonded laminates, Fatigue & Fracture of Engineering Materials and Structures 20 (1997) 1699–1708.

[21] R. C. Alderliesten, Fatigue crack propagation and delamination growth in glare, Ph.D. thesis, Delft University of Technology, Delft (2005).

[22] C. D. Rans, R. C. Alderliesten, Formulating an effective strain energy release rate for a linear elastic fracture mechanics description of delamination growth, in: Proceedings of 17th International Conference on Composite Materials (ICCM-17), 2009.

[23] S. Mall, S. Johnson, R. A. Everett Jr., Cyclic debonding of adhesively bonded composite, in: K. L. Mittal (Ed.), Adhesive joints: Formation, Characteristics, and Testing, American Chemical Society,, Plenum Press, 1982, pp. 639–658.

[24] S. D. Downing, D. F. Socie, Simple rainflow counting algorithms, International Journal of Fatigue 4 (1) (1982) 31–40.

[25] I. Rychlik, A new definition of the rainflow cycle counting method, International Journal of Fatigue 9 (2) (1987) 119–121.

[26] ASTM, Standard practices for cycle counting in fatigue analysis, Tech. Rep. ASTM E 1049-85, ASTM International (2005).

[27] M. L. C. E. Verbruggen, Aramid reinforced aluminium laminates:arall adhesion problems and environmetnal effects: Vol. a : Adhesion and delamination, Tech. Rep. LR-503, Delft University of Technology, Delft, The Netherlands (November 1986).

[28] G. H. J. J. Roebroeks, Constant amplitude fatigue of arall-2 laminates, Tech. Rep. LR-539, Delft University of Technology, Delft, The Nether-lands (October 1987).

[29] G. H. J. J. Roebroeks, Towards glare, the development of a fatigue insensitive and damage tolerant aircraft material, Ph.D. thesis, Delft University of Technology, Delft (1991).

[30] D. Purslow, Matrix fractography of fibre reinforced epoxy composites, Composites 17 (1986) 289–303.

[31] G. H. J. J. Roebroeks, Observation on cyclic delamination in arall under fatigue loading, Tech. Rep. LR-496, Delft University of Technology, Department of Aerospace Engineering, (1986).

Chapter 4

DELAMINATION SHAPE

When you are describing a shape, or sound, or tint:
Don't state the matter plainly, but put it in a hint;
And learn to look at all things with a sort of mental squint

Lewis Carroll
(1832-1898)

This chapter presents a study on the influence that load variations have on delamination shapes in Fibre Metal Laminates. Previously fatigue tested centre-crack tension specimens have been chemically etched to obtain the final delamination shapes. In addition, fatigue crack growth tests on similar specimens have been performed to investigate the formation of delamination shapes. For this purpose, digital image correlation has been used as strain measurement technique to record the delamination shapes in-situ testing. An explanation is put-forward in order to understand the effects of variable amplitude loading on the formation of delamination shapes. A transition in delamination shapes was observed, but evaluating this observation using an analytical fatigue crack growth prediction model including the observed change in delamination shapes revealed no significant effect on subsequent crack growth.
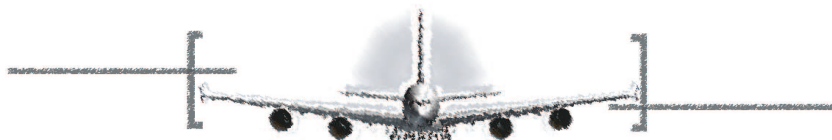
In principle, the delamination growth and fatigue crack growth are balanced and coupled phenomena that significantly influence each other. During constant amplitude *(CA)* loading, this balance between the delamination and crack growth is
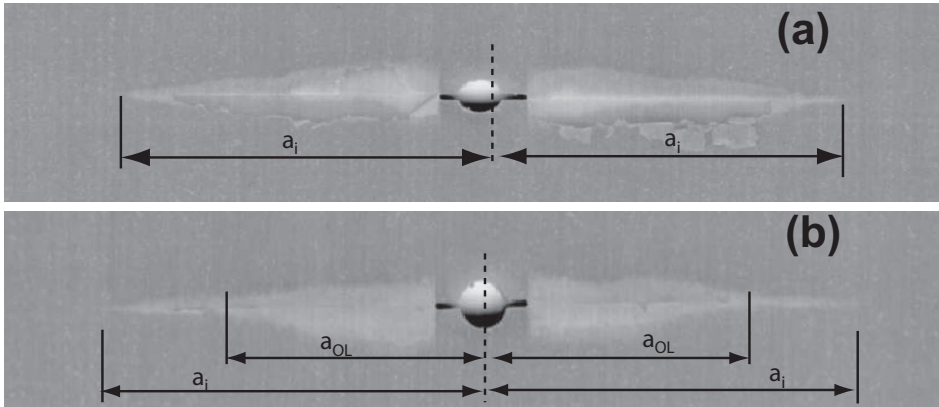
Figure 4.1: Delamination between outer aluminium layer and adjacent fibre/adhesive layer for Glare 3-3/2-0.3 loaded with S_{appl} = 6 - 120 MPa, in case no overload is applied (a) and in case an overload of Smax = 200 MPa is applied (b) [2]

achieved after a certain crack extension . An illustration of the geometry of a delamination in the wake of a crack is given in figure 2.3.

To understand this balance during variable amplitude *(VA)* loading, one must understand the behaviour of crack growth and delamination growth under *VA* loading independently. For the fatigue crack configuration illustrated in Figure 2.3, interaction effects due to overloads have already been reported [1]. On the other hand, interaction effects were not observed when looking only at delamination growth, as discussed in Chapter 3.

So, hypothetically, both these observations come together for the configuration in Figure 2.3 under *VA* loading. For example, Alderliesten and Woerden [2] reported tests with overload sequences. They observed a change in delamination shape after the application of the overload (see Figure 4.1). The observed kink in the delamination shape appeared to depend on the overload ratio. They attributed the transition in delamination shape to a process similar to post-stretching induced by the overload, as discussed in section 2.4.

However, based on the current understanding of the mechanisms, the author believes that even if post-stretching may contribute to the delamination shape transition, it may not be the dominating mechanism. In fact, crack tip plasticity induced by the overload may have a greater impact on the formation of the delamination than local stress reversal related to the same plasticity. This can be explained with the illustration given in Figure 4.2. After the application of an overload, the crack growth in the metal layers retards for a certain number of cycles, known as delay cycles (N_D), as illustrated
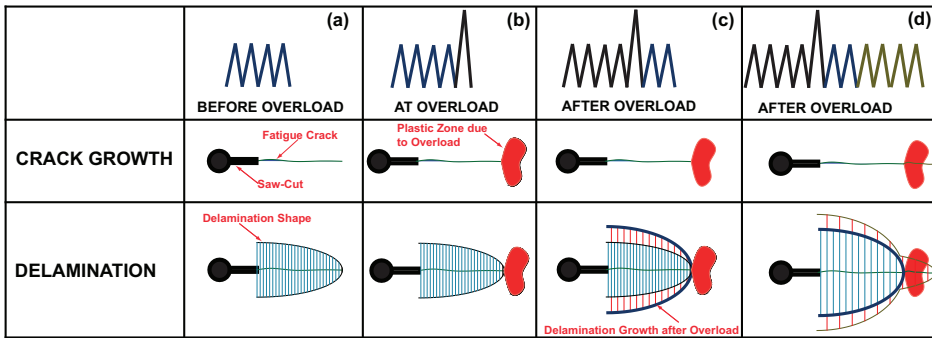
Figure 4.2: Illustration of delamination extension after application of OL

in figure 4.2-b. Although the crack retards, the delamination present in the wake of the crack continues growing perpendicular to the crack as result of the continuing cyclic loading (figure 4.2-c). After about N_D cycles, the crack continues propagating at its original rate, inducing new delaminations to be formed in the wake of the subsequent crack length increments Δa. This is illustrated in figure 4.2-d. The shape of the new delamination may appear different from the delamination shape before the application of overload, but may have been formed under the same conditions.

To verify this explanation, several aspects had to be addressed prior to the current work. The first aspect is covered by another study performed by the author [3]. In that experimental study, crack tip plasticity and crack growth retardation were observed to be similar to monolithic metals, but limited in magnitude due to fibre bridging. The second aspect relates to the response of delamination growth itself to *VA* loading. This work has been discussed in chapter 3.

To correlate the work on crack tip plasticity and delamination growth inter-actions, this chapter focuses on centre-crack tension *(CCT)* specimen to com-bine the mechanisms of crack growth and delamination growth while acting together and influencing each other. In this specimen geometry, the crack growth can be easily monitored in the outer metal layers in situ-testing. To obtain information about the delaminations, both Digital Image Correla-tion *(DIC)* and chemical etching techniques have been exploited in-situ and after testing. In earlier studies [4] only the delaminations obtained after chemical etching were reported, but the specific questions in the current study require the observation of the shape and extension of the delamina-tions in-situ. Therefore, *DIC* being a rapid, effective, non-destructive and non-contact strain measurement technique was applied to measure the de-lamination shapes. The principle of visualising the subsurface delaminations by this surface measurement technique are explained in this chapter.

To determine the effect of overloads on the subsequent formation of delaminations, a distinction must be made between the case without and the case with the application of the overload. For this reason, an analytical prediction model for constant amplitude fatigue in *FMLs*, presented in chapter 6, has been used to evaluate the crack and delamination growth for the cases tested. In addition, the correlation between the experiments and the predictions enables to determine the effect of overload application on the bridging stress directly, and to describe the effect on the stress intensity factor driving crack growth.

4.1 EXPERIMENTAL PROGRAM

To investigate the delamination shape, it was necessary to observe its development in-situ testing and to capture the final shape after finishing the test. Two sets of *CCT* specimens were studied; The first set consisted of postmortem investigation of specimens from a previous study [1, 3], while the second set consisted of new specimens tested with in-situ delamination observation using *DIC*.

4.1.1 Test specimens

The specimen for postmortem investigation were *CCT* specimens illustrated in figure 4.3. These specimens had 4 metal layers with 0.3 mm thickness and 3 composite cross-ply fibre layers with a nominal thickness of 0.266 mm (i.e., Glare3-4/3-0.3). These specimens had three parallel starter notches of approximately 5 mm, made by drilling 3 mm diameter holes and subsequent cutting both sides.

The newly tested specimens were *CCT* specimens shown in Figure D.1. These specimens were manufactured with 5 metal layers of 0.4 mm thickness and 4 composite cross-ply fibre layers with a nominal thickness of 0.266 mm (i.e., Glare3-5/4-0.4). The starter notches were made by drilling a hole of 3 mm diameter with two saw cuts oriented perpendicular to the loading direction. The length of the starter notch ($2a_0$) was approximately 5 mm.

4.1.2 Test Matrix

The postmortem specimens had been tested and reported by Plokker et. al. These tests were performed using a *CA* baseline cycle with S_{max}=120 MPa and R = 0.1. A single overload of S_{OL}=175 MPa was applied at crack length
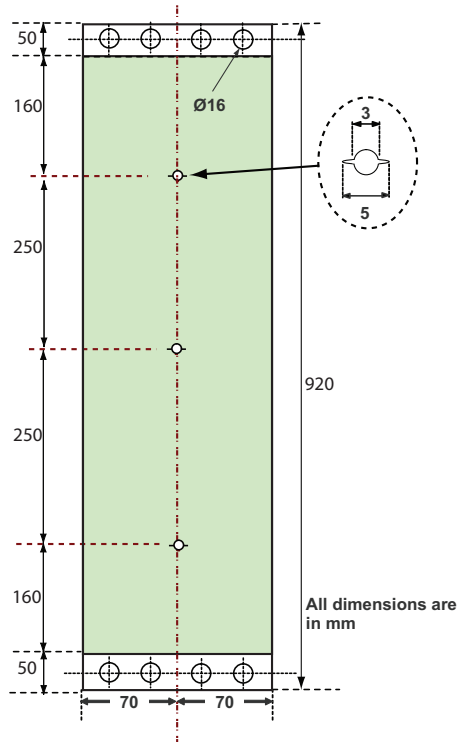
Figure 4.3: Postmortem crack growth specimen geometry [3]

of a_{OL}=9.5 mm. A multiple block overload spectrum consisted of 1000 cycles of 160 MPa was applied at crack length a_{TR}=6.92. For the block load tests, two block load sequences i.e., LO-HI and HI-LO were used. Both of the block loads had the same stress levels i.e., $S_{max,LO}$ = 100 MPa and $S_{max,HI}$ = 140 MPa. In case of LO-HI sequence, the transition crack length was a_{TR}=6.9 mm and for HI-LO a_{TR}=12.7 mm.

The new specimens have been tested using a *CA* baseline spectrum with a maximum stress S_{max} = 100 MPa and a stress ratio R = 0.1. The single overload spectrum has an overload S_{OL} = 145 MPa at a_{OL}=10 mm. The multiple overload spectrum has three overloads i.e. S_{OL1} = 145 MPa; S_{OL2} = 130 MPa and S_{OL3} = 115 MPa at a_{OL}=9, 12 and 15 mm respectively. Block load spectra are constituted of two stress levels $S_{max,LO}$ = 100 MPa and $S_{max,HI}$ = 140 MPa.

Detail of both test programs are given in table 4.1 and D.1. Tables D.2 and D.3 were part of the same experimental program but will be discussed
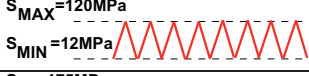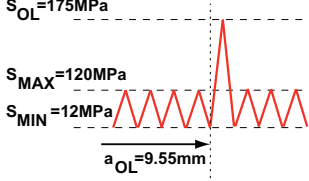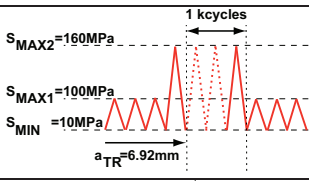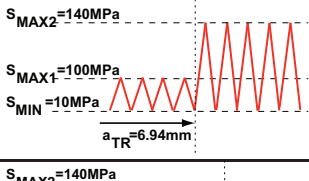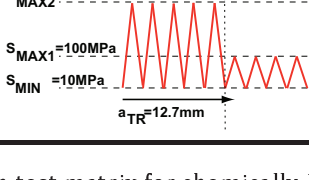
	Load variation	CA cycles		Load variation
		Maximum stress [MPa]	Stress ratio	[MPa]
A1	Constant amplitude — $S_{MAX}=120$ MPa, $S_{MIN}=12$ MPa	120	0.1	
A2	Single overload — $S_{OL}=175$ MPa, $S_{MAX}=120$ MPa, $S_{MIN}=12$ MPa, $a_{OL}=9.55$ mm	120	0.1	175
A3	Multiple block overload — 1 kcycles, $S_{MAX2}=160$ MPa, $S_{MAX1}=100$ MPa, $S_{MIN}=10$ MPa, $a_{TR}=6.92$ mm	100	0.1	160
A4	Block loading-LO-HI — $S_{MAX2}=140$ MPa, $S_{MAX1}=100$ MPa, $S_{MIN}=10$ MPa, $a_{TR}=6.94$ mm	100	0.1	140
A5	Block loading-HI-LO — $S_{MAX2}=140$ MPa, $S_{MAX1}=100$ MPa, $S_{MIN}=10$ MPa, $a_{TR}=12.7$ mm	140	0.1	100

Table 4.1: Fatigue crack growth test matrix for chemically Etched (Postmortem) specimen

in chapter 5

4.1.3   Test Equipment & Procedure

The postmortem specimens were already/previously tested at a 6 metric tons servo-hydraulic testing system and measurements were made using a potential drop measurement technique. Details about the second set of specimens, testing procedures and equipments are given in Plokker et. al. [1, 3].

The new specimens were tested in lab air at room temperature in a clo-

sed loop mechanical and computer controlled servo-hydraulic testing system with a load capacity of 25 metric tons. The test frequency was 10Hz. The test setup is shown in figure D.2.

4.1.4   Measurement Technique – Digital Image Correlation

DIC is a fully non-contact and non-destructive image evaluation technique used to track the surface displacements of deforming materials. It is based on the comparison of two images acquired using a *CCD* camera at different defined stages, one before the deformation (known as reference image) and the other one after the deformation (known as deformed image) [5, 6]. The displacement of applied grid points is computed from the positions in each of the two images. It has been widely used to examine the deformations of engineering materials including monolithic metals, *FMLs* and adhesives [7, 8]. Comparing with other strain and delamination measurement techniques like C-scan [9] and fibre-bragged grating sensors [9], *DIC* is considered to be one of the most versatile and suitable non destructive and in-situ technique for detailed full-field strain measurements in *FMLs*.

For the current research, an in-house developed *DIC* tool has been used. This tool is programmed in Matlab in such a generic way that it can be used independent of the test type, the amount of images per test or the size and shape of the grid as long as only in-plane deformations are present. This *DIC* tool is described in detail in [6, 7].

The principle of observing subsurface delamination shapes by recording surface deformations is based on the strain difference between delaminated and non-delaminated areas. The delaminated metal layers do not carry any load as most of this load is transferred to the fibre layers, schematically shown in figure 2.3. This 'zero strain' (or in other words delaminated) region can easily be detected with *DIC*, as illustrated by the dark region in Figure 4.4-(a). Details about the validation of this technique for delamination shape measurements can be found in [8, 10].

Delamination shapes acquired using *DIC* at different crack lengths are shown in figure 4.4-(b). The final delamination shape in the specimen observed after chemical etching the surface is added to the same figure. An excellent correlation between delamination shape observed using *DIC* and after chemical etching has been obtained.
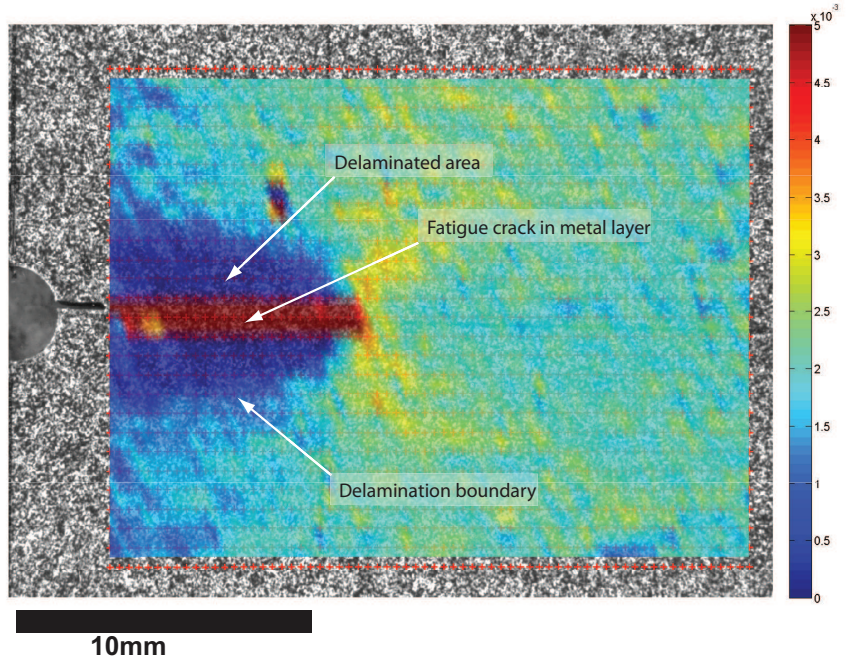
(a)
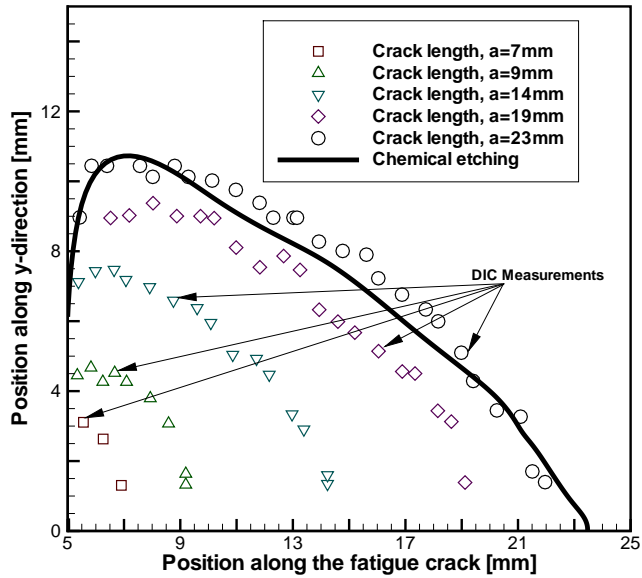
(b)

Figure 4.4: a. Fatigue delamination shape acquired using DIC in GLARE 5/4 – 0.4 with S_{max} = 100 MPa, R = 0.1, a = 19 mm , b. Fatigue delamination growth measured using DIC and comparison with chemical etching. FML 2-2/1-0.4 2024-T3/M30-carbon, S_{max} = 150 MPa, R = 0.05 [8]

(a)

(b)

(c)

(d)

(e)
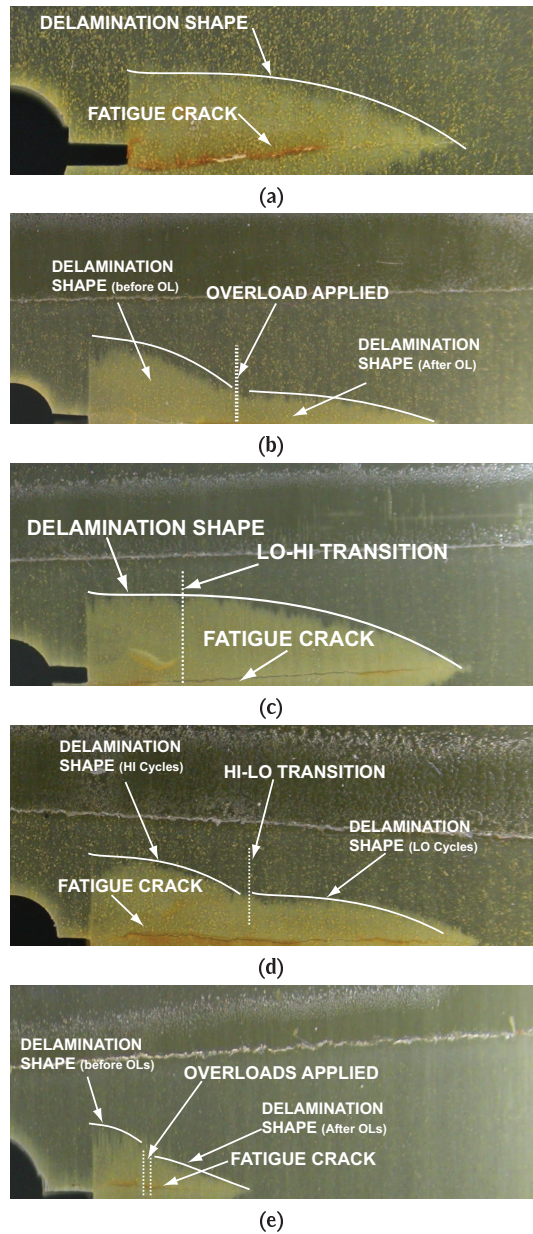
Figure 4.5: Delamination shape in postmortem specimens: a Constant amplitude, b Single overload, c Block load (LO-HI), d Block load (HI-LO), e Block of loads

4.2   RESULTS & DISCUSSION

The delamination shapes observed after etching the outer metallic layers as well as those observed in-situ fatigue testing are discussed here. In addition, delamination shapes predicted using the *FMLs* fatigue crack growth prediction *VA* loading model, detailed in section 6.2, are compared with the observed shapes. The effect of the change in the delamination shape in the fatigue crack growth parameters and fatigue crack growth prediction is also discussed in detail.

4.2.1   Observed Delamination Shape

The observed delamination shapes in both sets of specimens are discussed in this section. A detailed study is presented comparing observed and predicted delamination shapes.

Chemical Etching

Figure 4.5 shows the delamination shapes observed in post-mortem specimens. It is observed that after a change in the load sequence (i.e., overload or HI-LO), the delamination shape changes from a semi-elliptical shape to a shape containing a kink at the location where the load sequence is changed, as shown in figures 4.5-(b),(d), and (e). The delamination shape of the *CA* test (figure 4.5-(a)) is given to highlight the effect of *VA* load sequences. Figure 4.5-(b) shows the delamination shape, after the application of a single overload. The kink and change is visible in figure 4.5-(b). In case of block load sequences, no change was observed for LO-HI sequence (Figure 4.5-(c)). For HI-LO and block of overloads, a change in shape has been observed after the load transition (Figures 4.5-(d) and 4.5-(e)).

Figure 4.6 shows the comparison of final delamination shape predicted using the *VA* Yield zone mode for *FMLs* and measured after chemical etching, for *CA* and single overload cases. The details about the prediction model can be looked in section 6.2. The prediction model seems to underpredict the delamination shape in both the cases.

Digital Image Correlation-DIC (In-situ fatigue test)

Figure 4.7 shows the *DIC* results of the second set of tested specimens for different load cases. A comparison between single overload and *CA* loading results is shown in Figure 4.7-(a).
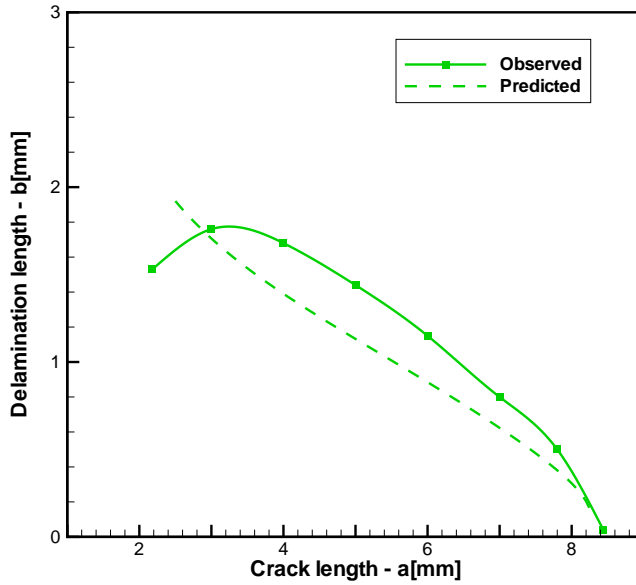
(a)
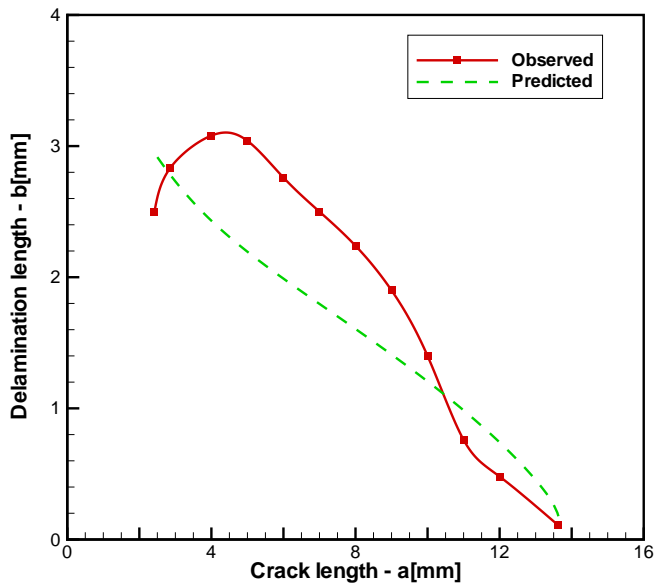
(b)

Figure 4.6: Comparison of Delamination shape, predicted and actual: a Constant Amplitude case , b Single overload case.
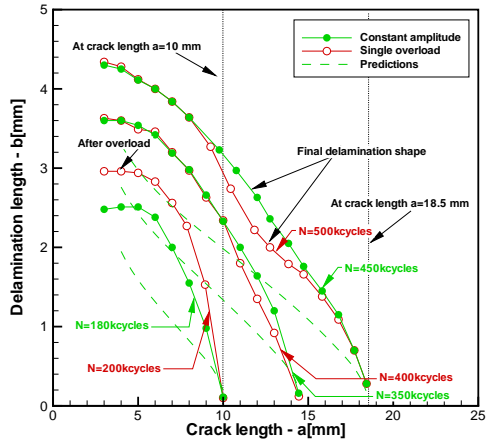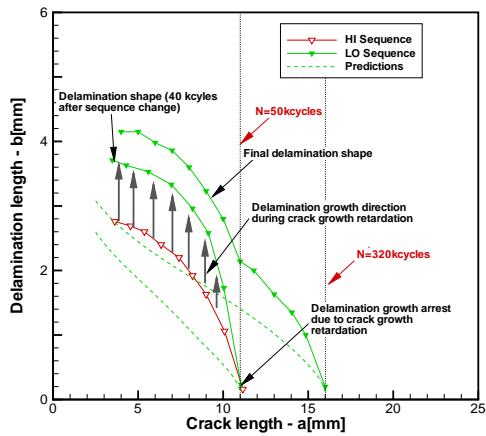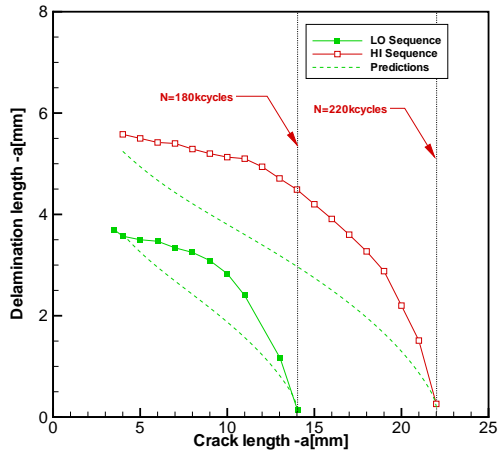
Figure 4.7: Postmortem specimens delamination growth tests results: a. Constant amplitude and single overload, b. Block load (HI-LO), c. Block load (LO-HI

After application of the overload, the crack growth was retarded for 10 kcycles. Although the crack growth was retarded, the delamination present in the wake of the crack remained growing perpendicular to the crack due to the continuing cyclic loading. But as soon as the crack continued to propagate, a kink can be observed between the new and the already present delamination shape.

Similarly, for the HI-LO block load sequence, a change in the delamination shape was observed. Due to the large number of higher stress cycles the observed number of delay cycles was 40 kcycles. After the change of load sequence, delamination extension was observed only in the loading direction. A kink was observed in the final delamination shape.

Figure 4.7-(c) shows the delamination shape of the LO-HI block load sequence. No change or kink was observed in the delamination shape, because of the absence of any interaction effect that can cause crack growth retardation.

The change in the delamination shape for the single and HI-LO block load sequence was due to the application of overloads or because of crack-tip plasticity that retarded the crack growth. During the *CA* baseline loading (figure 4.2-(a)), cracks started to grow in the metallic layers accompanied with the delaminations at the metal-fibre interface around the crack. After application of the overload, the crack growth was retarded that stopped the delamination growth (in the wake of propagating crack, perpendicular to the loading direction). However, the delamination continued to grow parallel to the loading direction, because delamination growth has been observed to be independent of any interaction effects (3), as shown in figure 4.2-(c). The delamination started to grow perpendicular to the loading direction, as soon as the crack-tip was out of the retardation region. A kink was observed between the delamination shapes before and after the location of overload, as illustrated in figure 4.2-(d). Similarly for block loads, when the load was changed from HI to LO, crack growth retardation occurred and affected the delamination shape.

Figure 4.8 shows the comparison of the delamination shape and its extension predicted with and without considering crack-tip plasticity due to an overload. The prediction without considering the crack growth retardation (*CA* represented by thin lines) did not show any change in the delamination shape. While the predictions considering crack growth retardation showed a change in the delamination shape after the application of the overload. However, it is also shown in the same figure that the final delamination shapes predicted with and without considering crack growth retardation are almost identical.

One major observation about the delamination shape predictions is that the model underpredicts the delamination shape (shown in Figures 4.6 and 4.7).
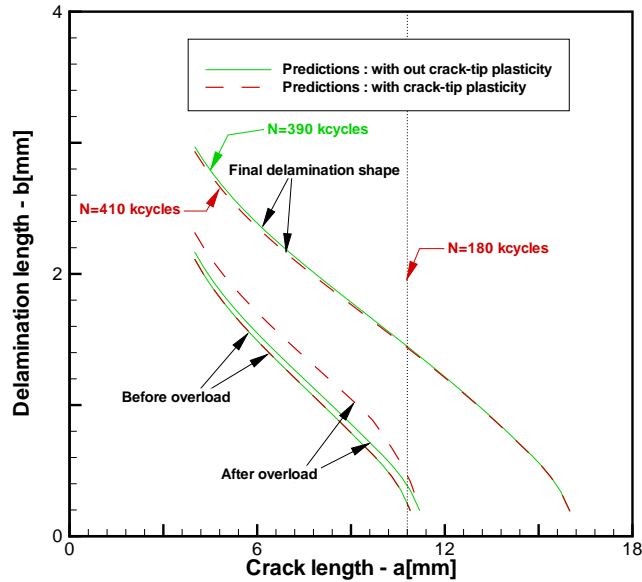
Figure 4.8: Delamination growth test results of single overload case compared with the predictions.

This can be attributed to the fact that the interface adjacent to the outer metallic layer faces higher cyclic shear stresses, because the load is transferred through a single metal-fibre interface, while the middle layers distribute the load through two interfaces. The predicted results come from an imposed average calculation of the delamination that occurs at each metal-fibre interface. The extra load transfer occurring at the outer interfaces increase the mode II delamination which results in larger delamination compared to the predicted one. The prediction model is based on the average behaviour of all the interfaces and excludes any through the thickness variation, but the delamination occurring at the middle layers is smaller that the one at the outer layers. Rodi et. al [11], observed a difference in the predicted and observed final delamination shapes in most of the cases.

It can be seen in figure 4.8 that the delamination propagates only parallel to the loading direction when the crack growth is retarded. Without including crack growth retardation, the delamination would have been growing in both the directions. Following from the discussion above, crack growth retardation indeed seems to be the major phenomenon causing the kink in the delamination shape. However, as shown in figure 4.8, a mismatch is observed between the delamination shapes predicted using crack growth retardation and the measured shapes at the point where the test is stopped.

The mismatch may imply that the currently proposed crack growth retardation theory alone is insufficient to describe the change in delamination. Thus, there may be still some effect of local pre-stretching as proposed by Alderliesten and Woerden [2].

The question arises whether this difference in delamination shape and area has an effect on the subsequent crack growth and whether it needs to be considered during fatigue crack growth prediction. These questions are addressed hereafter.

4.2.2   Effect of Delamination Shape

The modified Wheeler model (will be discussed in details in 6.2), being a crack-tip plasticity based retardation model, is used to predict the fatigue crack growth in *FMLs*. To investigate the effect of the delamination shape change on fatigue crack growth, the delamination shape acquired from the single overload test (Figure 4.6-(a)) after chemically etching the specimen, is used as an input to compute the fibre bridging stress as well as stress intensity factor at the crack tip, K_{tip}, the stress intensity factor describing fibre bridging, K_{br}, and far-field stress intensity factor K_{∞} [12]. In general, K_{tip} is computed as the difference of between far-field and fibre bridging [12], and it is used to calculate fatigue crack growth in *FMLs*. For this investigation, two delamination shapes were studied for the case where the crack continues propagating from the length where the test was terminated:

1. Delamination shape predicted with the model including plasticity

2. Delamination shape measured at the end of the test.

For the predicted delamination shape, a typical bridging stress profile was computed that is approximately constant along the crack, except for the area near the crack tip. For the measured delamination, a shape is calculated that shows significant variation along the crack. Both profiles are shown in figure 4.9-(a), and figure 4.10-(a).

It is observed from the measured shape that after application of the overload, a larger delamination is present that corresponds to low bridging stresses. These low bridging stresses will result in subsequent slow delamination growth, while the area having high bridging stresses will grow at higher rate. This means that in the subsequent cycles, the delamination shape will form a shape closer to delamination shape predicted with the model including plasticity. As a result, the stress intensity factor K_{tip} calculated with the model originally underestimates the value that is expected based on the measured delamination shape. However, as illustrated in Figure 4.9-(b) and 4.10-(b),
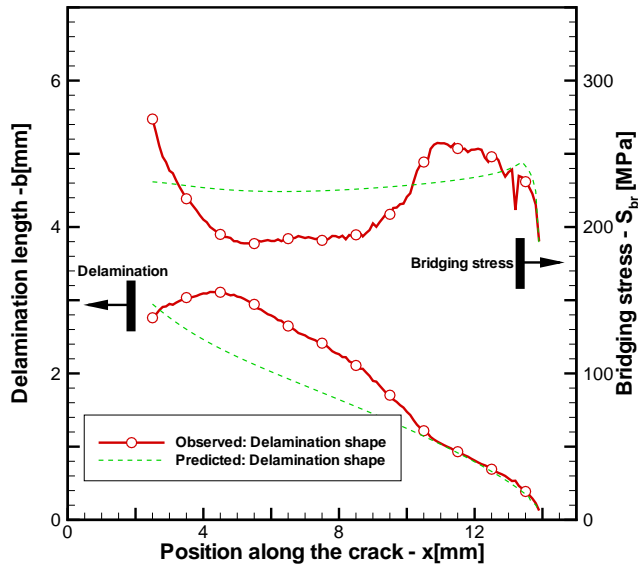
(a)
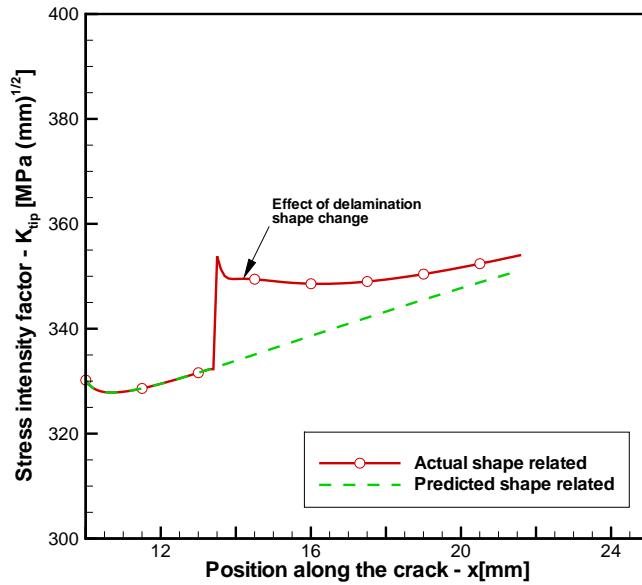
(b)

Figure 4.9: Effect of delamination shape changes, in postmortem specimen, on: (a) The bridging stress,(b) Stress intensity factors
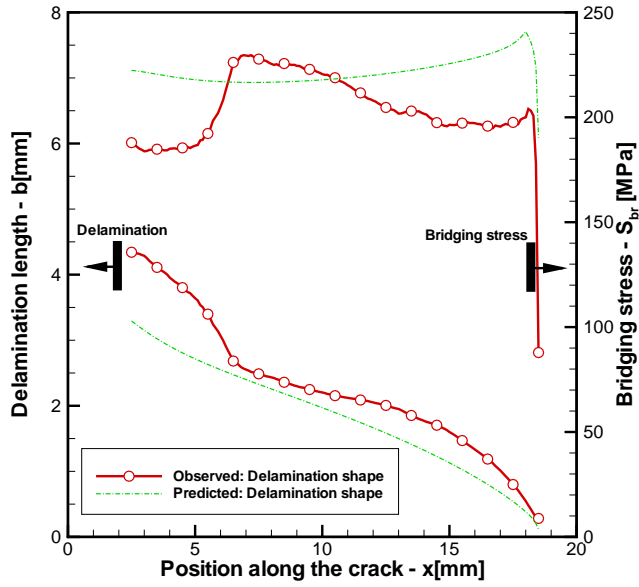
(a)
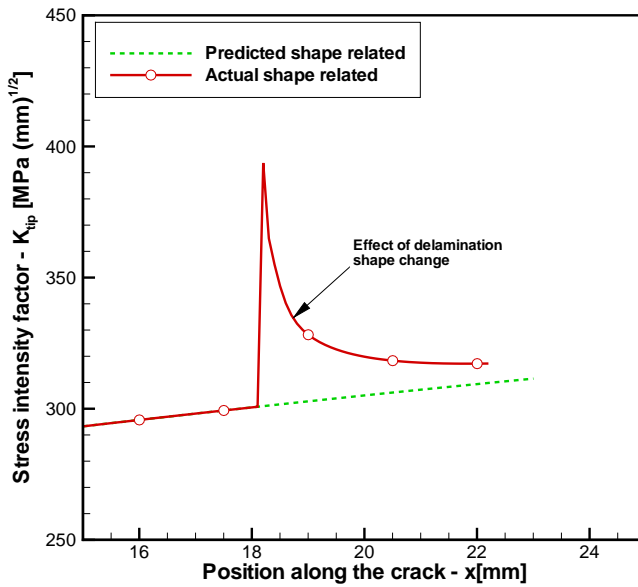
(b)

Figure 4.10: Effect of delamination shape changes, in DIC specimen, on: (a) The bridging stress, (b) Stress intensity factors

K_{tip} decreases towards the value calculated with the model. This highlights the fact that a change in the delamination shape has insignificant effect on the parameter governing fatigue crack growth in *FMLs*. This observation is validated when the fatigue crack growth predictions are correlated with the test data (discussed in the next section). This was also observed for the specimen with delamination shapes measured using *DIC*, as shown in figure 4.10.

4.3   Summary

The load variations slightly change the delamination shape. This change in delamination shape is predominantly related to the crack growth retardation in metal layers after application of overload. However, this cause is insufficient to completely describe the transition of the delamination after the application of an overload. If in addition, the post-stretching mechanism locally near the crack tip is considered, the transition can be fully understood.

The effect of this transition in delamination shape on subsequent fatigue crack growth has been related to the change in stress intensity, which factor is used in the fatigue crack growth prediction model for *FMLs*. This investigation has evidently shown that the transition in delamination shape has no significant effect on subsequent the fatigue crack growth.

In other words, for predicting the fatigue crack growth after an overload accurately, it will be sufficient to attribute the transition of delamination shape solely to the crack retardation, thus ignoring post-stretching.

References

[1] H. M. Plokker, R. C. Alderliesten, R. Benedictus, Crack closure in fiber metal laminates, Fatigue & Fracture of Engineering Materials & Structures 30 (7) (2007) 608–620.

[2] R. C. Alderliesten, H. J. M. Woerden, Load history effects during fatigue crack propagation in glare, in: M. Guillaume (Ed.), Fatigue of Aeronautical structures as an Engineering Challenge, Vol. I, 2003, pp. 509–530.

[3] H. M. Plokker, S. U. Khan, R. C. Alderliesten, R. Benedictus, Fatigue crack growth in fibre metal laminates under selective variable-

amplitude loading, Fatigue Fracture Engineering Materials & Structures 32 (2009) 233–248.

[4] H. M. Plokker, Crack closure in glare (2005).

[5] M. A. Sutton, M. S. R., J. D. Helm, Y. D. Chao, Advances in two-dimensional and three-dimensional computer vision., Photomechanics, Topics Applied Physics 77 (2000) 323–372.

[6] D. Corr, M. Accardi, L. Graham-Brady, S. Shah, Digital image correlation analysis of interfacial debonding properties and fracture behavior in concrete, Engineering Fracture Mechanics 74 (2007) 109–121.

[7] H. J. K. Lemmen, R. C. Alderliesten, R. Benedictus, J. C. J. Hofstede, R. Rodi, The power of digital image correlation for detailed elastic-plastic strain measurements, in: M. K. Nikolinakou, G. Tsekouras, V. Gekas, D. G. Pavlou (Eds.), New aspects of engineering mechanics, strucutres and enginereing geology, WSEAS, WSEAS Press, Athens, 2008, pp. 73–89.

[8] R. Rodi, R. Alderliesten, R. Benedictus, An experimental approach to investigate detailed failure mechanisms in fibre metal laminates, in: M. J. Bos (Ed.), ICAF 2009, Bridging the Gap between Theory and Operational Practice - Proceedings of the 25th Symposium of the International Committee on Aeronautical Fatigue, Rotterdam, The Netherlands,27–29 May 2009, Springer Netherlands, 2009, pp. 493–512.

[9] T. S. P. Austin, M. M. Singh, P. J. Gregson, P. M. Powell, Characterisation of fatigue crack growth and related damage mechanisms in frp-metal hybrid laminates, Composites Science and Technology 68 (6) (2008) 1399 – 1412.

[10] R. Rodi, G. Campoli, R. C. Alderliesten, R. Benedictus, Characterization of the crack tip behavior in fibre metal laminates by means of digital image correlation, in: 50th AIAA/ASME/ASCE/AHS/ASC Structures, Structural Dynamics, and Materials Conference, Palm Springs, CA., no. AIAA-2009-2586 in AIAA, 2009, pp. 1–18.

[11] R. Rodi, R. C. Alderliesten, R. Benedictus, The effect of external stiffeners on the fatigue crack growth in fibre metal laminates, in: A. S. L. Lazzeri (Ed.), ICAF 2007- Durability and damage tolerance of aircraft structures: Metal Vs. Composites-24th Symposium of the International Committee on Aeronautical Fatigue, Naples, Italy, 2007, pp. 858–875.

[12] R. C. Alderliesten, Fatigue crack propagation and delamination growth in glare, Ph.D. thesis, Delft University of Technology, Delft (2005).

Chapter 5

CRACK-TIP PLASTICITY

It doesn't matter how beautiful your theory is, it doesn't matter how smart you are. If it doesn't agree with experiment, it's wrong.

Richard Feynman
(1918-1988)

This chapter presents a quantitative study of crack-tip plasticity under selective variable amplitude (VA) fatigue loading. Centre crack tension specimens made from three types of materials (i.e., monolithic aluminium, laminated aluminium sheets and fibre metal laminates (FMLs)) were used for this research. Plastic zone sizes induced by overloads were calculated using Irwin crack-tip plasticity relation and compared with the ones measured using Digital Image Correlation for the three materials. A better correlation is observed for FMLs in comparison with other two materials between the measured and calculated plastic zone size. From the comparison it is deduced that the Irwin relation combined with a Paris crack growth relation can be utilized in FMLs for predicting fatigue crack growth under VA loading. This hypothesis has been validated by comparing the test results with the predictions using the extended fatigue crack growth prediction model incorporating both relations.

Fatigue crack growth is commonly predicted using stress intensity factors that are based on the linear elastic fracture mechanics principles. Although the linear elastic representation

is convenient from an engineering perspective, it is common knowledge that small scale plasticity occurs at the crack tip, which influences the crack propagation. This is particularly true for *VA* loading, where interaction phenomena are observed for crack tip plasticity related to different load cycles.

To develop a crack growth prediction method for *FMLs* based on the similar principles as currently applied for monolithic metals, one should not only understand the influence of delamination growth, as discussed the previous two chapters. One should also investigate to what extent the small scale plasticity and related phenomena in the thin sheets of *FMLs* are similar to monolithic aluminium.
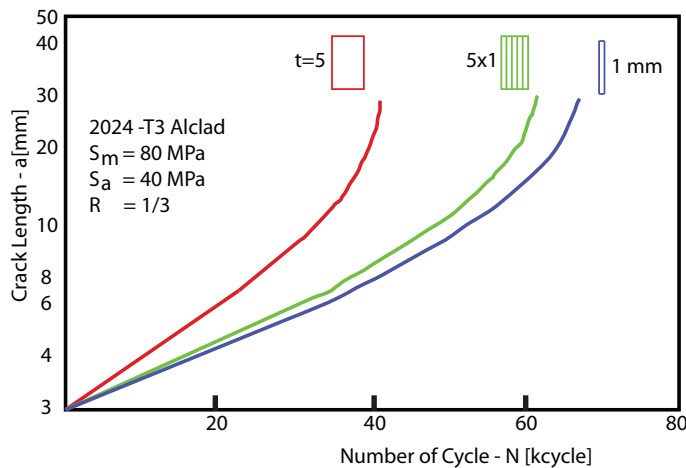
Figure 5.1: Crack growth curves in solid and laminated panels with central crack [1]

Obviously the first question to address is whether the general appearance of the fracture surface is similar for monolithic aluminium and *FMLs*. Typical features as shear lip formation and the transition from a mode I to a mixed mode I/III, often denoted as crack slanting have to be evaluated. In addition, the application of *VA* loading requires a more detailed investigation specifically about the crack tip plasticity in addition to the earlier mentioned delamination phenomena in chapters 3 and 4.

Schijve et al. [1] have tested and compared monolithic metals with the laminated sheet specimens for part-through and through cracks. According to them, the laminates have 1.5 times slower crack growth than solid materials (as shown in figure 5.1). In addition, it was concluded in their investigation that, the laminated material implied some extra weight for the adhesive, which made the improvement rather small and the transition from tensile mode to shear mode suggested that the five sheets of the laminated material

didn't behave like they are fully separated sheets.

However, even more straightforward it may seem to determine whether the amount of small scale plasticity, which in Linear Elastic Fracture Mechanics *(LEFM)* is related to the Stress Intensity Factor *(SIF)* is still valid for the thin sheets in *FMLs*. Here, is it commonly known that in thick monolithic sheets the plastic zone varies over the thickness. This variation is attributed to the transition of stress state from the surface (plane stress) towards the middle of the sheet (plane strain). It may be expected that the thin sheets used in *FMLs* exhibit smaller plastic zone sizes through-thickness that correlate to a plane stress state.
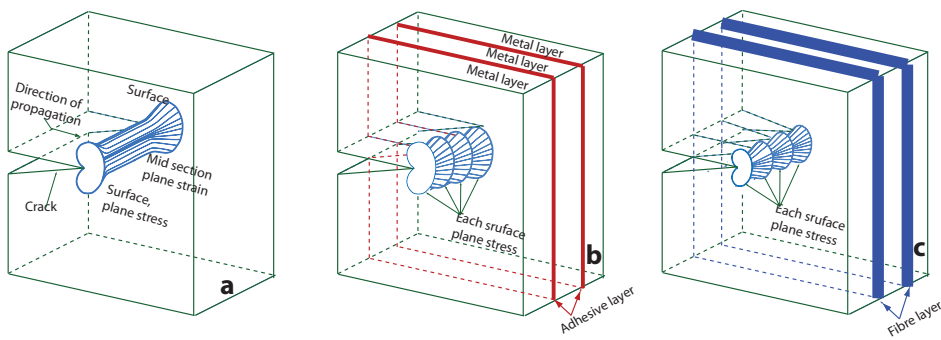
Figure 5.2: Plane stress/strain formation in: a. Monolithic metal, b. Metal laminate (without fibres), c. *FMLs*

Plastic zone sizes under *VA* loading are used as a comparison criterion for the three types of materials i.e., monolithic metals, metal laminates (without fibres) and fibre metal laminates (with fibres). Digital Image Correlation *(DIC)* is used to quantitatively compare the plastic zone sizes these materials. *DIC* is explained in detail in section 4.1.4.

Figure 5.2-a illustrates a typical plastic zone with plane stress (at surface) and plane strain (through the thickness). It is also illustrated in figure 5.2-b the hypothetical effect of reducing the thickness (Metal laminate) and figure 5.2-c shows the hypothetical effect of further adding the fibre layers to the metal laminate. It is illustrated in figures 5.2-a and 5.2-b, the hypothetical effects of reducing the thickness (monolithic metal to laminated sheet of metal). By reducing the metal thickness, plane stress becomes the dominant stress state and results in large plastic zone sizes at each metal sheet surface. While in case of thick monolithic metal the plastic zone is large on the surface (plane stress) and smaller through the thickness (Plane strain). The stress intensity factor is reduced by the addition of fibres that contribute to the load transfer with the fibre bridging stress. This reduction in the stress intensity factor

correlates to a decrease in the plastic zone size. This effect is illustrated in figures 5.2-b and 5.2-c.

To determine whether the basic assumptions underlying the *LEFM* approach for crack propagation in *FMLs* are valid for *VA* loading, the strain fields in the vicinity of the fatigue cracks in the specimens discussed in the previous chapter (Chapter 4) have been measured with *DIC* and subsequently analysed. In addition, the fracture surfaces of these specimens have been evaluated after the tests to obtain detailed information about the fatigue fracture features.

5.1   Plastic Zone Measurement Techniques

Uguz and Martin [2] have compared different plastic zone measurement techniques. Their remarks about these techniques are summarized in table 5.1, which lists the various plastic zone measuring techniques with their advantages, disadvantages, reference and material on which these techniques were applied. In 1982, Sutton and McNeill [3–6] raised the idea of *DIC*. *DIC* has a number of advantages like the quite ease of test set-up and specimen preparation, specimen size is not a issue, insensitivity to vibrations and large strains or significant body movements do not cause difficulties. However, out-of-plane movement can be quite challenging and complicated. In order to measure out-of-plane displacement more equipment (i.e, 3D or two cameras, etc.), expertise and complex mathematics are needed, which can be a disadvantage.

Becasue of these advantages of *DIC*, it was selected to use for this research as a plastic zone size measurement technique. A *DIC* tool developed at Delft University of Technology is used [7–9]. This tool is programmed in Matlab and is independent of the test type, the amount of images per test or the size and shape of the grid as long as only in-plane deformations have to be measured.

Plastic zones created by the overload cycles were calculated for monolithic metal, metal laminate and *FMLs* using the plastic zone relation (Equation 2.4). Subsequently, the *DIC* technique was used to measure the plastic zone sizes for all of these materials. The plastic zone size in the *DIC* images is defined as the plastic deformation at the $\varepsilon_{0.2}$, this assumption is validated and used by Lemmen [10] and Rodi [11].

Method	Plane strain/ Plane stress	Advantages	Disadvantages	Material
Deformed grains	both	Strain distribution can be determined	Applicable to very fine grained materials	HSLA
Digital Image Correlation	Plane stress	Direct observation of plastic zone, practical and rapid	Sensitive to motion	2024-T3, 7475 Al-Alloy, FMLs
Electron Channeling contrast imaging (ECCI)	Both	More rapid than SACP	With EBSD can measure strains within the PZ	Low-C steel,
Etching	Both	Direct observation of the plastic zone is possible	Etchants and etching conditions should be determined for each material:Time consuming	Fe-3Si, INCO 718
Foil strain-gauges	Plane stress	Strain distribution within the plastic zone can be determined	Delicacy of delaying with tiny strain-gauges	Al-alloys and NI-AL alloy, MA87 Al P/M alloy
Image distortion	Plane stress	Direct observation of the plastic zone is possible	Not very sensitive	7075 Al-alloy
Microhardness	Both	Practical and rapid	Applicable to strongly work hardening or softening materials : Sensitivity depends on the indentation size	Maraging and austenitic stain-less steels
Moire interferometry	Plane stress	Submicron displacements and the amount of deformation can be determined	Vibration-free environment is needed	2024, 7075 Al-Alloy, 4340 steel
Optical interference	Plane stress	Direct observation of the plastic zone is possible : Very sensitive	Interference microscope and perfect polishing of the specimen surface needed	2024, 7075 Al-alloy
Photoelectron microscopy	Plane stress	Direct observation of plastic zone is possible	Photoemission microscope is needed and not very sensitive	SAE 1018 and 1015 steel
Recrystallization	both	Real shape and size of plastic zone can be observed, strain distribution can be constructed	Less that 2% deformation cannot be measured:In carbon-contraining materails decarburization may result	304 stainless steel, Mild steel
Selected area channeling patterns (SACP)	Both	Measurements can be repeated:Sensitivity is good:Applicable to any crystalline material	Specimen preparation may be time consuming:Selected area size should be smaller than the grain size	6061 AL-alloy
Shear lip size measurements	Plane stress	Practical and rapid	Sensitive measurements cannot be made	Steel and 7075 Al-alloy
X-ray microbeam	Both	The amount of plastic deformation can be determined in depth:PZS can be measured on fracture surfaces	Sensitivity is limited owing to probe size	Al-alloy, Low C steel, Cr-alloyed steel

Table 5.1: Plastic zone size measurement techniques for metallic materials [2]

5.2   Experimental Program

Fatigue crack growth experiments on monolithic aluminium 2024-T3, laminated aluminium 2024-T3 sheets and GLARE 3-5/4-0.4 have been performed. Details are given in tables D.1, D.2 and D.3. The thickness of specimens was selected to be approximately equal (i.e., 2 mm). The thickness of monolithic metal specimens was 2 mm while for metal laminate and $GLARE$, the metal layer thickness was $5 \times 0.4 = 2$ mm, excluding adhesive and fibres. The geometry of CCT specimen and cross section of the three materials are illustrated in figure D.1. The starter notches were made by drilling a hole of 3 mm diameter with two saw cuts at both opposite sides oriented perpendicular to the loading direction. The total length of the starter notch $(2a_0)$ was approximately 8 mm.

5.2.1   Test Matrix

Load variations were applied in a CA baseline spectrum with a maximum stress $S_{max} = 100$ MPa and a stress ratio $R = 0.1$. The single OL spectrum has an overload $S_{OL} = 145$ MPa at $a_{OL} = 11$ mm. The multiple OL spectrum has three overloads i.e. $S_{OL1} = 145$ MPa; $S_{OL2} = 130$ MPa and $S_{OL3} = 115$ MPa at 9, 12 and 19 mm respectively. Block loading spectra are constituted of two stress levels $S_{max1} = 100$ MPa and $S_{max2} = 140$ MPa and vice versa with stress ratio $R = 0.1$. Details of these tests are given in table D.1, D.2 and D.3.

5.2.2   Test Equipment & Procedure

The tests were conducted in lab air at room temperature on a closed loop mechanical and computer controlled servo-hydraulic testing system with a load capacity of 250 KN. The test frequency was 10 Hz. The test setup is shown in figure D.2.

5.3   Results & Discussion

The output of the DIC software is shown in figures 5.3, 5.4 and 5.5 for all three materials. Figure 5.6(a) shows the method used to measure the plastic zone size from the data acquired with the DIC. Figure 5.6(b) shows the comparison of plastic zone contours acquired using DIC for monolithic 2024-$T3$, laminate aluminium sheets and $FMLs$ for CA and OL cases. It is seen in the figure 5.6-(b) that the plastic zone in the laminated aluminum sheets

(a)

(b)
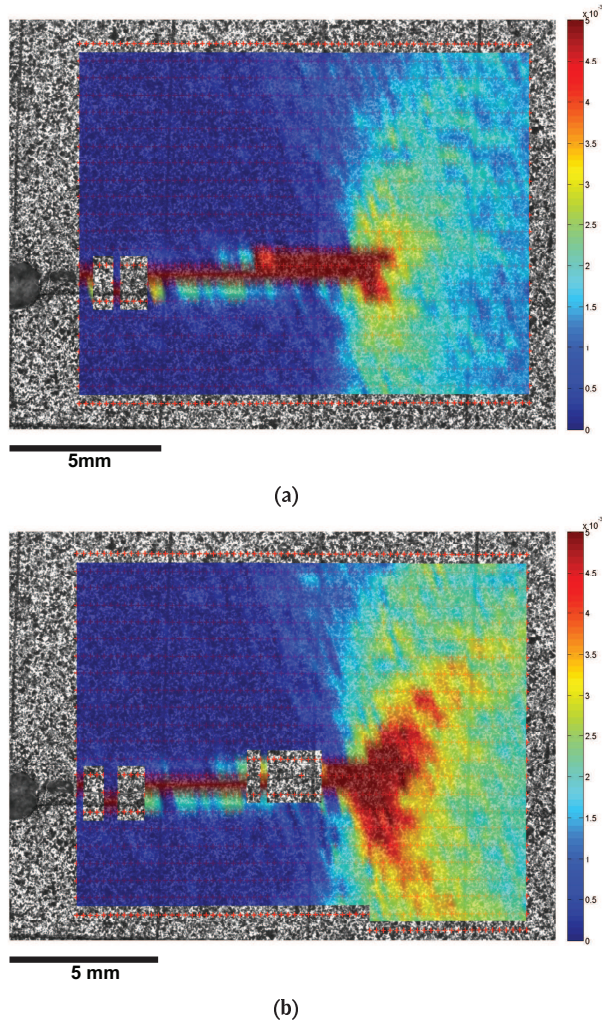
Figure 5.3: DIC Outputs: (a) Monolithic Metal – CA, (b) Monolithic Metal – OL

without fibres is larger than the other two materials. The larger plastic zone in the metal laminate is due to the presence of plane stress as the major stress state due to the thin metallic sheets. While for the *FMLs* the plastic zone size is quite small due to the presence of the fibres. with the addition of fibres the stress intensity factor becomes quite small, which results in smaller plastic zone sizes. The quantitative plastic zone size comparison between calculation and measurement is given in table 5.2.

In case of monolithic metal and metal laminates the calculated plastic zone is
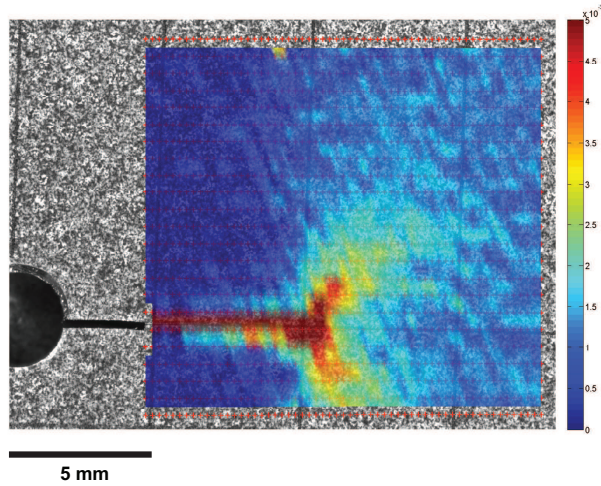
(a)
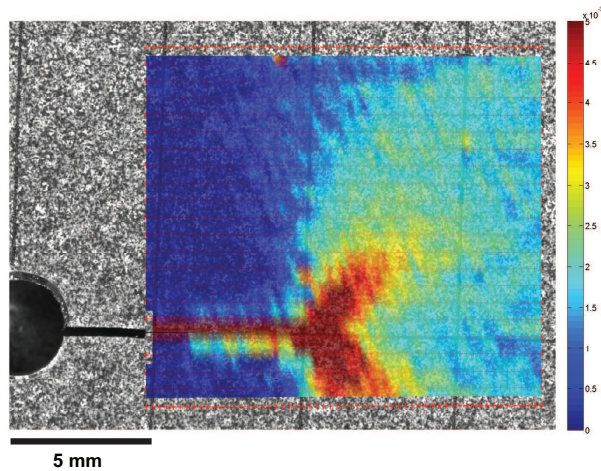
(b)

Figure 5.4: DIC Outputs: (a) Laminated Aluminium sheets – CA, (b) Laminated Aluminium sheets – OL

smaller than the one measured using *DIC*. This means that predictions using only the plastic zone calculation combined with the Paris's crack growth relation (Wheeler) will be erroneous. This mismatch between the calculation and measurement also indicate the existence of other overload related phenomena such as delayed retardation, gradual increase of crack growth rate after retardation, etc. On the other hand, for *FMLs* the difference between the calculated and measured plastic zone size is quite small. This may allow

(a)

(b)
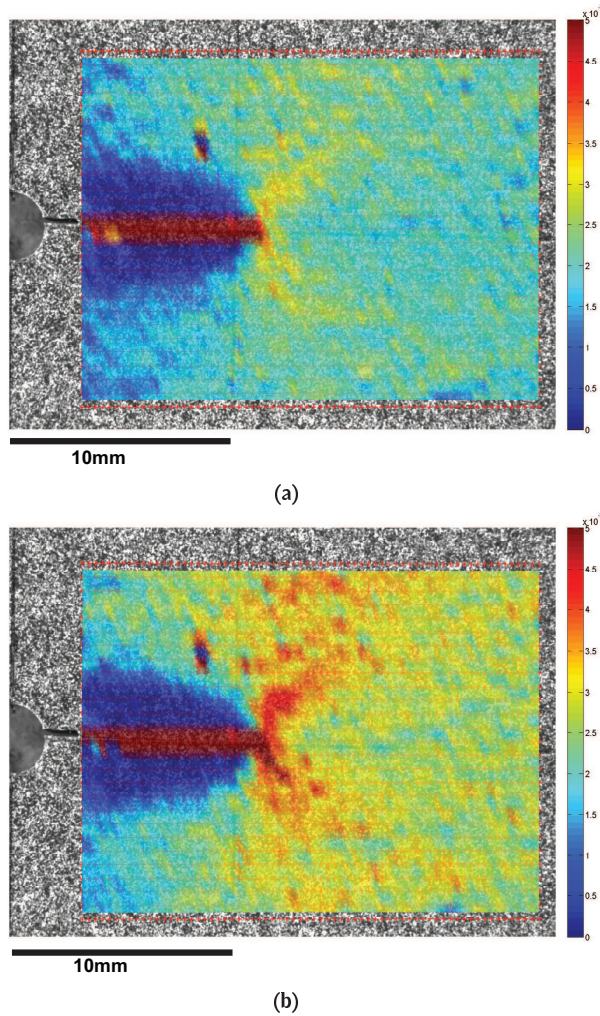
Figure 5.5: DIC Outputs: (a) FML – CA, (b) FML – OL

to use a plastic zone relation in combination with a crack growth relation. Here, the Wheeler yield zone retardation model [12] is chosen as the model that combines the Irwin approach and, the Paris crack growth relation.

Other observations with the *DIC* measurement is the almost constant plastic zone size in *FMLs*, while in the case of monolithic and metal laminate the plastic zone increased with the increase in crack length, as illustrated in figure 5.7. From equation 2.4, it is known that the plastic zone is directly related to the crack-tip stress intensity factor (K_{tip}). In monolithic metals
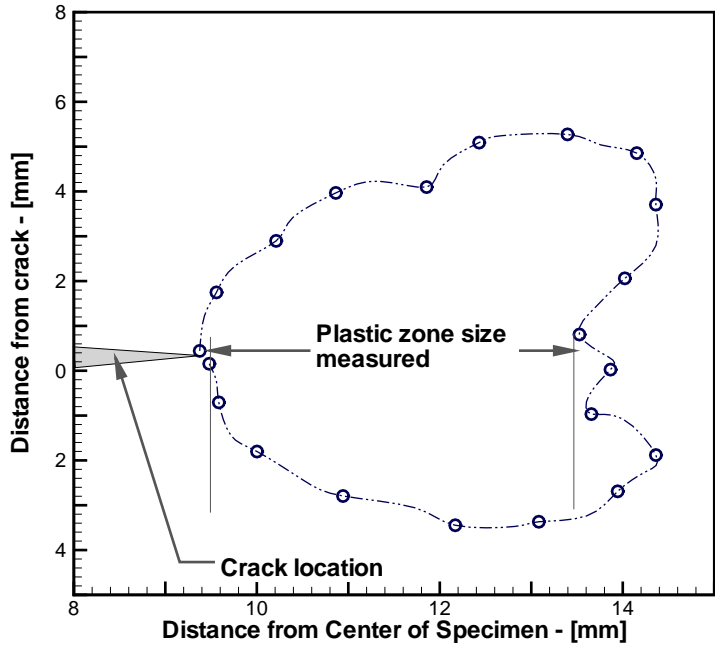
(a)
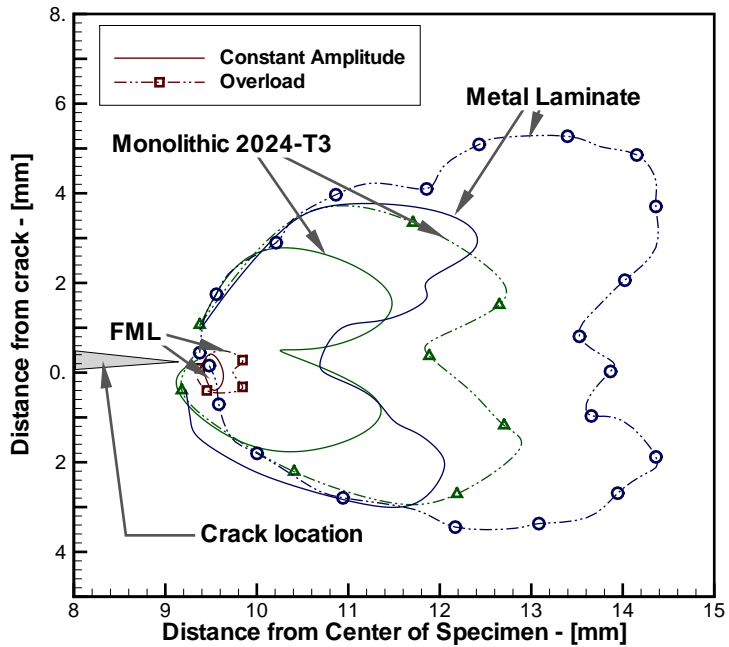
(b)

Figure 5.6: Plastic zone size : (a). Measurement technique, (b). Comparison of Plastic zone measurement for CA and OL (Monolithic, Aluminium laminate and FML)
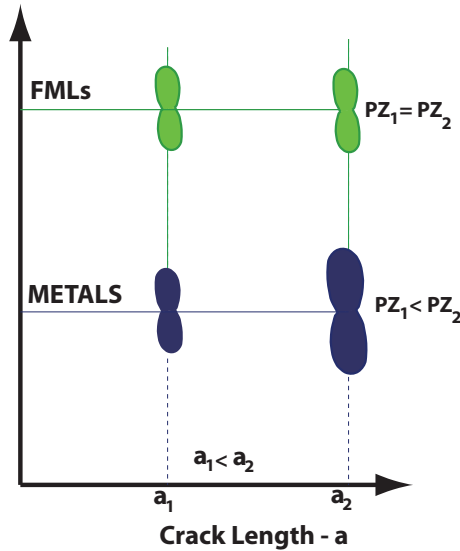
Figure 5.7: Plastic zone formation and sizes comparison in Metals and *FMLs*

and metal laminates, K_{tip} depends on the crack length and increases with the corresponding increase in crack length. But in case of *FMLs*, the plastic zone size remained constant. One expect that increasing the crack length, for the same stress, will increases the K_{tip}. However, increase in crack length results in the increase of number of fibres bridging the crack and fibre bridging stress intensity factor K_{br}. According to equation 5.1, K_{tip} will remain almost constant, resulting in constant plastic zone size.

$$K_{tip} = K_{ff} - K_{br} \qquad (5.1)$$

5.3.1   Shear-Lip Formation & Topology

Figures 5.8, 5.9 and 5.10 shows the comparison of shear-lip formation and topology in monolithic metal, laminated metal sheets and *FMLs*. Figure 5.8 shows the shear-lips formation in monolithic metal for *CA*, single *OL*, multiple *OL* and block *OL*. The shear-lips shown in this figure have typical surface topology of tensile mode in start and followed by shear mode. The crack starts with a pure tensile mode, followed by the change in mode from pure tensile to a shear mode or mix-mode causing a shift in crack surface (flank) from flat to slant. In addition, dark markings are observed for single and multiple *OL*. Details about this typical formation of shear-lips can be found in [13–15].

Monolithic Aluminium 2024-T3

	Crack length	Plastic zone size	
		Calculated	Measured (DIC)
	[mm]	[mm]	[mm]
A1	11.25	0.95	1.25
A1	13.5	1.134	2.2
A2	11.25	0.95	1.5
A2	11.25 (at OL)	1.987	3.0
A3	6	0.504	1.25
A3	6 (at OL_1)	1.06	3.0
A3	9	0.76	2.0
A3	9 (at OL_2)	1.28	3.0

Laminated Aluminium Sheets

B1	13	1.092	1.6
B1	16	1.344	2
B2	15	1.26	1.8
B2	15 (at OL)	2.65	4.0
B3	9	0.84	1.2
B3	9 (at OL_1)	1.77	2.2
B3	11	1.04	1.5
B3	11 (at OL_2)	1.76	3
B5	12.6	2.226	4.6
B5	12.6 (HI->LO)	1.0586	2.2

GLARE3 5/4-0.4

C1	12.75	0.2	0.25
C1	19.25	0.2	0.25
C2	11.1	0.2	0.25
C2	11.1 (at OL)	0.41	0.5
C3	9.25	0.2	0.25
C3	9.25 (at OL_1)	0.37	0.4
C3	12.3	0.2	0.25
C3	12.3 (at OL_2)	0.25	0.35
C5	13.2	0.35	0.4
C5	13.2 (HI->LO)	0.2	0.25

Table 5.2: Plastic zone measurement

Figure 5.9 shows the shear-lip formation in laminated metal sheets without fibres. The shear-lips are quite small compared to the monolithic metal and it occurs very late during the fatigue crack growth. This shows a smaller tensile region than observed in the case of monolithic metals. The same observations were reported by Schijve et al. [1] when comparing monolithic metal and metal laminate. While for the multiple *OL* and block *OL* case, a bold striation mark is observed on the crack surface at the a_{OL}. It is observed in the overload specimens that the crack lengths in all the metal layers are equal. This confirms equal crack growth rate in all the layers.

Figure 5.10 shows the shear-lip formation in *FMLs*. It was observed during the test that cracks grow almost in a straight line. After removing the specimens from the test machine, it was quite hard to see the crack because of the presence of fibres closing the crack. In addition, the crack flanks are straight

Figure 5.8: Shear lip formation in Monolithic metal: a.Constant amplitude, b. Single overload, c. Multiple overloads, d. Block overload (HI-LO)

and quite smooth having a perfect match with each other. Figures 5.10 shows similar findings. In case of monolithic metal and laminated metal sheets, it is quite clear to see the shear-lip and overload markings with the naked eye or with an optical microscope while in case of *FMLs* it is quite difficult to use either of these techniques to see the shear-lip. Rodi et al. [16] has used *SEM* to investigate the shear-lips topology in *FMLs* under static loads. For this investigation, although they has removed the fibre layers but have the similar observations.

The crack growth rate and stress intensity factors of metal laminate, monolithic metal and *FMLs* are shown in figure 5.11. The crack growth rate of monolithic metal is faster than the two other materials and the same is the case for the stress intensity factor range. The curves for monolithic metal and metal laminate are quite similar to each other with the only difference in the shear-lips transition. In the metal laminate, the shear-lips transition is later than in the monolithic metal, but the transition is faster in comparison with monlithic metal. The shear lips transition is indicated in the figure with a dotted box. For the *FMLs* no shear lip transition is observed because the crack surface remained quite smooth.

The other noticeable observation is the equal crack length in the different
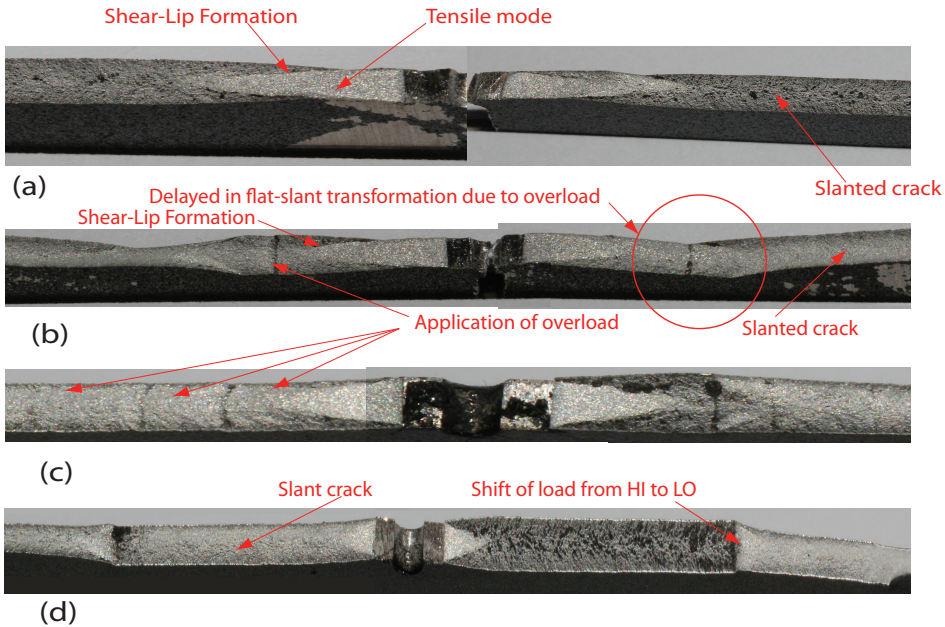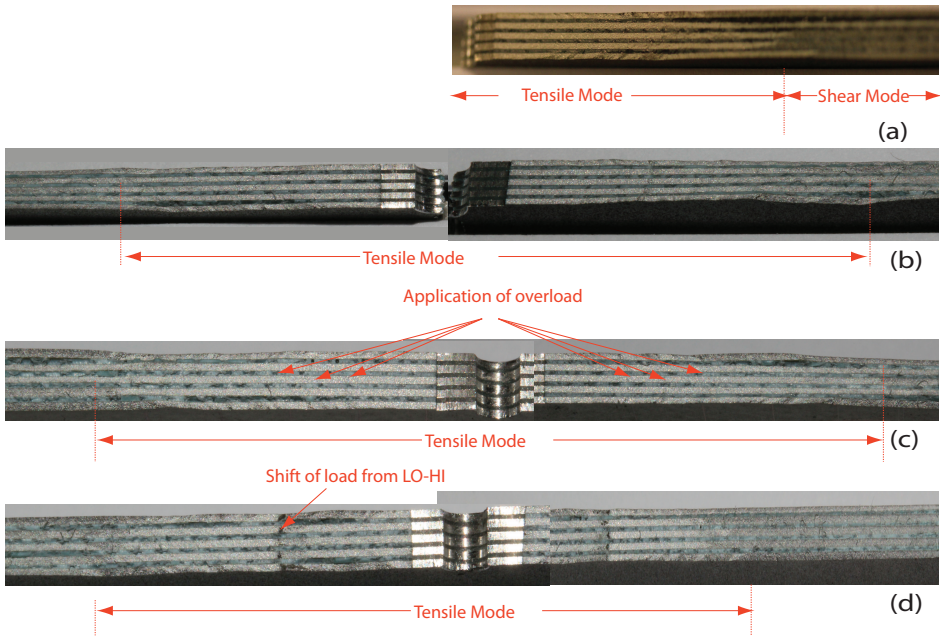
Figure 5.9: Shear lip formation in Laminated Metal Sheets: a. Constant amplitude, b. Single overload, c. Multiple overloads, d. Block overload (HI–LO)

metal layers of *FMLs*. During all the previous studies, equal crack length was assumed. But during this study, it was proven to be a quite accurate assumption. The overload mark on all the metallic surfaces and the crack lengths at the end of fatigue crack growth test were quite close to each other.

Summary

DIC was used for measuring plastic zone sizes in monolithic metal, metal laminates and *FMLs*. Plastic zones created by overloads were predicted using a simple theory and measured using *DIC*. In case of monolithic metals and metal laminates, a big difference was observed between the predicted and measured sizes. On the other hand, a small difference was observed between the predicted and measured plastic zone size in *FMLs*. The plastic zone size calculated as well as measured for *FMLs* is almost constant at any crack length, which is corresponding to the constant K_{tip} observed for *FMLs*.

In addition, shear-lip formation was compared for monolithic metal, metal laminates and *FMLs*. Monolithic metals showed typical shear-lip profiles

REFERENCES 97
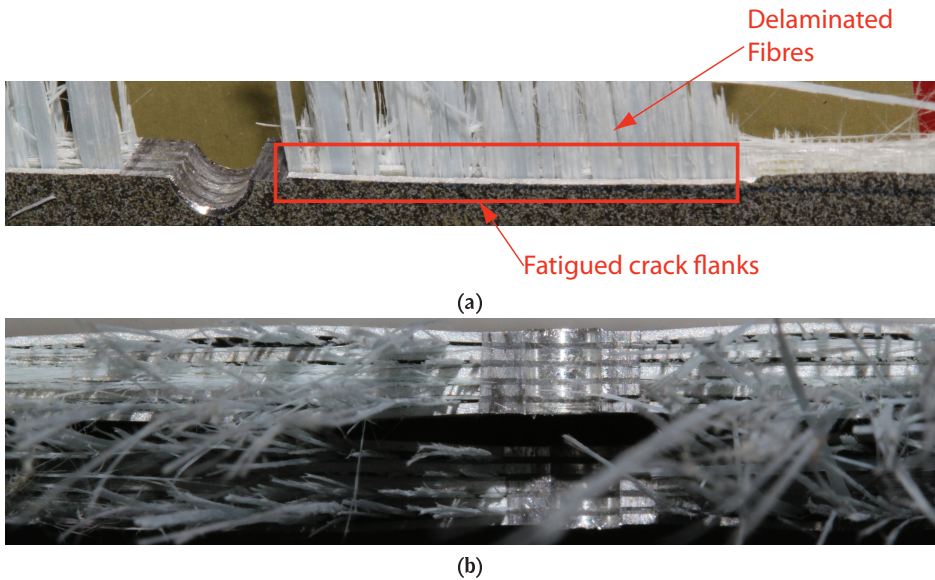
Figure 5.10: Shear lip formation in Fibre metal laminates : (a).Constant amplitude, (b).Block overload (HI-LO)

with the tensile mode followed by a transition mode and finally a shear mode. For metal laminates (without fibres) the mode transition happens quite late during the fatigue crack growth, but the transition length is smaller as compared to monolithic metals. In *FMLs*, it is quite difficult to see the shear-lip profile with naked eye or optical microscope. Like the metal laminate, the major part of crack surface is flat and apparently no shear-lips formation is observed on the crack surface.

References

[1] J. Schijve, H. T. M. van Lipzing, A. H. W. Hoeymakers, Fatigue properties of adhesive-bonded lamianted sheet materal of aluminium alloys, Report LR-276, Delft University of Technology (December 1978).

[2] A. Uguz, J. W. Martin, Plastic zone size measurement techniques for metallic materials, Materials Characterization 37 (1996) 105–118.

[3] W. T. Riddell, R. S. Piascik, M. A. Sutton, W. Zhao, S. R. McNeill, J. D. Helm, Determining fatigue crack opening loads from near-crack-tip displacement measurements, in: R. C. McClung, J. C. Newman
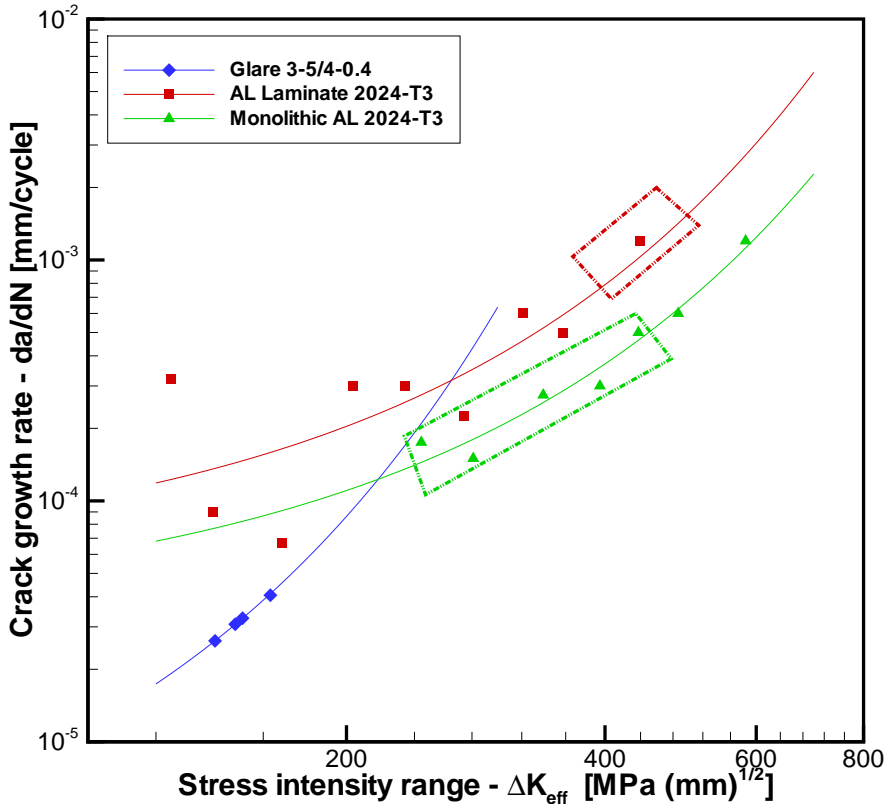
Figure 5.11: Crack growth rates for laminated metal, Monolithic metal and FMLs

(Eds.), Advances in Fatigue Crack Closure Measurement and Analysis: Second Volume, no. 1343 in ASTM STP, American Society for Testing and Materials, West Conshohocken, PA,, 1999, pp. 157–174.

[4] M. A. Sutton, W. J. Wolters, W. H. Peters, W. F. Ranson, S. R. McNeill, Determination of displacements using an improved digital correlation method, Image and Vision Computing 1 (3) (1983) 133139.

[5] M. A. Sutton, M. Cheng, W. H. Peters, Y. J. Chao, S. R. McNeill, Application of an optimized digital correlation method to planar deformation analysis, Image and Vision Computing 4 (3) (1986) 143150.

[6] M. A. Sutton, J. L. Turner, H. A. Bruck, T. A. Chae, Full-field representation of discretely sampled surface deformation for displacement and strain analysis, Experimental Mechanics 31 (1991) 168177.

[7] H. J. K. Lemmen, R. C. Alderliesten, R. Benedictus, J. C. J. Hof-
stede, R. Rodi, The power of digital image correlation for detailed
elastic-plastic strain measurements, in: M. K. Nikolinakou, G. Tse-
kouras, V. Gekas, D. G. Pavlou (Eds.), New aspects of engineering
mechanics, strucutres and enginereing geology, WSEAS, WSEAS Press,
Athens, 2008, pp. 73–89.

[8] R. Rodi, G. Campoli, R. C. Alderliesten, R. Benedictus, Characteri-
zation of the crack tip behavior in fibre metal laminates by means of
digital image correlation, in: 50th AIAA/ASME/ASCE/AHS/ASC Struc-
tures, Structural Dynamics, and Materials Conference, Palm Springs,
CA., no. AIAA-2009-2586 in AIAA, AIAA, 2009, pp. 1–18.

[9] H. J. K. Lemmen, Fatigue and damage tolerance of friction stir wel-
ded joints for aerospace applications, Ph.D. thesis, Delft University of
Technology (2010).

[10] H. J. K. Lemmen, Fatigue and damage tolerance of friction stir wel-
ded joints for aerospace applications, Ph.D. thesis, Delft University of
Technology, Delft, The Netherlands. (2011).

[11] R. Rodi, The residual strength failure sequence in fibre metal lami-
nates, Ph.D. thesis, Delft University of Technology, Delft, The Ne-
therlands. (2012).

[12] O. Wheeler, Spectrum loading and crack growth., Tech. rep., ASMR 72
MetX also G.D. Report FZM 5602 (1970).

[13] J. Schijve, Shear lips on fatigue fractures in aluminium alloy sheet ma-
terial, Engineering Fracture Mechanics 14 (4) (1981) 789–800.

[14] J. Schijve, Fatigue damage accumulation and incompatable crack front
orientation, Engineering Fracture Mechanics 6 (1974) 245–252.

[15] J. Zuidema, H. S. Blaauw, Slant fatigue crack growth in aluminium 2024
sheet material, Engineering Fracture Mechanics 29 (4) (1988) 401–413.

[16] R. Rodi, R. C. Alderliesten, R. Benedictus, Experimental characteriza-
tion of the crack-tip-opening angle in fibre metal laminates, Enginee-
ring Fracture Mechanics 77 (2010) 1012–1024.

[17] R. Marissen, Fatigue crack growth in arall, a hybrid aluminium-aramid
composite material, crack growth mechanisms and quantitative predic-
tions of the crack growth rate, Ph.D. thesis, Delft University of Tech-
nology, Delft (1988).

Chapter **6**

PREDICTION MODEL

The only relevant test of the validity of a hypothesis is comparison of prediction with experience.

Milton Friedman
(1912-2006)

This chapter presents the experimental and analytical research on the applicability of the fatigue crack growth prediction models to Fibre Metal Laminates under variable amplitude loading. A recently developed constant amplitude analytical prediction model for Fibre Metal Laminates has been extended to predict fatigue crack growth under variable amplitude loading using Linear Damage Accumulation, Yield Zone and Crack Closure Models. These updated models have been compared with crack growth tests on Fibre Metal Laminates center-cracked tension specimen. In the end it is discussed to what extent or under which conditions the predictions from these models are sufficiently accurate for Fibre Metal Laminates structures.

Many investigations have been performed to understand the fatigue behaviour of different materials under *VA* loadings. This resulted in the development of a number of prediction models ranging from simple non-interaction models to more advance interaction models [1].

101

One main advantage of *FMLs* is the slow and almost constant rate of crack growth under constant amplitude *(CA)* fatigue loading. This property is due to the load bridging behaviour of the intact fibre layers around a cracked metallic layer. This bridging effect reduces the effective stress intensity factor in the cracked metallic layers, resulting in a smaller crack tip plastic zone, and thus smaller interaction effects under variable amplitude *(VA)* loading. As far as interaction effects are concerned, Plokker et. al. [2] have reported the absence of crack growth acceleration effects in *FMLs* under different underloads and over/under load combinations and highlighted the presence, although to a lesser degree compared to monolithic metals, of crack growth retardation in *FMLs*. Due to this limited retardation, fatigue crack growth predictions under *VA* based on Linear Damage Accumulation (a simple non-interaction model [2, 3]), correlate well with experimental data for load spectra with minor variations. However, a mismatch is observed in case of spectra where load variations are more distinct.

A major follow up question is whether a simple interaction model would be sufficient to describe the retardation effects during the large and distinct load sequences occurring in these load spectra. To answer this question, the Wheeler crack growth prediction model [4], being one of the simplest and most widely employed [5–19] model to quantify the fatigue crack growth retardation under selective *VA* loadings, is selected for fatigue crack growth prediction in *FMLs*. Fatigue crack growth predictions made with the Wheeler model for monolithic metals are quite inaccurate due to the existence of large plasticity due to overloads, details can be found in [1, 7, 20–24]. An additional modification to the Wheeler model is also included to incorporate crack closure effects in addition to the plastic zone effects.

Finally, CORPUS- the crack closure model is also models to compare the predicitons of Yield zone model with the crack closure model. This comparison facilitates the approach of simplified model for complex material like *FMLs*.

$$K_{tip} = K_\infty - K_{br} \tag{6.1}$$

6.1   Linear Damage Accumulation (LDA)

The linear damage accumulation model is based on a cycle-by-cycle analysis independent of proceeding load cycles. It is an integration of calculated crack growth increments Δa_i using crack growth relations [25] to obtain a prediction for the full load spectrum. As a result, it is the simplest model to predict the crack growth under VA loading. The advantage of the *LDA* rule is computational efficiency, while the disadvantage is non-consideration of non-linear fracture mechanics concepts such as plastic zone formation in

front of the crack tip, crack closure in the wake of crack, crack growth retardation and crack growth acceleration. In general, the *LDA* rule can be presented mathematically as:

$$a = a_0 + \sum_{i=1}^{n} f(\Delta K, r, ..) = a_0 + \sum_{i=1}^{N} \Delta a_i \qquad (6.2)$$

A model has been developed using the *LDA* rule (equation 6.2), in order
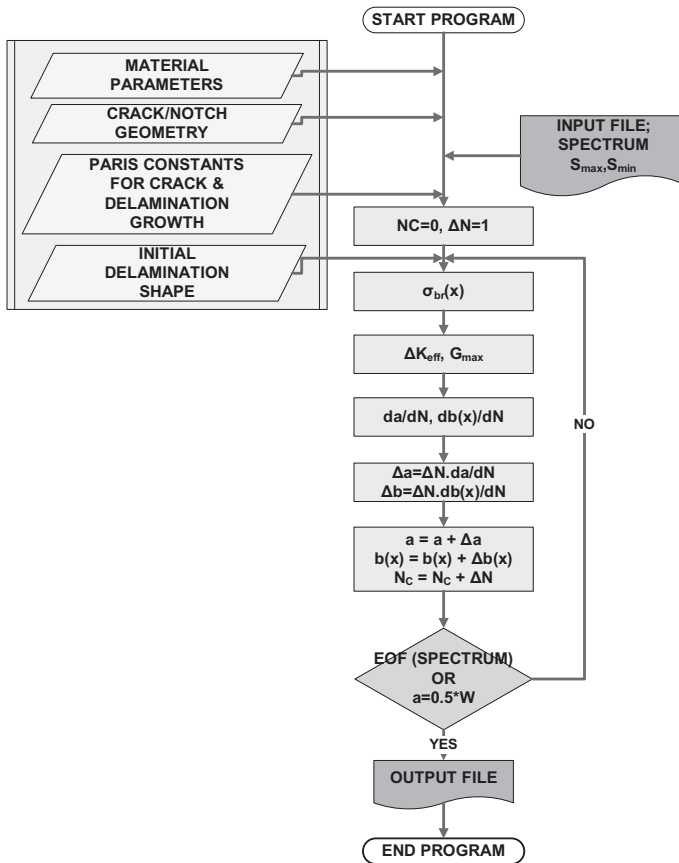
Figure 6.1: Flow diagram of the LDA crack growth prediction model

to investigate the prediction accuracy of the *LDA* rule for *FMLs* under *VA* loading. The *CA* model of Alderliesten[26, 27] has been used as the basis for development of this *VA* prediction model using *LDA* rule for *FMLs*. The flow diagram of the *LDA* prediction model is shown in figure 6.1.

6.2   Yield Zone Model

The *VA LDA* model is modified, using Yield zone model, to validate the hypothesis that limited retardation effects in *FMLs* as compared to monolithic aluminium are easier to predict with simple methods. A simple non-interaction model based on Linear Damage Accumulation *(LDA)* was developed . *LDA* model predicts well for the cases with limited crack growth retardation as observed in steep spectra with few high stress cycles. But the predictions were inaccurate for the load spectra causing large fatigue crack growth retardation as observed in flat spectra with a large number of high stress cycles. Details about the model and its performance can be found in [2, 3].

The next step in the model development is to include a simple retardation model. The yield zone model (equation 2.8) is selected for implementation for fatigue crack growth prediction in *FMLs*. The modified Wheeler model, equation 2.12, is used for calculating the crack growth rate. The flow diagram of the *VA FMLs* model with this modified Wheeler model is shown in figure 6.2.

6.3   Crack Closure Model

The details of the crack closure models are given in section 2.8.7. One of the famous crack closure model (CORPUS) is used, in this thesis, for the fatigue crack growth prediction in *FMLs*. The flow diagram of this model is shown in figure 6.3.

6.4   Model validation using test data

To validate the model, fatigue crack growth experiments on GLARE 3-4/3-0.3 with cross-ply fibre orientation have been performed. These fatigue crack growth tests have been performed on center-cracked tension *(CCT)* specimens, for which the geometry is illustrated in figure D.2. The starter notches are made by drilling a hole of 3 mm diameter with two saw cuts, directing perpendicular to the loading direction. The total length of the starter notch $(2a_0)$ is approximately 5 mm.
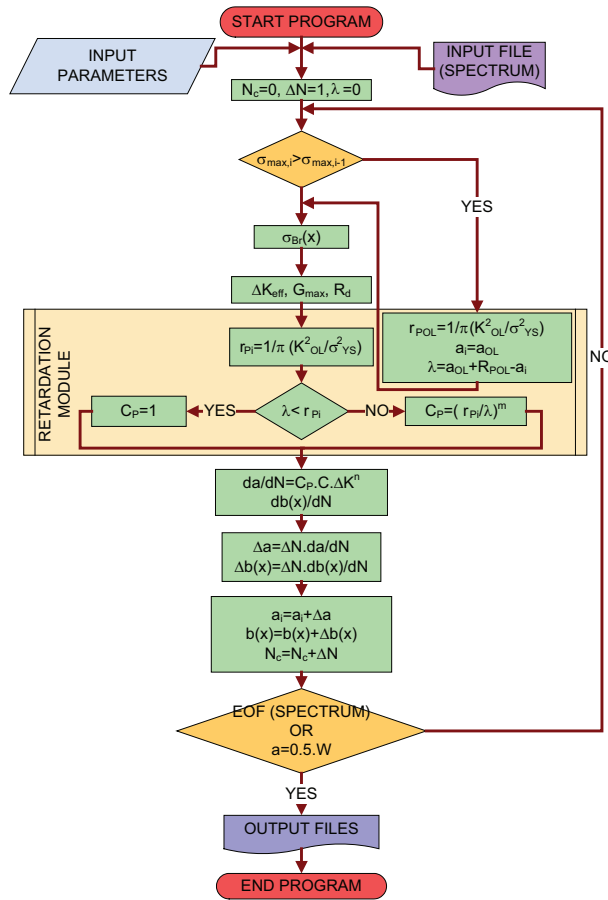
Figure 6.2: Flow diagram for the modified Wheeler crack growth prediction model
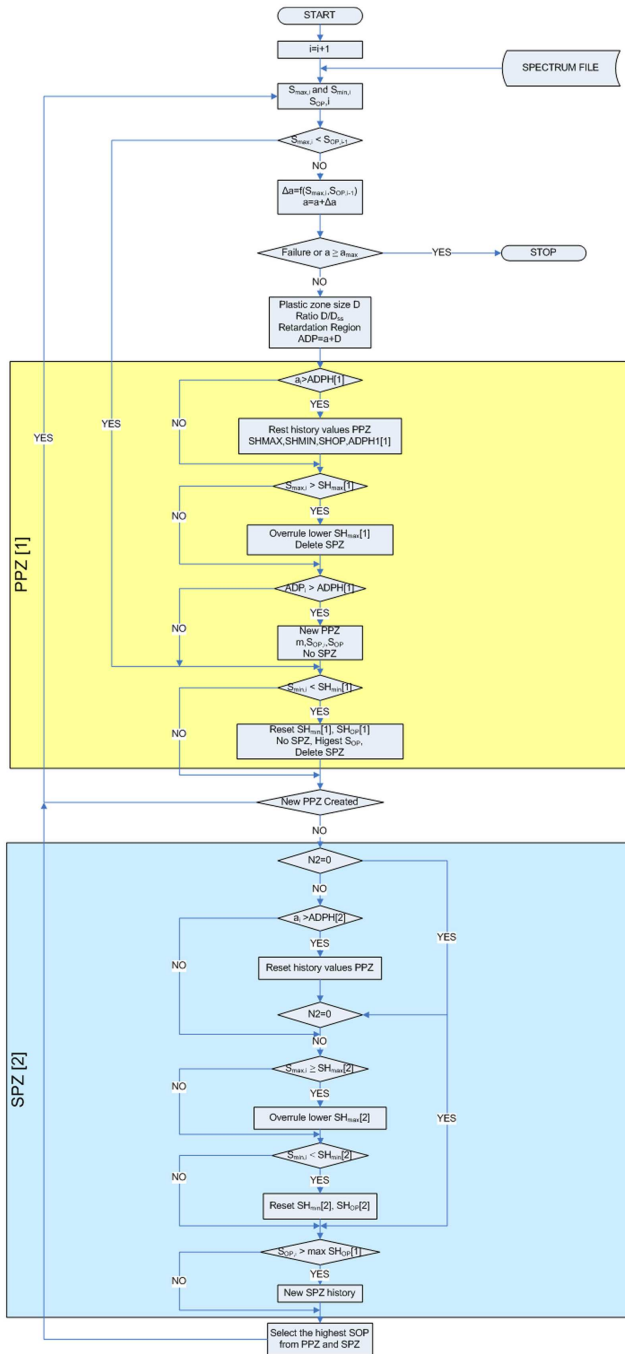
Figure 6.3: Flow diagram for the Crack closure model

6.4.1   Test Matrix

Four types of *VA* load sequences are used for the performance evaluation of all prediction models. Detail of these tests are given in table 6.1.

To study the retardation and other overload related phenomena, a building block approach is used; starting from a simple *OL* to complex flight spectra. For the single overload case a *CA* baseline spectrum with a maximum stress S_{max} = 120 MPa and a stress ratio $R = 0.1$ is used. A single overload of S_{OL}=175 MPa is applied at 100 kcycles equivalent to a crack length of a_{OL}=9.5 mm.

A multiple overload spectrum is the second load sequence type. The same *CA* baseline spectrum is used with three overloads of S_{OL1} = 175 MPa; S_{OL2} = 158 MPa applied at 100, 160 and 220 kcycles equivalent to a_{OL1} = 9.3 mm; a_{OL2} = 13.5 mm; a_{OL3} = 17.5 mm and respectively. The multiple overload spectrum is used to investigate whether the modified Wheeler model can be used to predict crack growth retardation after each overload and to what extent the three overloads interfere with each other.
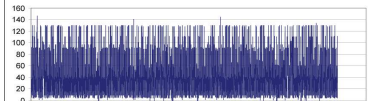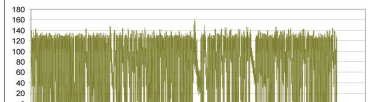
The third type of load sequences investigated is a block load sequence with two configurations i.e., LO-HI and HI-LO. The same stress levels are used for both the block load sequences. Two stress levels S_{max1} = 100 MPa for the LO cycles and S_{max2} = 140 MPa for the HI cycles with a stress ratio $R = 0.1$ are used. The change in the stress level is applied at 100 kcycles. In case of LO-HI sequence stress level are changed at a_{TR}=6.9 mm and for HI-LO a_{TR}=12.7 mm. These load sequences are used to investigate the effect of block of overload cycles on the fatigue crack growth.

Apart from these selective *VA* load spectra, representative complex flight spectra are also used for the model evaluation. Qualitatively, these spectra are Spectrum-I which is a typical wide body fuselage spectrum, spectrum-II which is a Mega linear front fuselage spectrum and Spectrum-III which is a Mega liner aft fuselage spectrum. Spectrum I and Spectrum II are almost identical with a small number of overloads while Spectrum-II is different and a more severe spectrum. Spectrum-II has a large number of overloads applied very close to each other.

6.4.2   Test Equipment & Procedures

The tests were conducted in lab air at room temperature on a closed loop mechanical and computer controlled servo-hydraulic testing system with a load capacity of 6 metric tons. The test frequency was 10 Hz.

Table 6.1: Fatigue crack growth test matrix

Type of Loading		CA cycles		Load variation
		Maximum stress [MPa]	Stress ratio	[MPa]
Single overload	$S_{OL} = 175$ MPa $S_{MAX} = 120$ MPa $S_{MIN} = 12$ MPa	120	0.1	175
Multiple overload	$S_{OL_1} = 175$ MPa $S_{OL_2} = 158$ MPa $S_{OL_3} = 139$ MPa $S_{MAX} = 120$ MPa $S_{MIN} = 12$ $a_{OL_1} = 9.33$ mm $a_{OL_2} = 13.54$ mm	120	0.1	175,158,139
Block loading-LO-HI	$S_{MAX_2} = 140$ MPa $S_{MAX_1} = 100$ MPa $S_{MIN} = 10$ MPa	100	0.1	140
Block loading-HI-LO	$S_{MAX_1} = 140$ MPa $S_{MAX_2} = 100$ MPa $S_{MIN} = 10$ MPa	140	0.1	100
Spectrum loading-I		Wide body fuselage spectrum		
Spectrum loading-II		Mega liner front fuselage spectrum		
Spectrum loading-III		Mega liner aft fuselage spectrum		

6.5   Results and Discussion

6.5.1   Linear damage accumulation

The comparisons of *LDA* predictions with the tests results are shown in figures 6.4-6.10.

Single Overload

Figure 6.4 shows the comparison for single overload of 175 MPa in the *CA* baseline cycles of $S_{max} = 120$ MPa and stress ratio $R = 0.1$.

The crack growth retardation is not predicted due to the limitation of *LDA* approach being a non-interaction model. The magnitude of retardation in case of a *FMLs* is less than the monolithic metals case making the *LDA* predictions slightly more reliable for *FMLs*. The comparison also shows that the crack growth rate gets back to the original rate as soon as the crack is out of retardation region (which is always larger than plastic zone size).

Multiple Overload

Similar to the single overload case (figure 6.4(a)), the crack growth rate in the multiple overload case (figure 6.5(a)) gets back to original level depending on the magnitude of S_{OL} and R_{OL}. Figure 6.5(a) shows the comparison for the case with multiple overloads of 175, 158 and 139 MPa respectively in the *CA* baseline cycles of S_{max}=120 MPa and $R = 0.1$. It is known from the literature that in metals the retardation region is highly influenced by the magnitude of S_{OL}, and similar behavior is seen in case of *GLARE*. By reducing the S_{OL} from 175 to 158 and then to 139 MPa the crack growth retardation keep decreasing (figure 6.5(a)).

Block load

Figures 6.6 and 6.7 show the comparison between *LDA* prediction and test results for the two different sequences of block loads. The stress values are S_{max1}=100 MPa, $R = 0.1$ and S_{max2}=140MPa, $R = 0.1$. Figure 6.6(a) shows the comparison for the Low-High block loading case. Since the loading sequence is going from low to high values, there will not be any retardation but due to increase in stress level, crack growth acceleration is observed. The error in this case is less than the cases shown in figures 6.4 and 6.5, because the interaction effects are absent in the test.

(a)
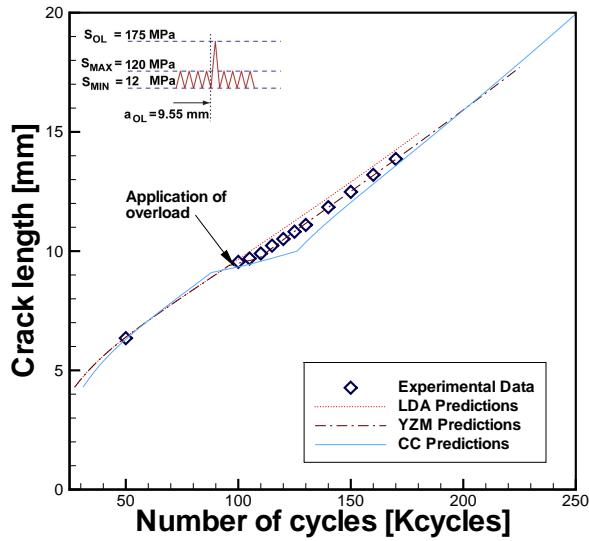
(b)

Figure 6.4: Correlation between experiment and predictions for single overload: (a). Crack growth rate Vs. Crack length, (b). Crack length Vs. Number of cycles

Figure 6.7(a) shows the comparison between test results and the *LDA* predictions in case of the high-low block loading sequence. The error in crack growth prediction is evident from this comparison. Due to the presence of

(a)

(b)
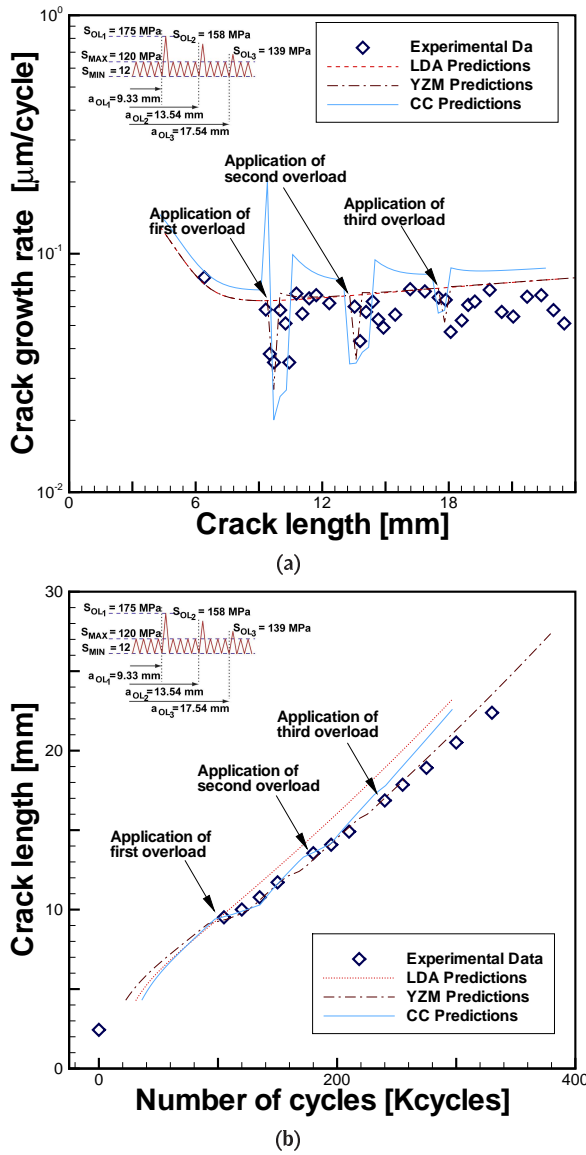
Figure 6.5: Correlation between experiment and predictions for multiple over-loads: (a). Crack growth rate Vs. Crack length, (b). Crack length Vs. Number of cycles

block of high (overload) cycles the crack growth retardation is more than the case of a single overload. Here it is clear that the LDA being a non-

interaction model is unable to predict the crack growth and retardation.

Flight spectra

Figure 6.8- 6.10 exhibit the comparison of crack growth test results with the *LDA* predictions for representative complex aircraft spectra. Three different spectra are used with different S_{max} values and sequences. Spectrum I is a wide body fuselage spectrum while spectrum II is a mega liner front fuselage spectrum and Spectrum III is mega liner aft fuselage spectrum, as detailed in table 6.1. The loading spectrum (Spectrum II) used in figure 6.9 is a severe spectrum with a lot of variations in the stress peaks.

The observed mismatch in *LDA* prediction and test result for spectrum II (figure 6.9), while only a small error is observed for the other two spectra (figures 6.8,6.10) can be attributed to the nature of these spectra. To avoid disclosing proprietary information, only the graphical representation of the three spectra in figure 6.8, 6.9 and 6.10 will be used for comparison and discussion. Comparing the spectra, one can observe that spectrum I and II have all loads randomly distributed between minimum and maximum values. Only spectrum III seems to have less amplitude cycles on the lower stress range, but that has no significant effect on crack growth, resulting in similar behavior as spectrum I. However, spectrum II has clearly large load cycles distributed throughout the spectrum with mostly stress cycles in the lower stress range. These high stresses have a retardation effect on the smaller stress cycles that are not captured by *LDA* predictions.

Comparing to a single overload situation figure 6.4, the crack in figure 6.9 seems unable to grow out of the retardation zone of previous high load in the spectrum II before facing subsequent high load. This continuous retardation not captured by *LDA* results in the systematic mismatch.

6.5.2   Yield Zone Model

Figures 6.4-6.10 show the comparisons of the predictions with the *FMLs* models with the tests results.

Single Overload

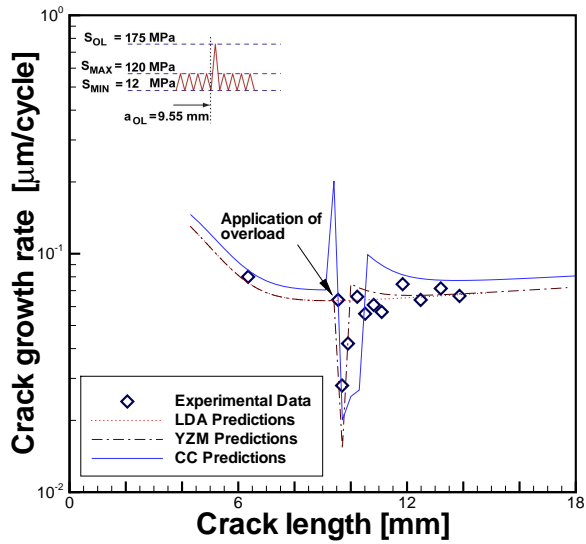The comparison for single overload of 175 MPa in the *CA* baseline cycles of $S_{max} = 120$ MPa and stress ratio $R = 0.1$ is shown in figure 6.4. The modified Wheeler is able to accurately predict the crack growth retardation observed for a single overload cycle as shown in figure 6.4. An interesting observation
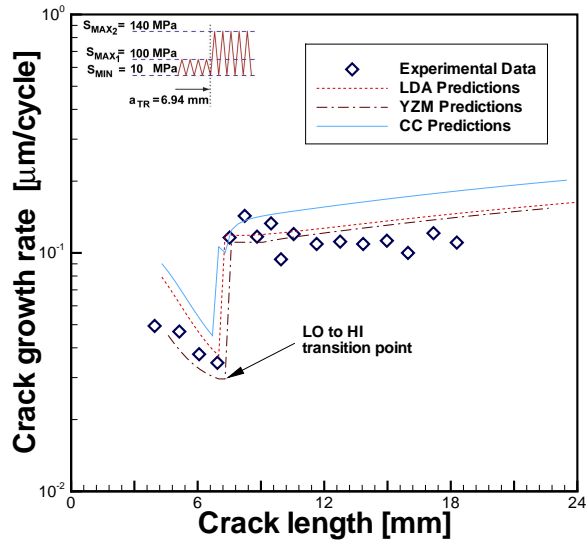
(a)
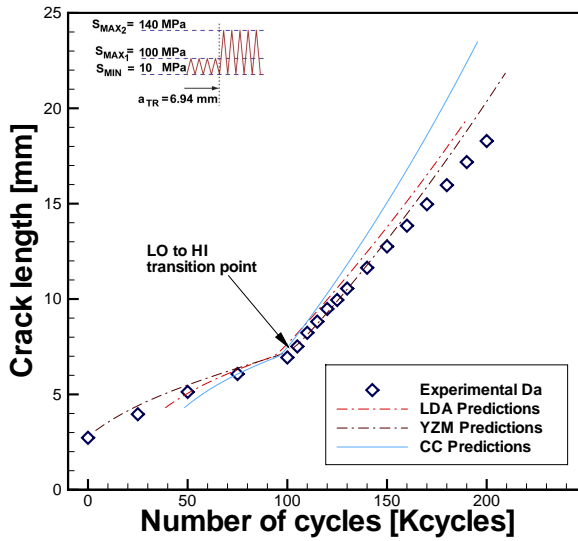
(b)

Figure 6.6: Correlation between experiment and predictions for block load sequence $(LO-HI)$: (a). Crack growth rate Vs. Crack length, (b). Crack length Vs. Number of cycles

(a)

(b)

Figure 6.7: Correlation between experiment and predictions for block load sequence $(HI - LO)$: (a). Crack growth rate Vs. Crack length, (b). Crack length Vs. Number of cycles

from figure 6.4 is that there is hardly any difference between the prediction and experimental data after the application of overload. In other words, the number of delay cycles predicted and observed in the test are almost equal. This can be attributed to the existence of intact fibers which restrain the crack opening and reduces the K_{tip} (equation 6.1) leading to the small plastic zone which is equal to the one calculated using Irwin's relation(equation 2.4). The crack growth rate returns to the previous level as soon as the crack tip is out of the plastic zone formed by the overload. Figure 6.4-(b) shows the crack length Vs. number of cycles for single overload case.

Multiple Overload

Figure 6.5 shows the comparison for the case with multiple overloads of 175, 158 and 139 MPa respectively in the CA baseline cycles of $S_{max}=120$ MPa and $R=0.1$. The crack growth rate in the multiple overload case, also returns to original level depending on the magnitude of S_{OL} and R_{OL}. This behaviour is similar to the one observed in single overload case, shown in figure 6.5. It is known from the literature that in metals the retardation region is highly influenced by the magnitude of S_{OL}, and similar behavior is observed in case of $FMLs$. By reducing the S_{OL} from 175 to 158 and then to 139 MPa the crack growth retardation effect decreases (figure 6.5. As far as predictions are concerned, the modified Wheeler model seems able to perform accurate predictions for isolated overload cases up to $R_{OL}=1.45$. Figure 6.5-(b) shows the crack length Vs. number of cycles.

Block Load

Figures 6.6 and 6.7 show the comparison between the modified Wheeler model prediction and test results for the two different sequences of block loads. The stress values are $S_{max1}=100$ MPa, and $S_{max2}=140$MPa, both at $R=0.1$. Figure 6.6 shows the comparison for the LO-HI block loading case. As the load sequence is going from low to high values, there will not be any retardation, but due to an increase in the stress level, the crack growth rate increases to the level associated with the higher stress level. The error observed in this case is less than the other cases shown in figures 6.4 and 6.5, because the interaction effects are absent in the test.

Figure 6.7 shows the comparison between test results and the modified Wheeler model predictions in case of the HI-LO block load sequence. Although a retardation level is computed with the modified Wheeler model, a delay retardation can be observed in the experiments that is not captured by the model predictions. Similar to metals, in $FMLs$ a large block of overload cycles creates larger plastic zones resulting in large retardation. As far as the

modified Wheeler model in case of HI-LO block loading is concerned, the initial retardation after the transition from HI-LO load is predicted, but the number of delay cycles is inaccurate. After predicting the initial retardation accurately, after the overload, a mismatch is observed in the prediction and experiment, as shown in figure 6.7-(b). This can be explained as, in case of large plasticity due to large number of high cycles the predictions are inaccurate.

Flight Spectra

Figures 6.8-6.10 show the comparison of crack growth test results with the the modified Wheeler model predictions for representative complex aircraft spectra. Three different spectra are used with different S_{max} values and sequences. The loading spectrum used in figure 6.9 is a severe spectrum with a lot of variations in the stress peaks. To avoid disclosing proprietary information, only the graphical representation of the three spectra in figures 6.8-6.10 will be used for comparison and discussion.

A mismatch is observed for the modified Wheeler prediction and test result for spectrum II (figure 6.9), while only a small error is observed for the other two spectra (figures 6.8-6.10). This can be attributed to the nature of these spectra. Comparing the spectra, one can observe that spectrum I and II have all loads randomly distributed between minimum and maximum values. Only spectrum III seems to have less amplitude cycles on the lower stress range, but that has no significant retardation effect on crack growth, resulting in similar behavior as spectrum I. However, spectrum II has clearly large load cycles distributed throughout the spectrum with the majority of the stress cycles in the lower stress range.

Comparing to a single overload situation figure 6.4-(a), the crack in figure 6.9 seems unable to grow out of the retardation zone of previous high load in the spectrum II before facing a subsequent high load. This continuous retardation, not captured by the modified Wheeler model, results in the systematic mismatch. This concept is illustrated in figure 6.11. In the modified Wheeler model, the crack growth rate returns to the original rate(prior overload) very quickly, while in reality it takes longer (larger number of delay cycles). Secondly, in case of the complex Spectrum II, the situation is further complicated by the application of additional overloads before the actual crack growth rate has reached its original level. A small error is generated due to the difference of actual and predicted crack growth rate when another overload is applied (point B shown in figure 6.11). This small error is compounded due to the application of consecutive overloads (point C in figure 6.11). Because of this, a lower crack growth rate is observed in experiments compared to the predictions (figure 6.9).
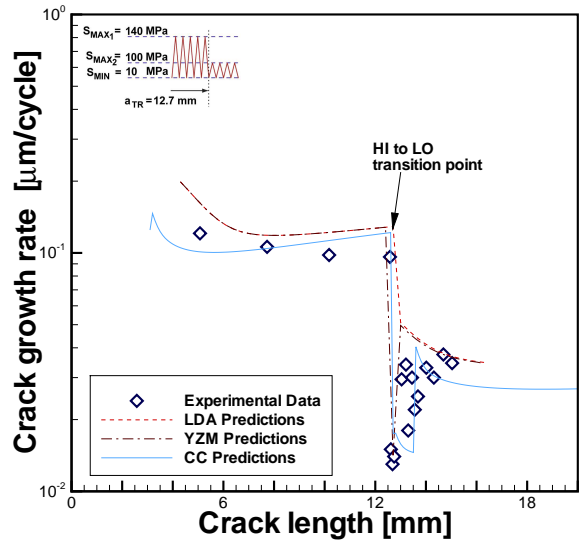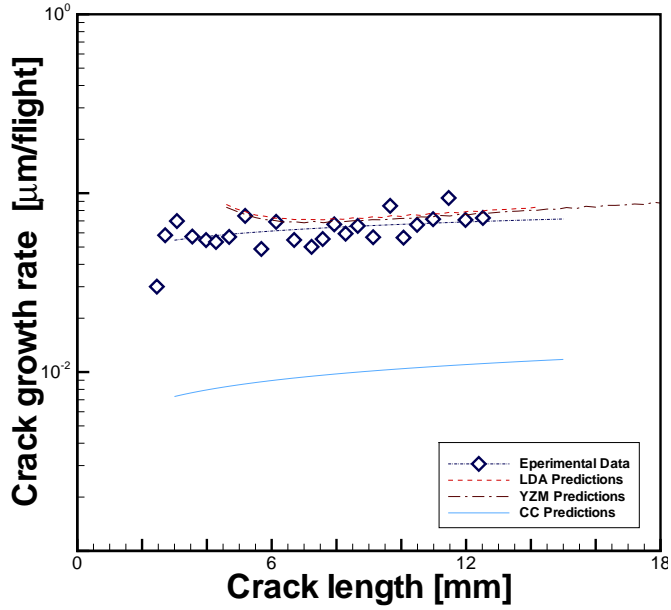
(a)
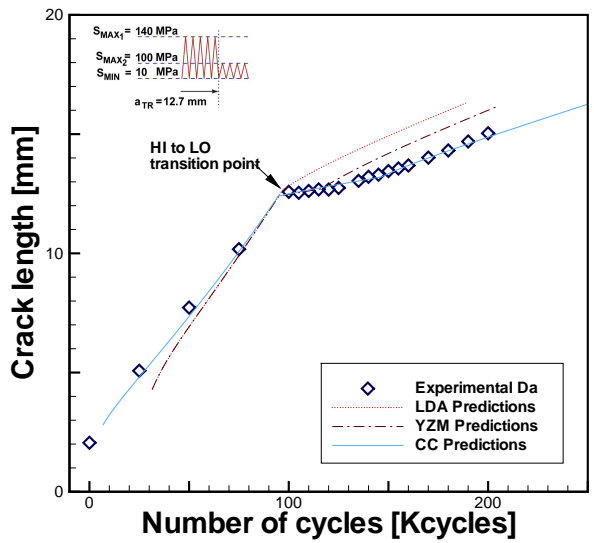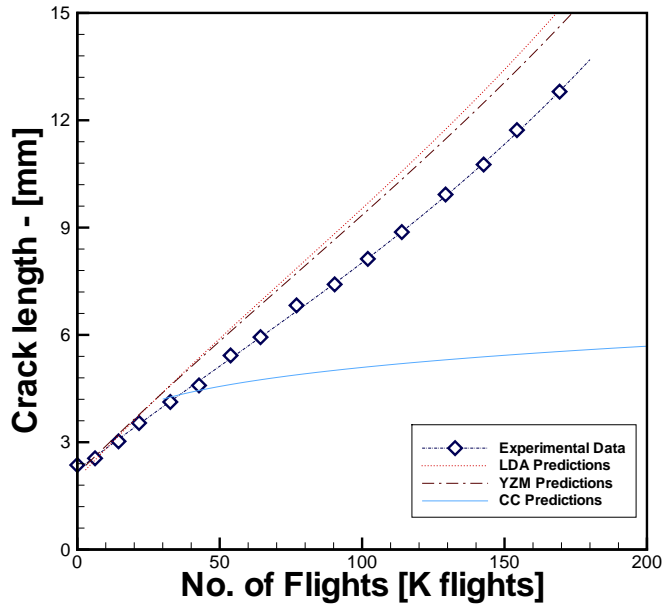

(b)

Figure 6.8: Correlation between experiment and predictions for Flight spectrum I: (a). Crack growth rate Vs. Crack length, (b). Crack length Vs. Number of Flights
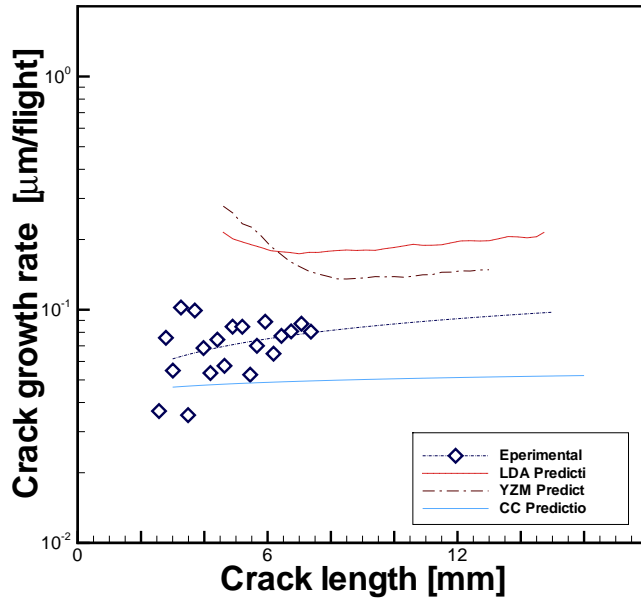
(a)
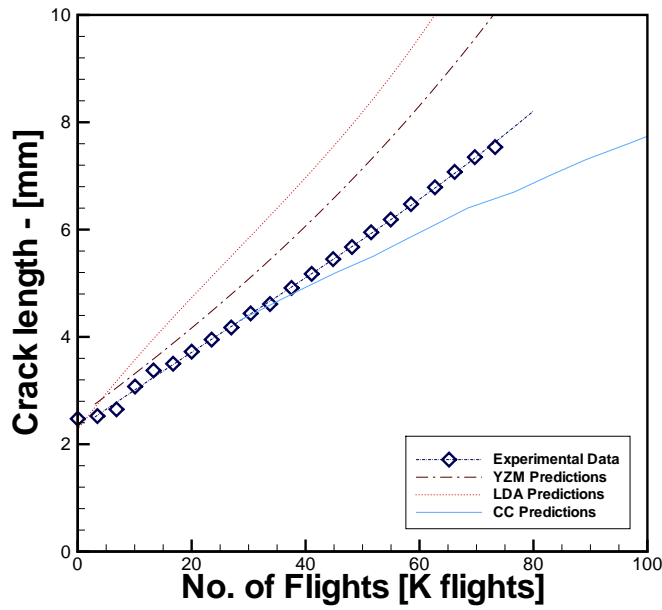
(b)

Figure 6.9: Correlation between experiment and predictions for Flight spectrum II: (a). Crack growth rate Vs. Crack length, (b). Crack length Vs. Number of Flights
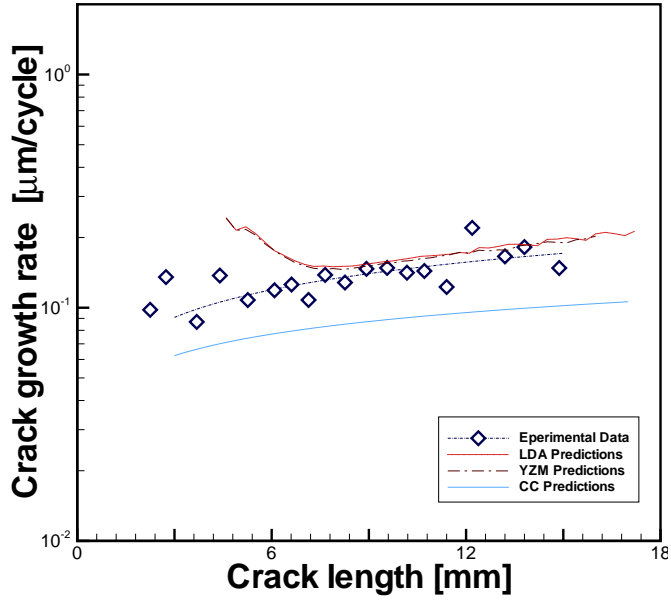
(a)
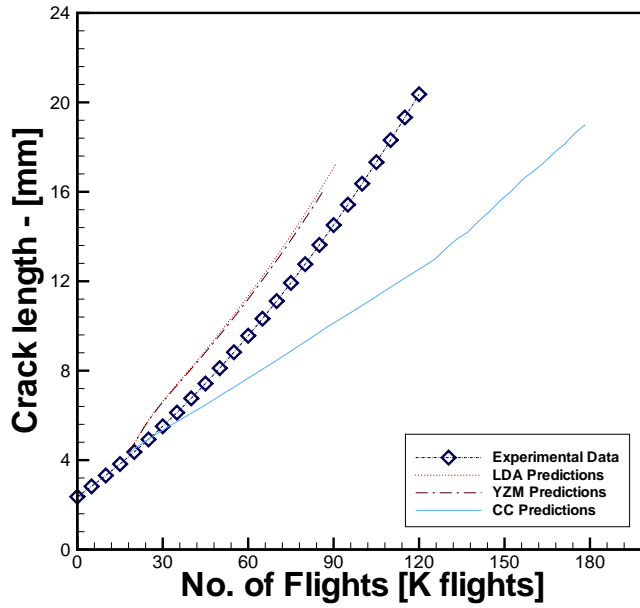
(b)

Figure 6.10: Correlation between experiment and prediction for flight spectra III: (a)crack Growth Rate vs. Crack Length, (b)Crack Length Vs. Number of Flights
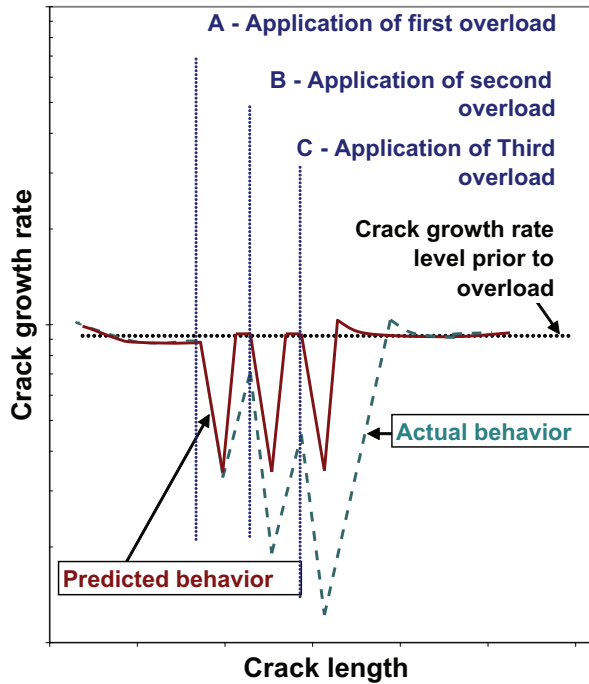
Figure 6.11: Illustration explaining the reason of mismatch for complex spectra (e.g. Spectrum II)

One may also relate this behavior to de Koning's [28] primary and secondary plastic zone concept that makes the large difference between the prediction and test results.

6.5.3 Crack Closure Model

Figures 6.4-6.8 show the comparisons of the predictions with the Crack closure *FMLs* model with the tests results.

Single Overload

The comparison for single overload of 175 MPa in the *CA* baseline cycles of $S_{max} = 120$ MPa and stress ratio $R = 0.1$ is shown in figure 6.4. The crack closure model is able to accurately predict the crack growth retardation observed for a single overload cycle as shown in figure 6.4-(a). An interesting

observation from figure 6.4-(a) is the prediction of delayed retardation at the time of application of overload. This phenomenon is not predicted by *LDA* and Modified yield Zone Model. In addition, unlike yield zone model the crack tip takes sometime to get back to the pre-overload crack growth rate. Figure 6.4-(b) shows the crack length Vs. number of cycles for single overload case.

Multiple Overload

Figure 6.5 shows the comparison for the case with multiple overloads of 175, 158 and 139 MPa respectively in the *CA* baseline cycles of S_{max}=120 MPa and $R = 0.1$. The crack growth rate in the multiple overload case, also show the delayed retardation at the application of overload. But the delayed retardation is very much depending on the overload ratio, since it is not quite prominent in the S_{OL}=158 and 130 MP cases. Similar to single overload case, crack-tip takes sometime to get back to the pre-overload crack growth rate. Figure 6.5-(b) shows the crack length Vs. number of cycles.

Block Load

Figures 6.6 and 6.7 show the comparison between the crack closure model prediction and test results for the two different sequences of block loads. The stress values are S_{max1}=100 MPa, and S_{max2}=140MPa, both at $R = 0.1$. Figure 6.6 shows the comparison for the LO-HI block loading case. As the load sequence is going from low to high values, there will not be any retardation, but due to an increase in the stress level, the crack growth rate increases to the level associated with the higher stress level. The error observed in this case is less than the other cases shown in figures 6.4 and 6.5, because the interaction effects are absent in the test.

Figure 6.7 shows the comparison between test results and the crack closure model predictions in case of the HI-LO block load sequence. Crack closure model is able to predict number of delay cycle quite close to the experimental data similar to single and multiple overload case. This statement can be observed in the crack length Vs. Number of cycle curve shown in figure 6.7-(b).

Flight Spectra

Figures 6.8-6.10 show the comparison of crack growth test results with the the crack closure model's predictions for representative complex aircraft spectra. Three different spectra are used with different S_{max} values and sequences.

The loading spectrum used in figure 6.9 is a severe spectrum with a lot of variations in the stress peaks. To avoid disclosing proprietary information, only the graphical representation of the three spectra in figures 6.8-6.10 will be used for comparison and discussion.

A mismatch is observed for the crack closure prediction and test result for all three spectra (figure 6.8-6.10). However, the difference between the prediction and experimental data is quite large for the Spectrum I while the difference is smaller for the other two spectra. But the model is under-predicting the crack growth rate and this is observed as well in the crack length Vs. Number of cycle curves. This mismatch can be attributed to the over estimation of crack-tip plastic zone size especially due to the secondary plastic zone.

6.6   Summary

A Linear Damage Accumulation based model has been introduced and evaluated with experimental results. It has been shown that the model does not predict the crack growth well, when distinct load sequences occur in the applied spectrum. However, for load variations with small interaction effects and full aircraft spectra with randomly distributed load cycles, the model correlated fairly well with experimental results.

Furthermore, it has been observed from the experiments, that the crack growth retardation after an overload gradually diminishes until the crack growth rate has reached its level prior to the application of the overload. Although different in magnitude, the phenomenon corresponds qualitatively with the behavior observed for monolithic metals. Similar to metals is the dependency of the crack growth retardation on the overload ratio R_{OL}. Small ratio's results in less retardation and smaller delay zones.

Out of the three evaluated aircraft fuselage spectra, two correlated quite well with the predictions based on non-interaction. The spectrum for which the correlation was insufficient contained distinct severe peak cycles as compared to the remainder of the spectrum cycles. This might induce more distinct crack growth retardation, which is not captured by the non-interaction model. This supports the conclusion that the *LDA* based prediction of crack growth in *FMLs* can only be accurate if the load cycles are evenly and randomly distributed throughout the applied load spectrum.

The fatigue crack growth behavior in *FMLs* has been further investigated using a simple interaction model. The experimental data for different selective variable amplitude loading and flight spectra reasonably correlates with the Yield Zone model predictions. The basic assumption of small interaction

effects due to crack bridging proves to be valid.

In case of selective *VA* loading the prediction model performs well. In single overload, modified Wheeler model is able to predict the crack growth retardation and number of delay cycles exceptionally well. The same can be concluded for multiple overload and block load *(LO-HI)*.

For block loading, *LO-HI* is the spectrum which cannot cause crack growth retardation. Modified Wheeler model predictions are in good agreement with the test data. The model is able to follow the trend as the S_{MAX} is changed from *LO* to *HI*. However, for the HI-LO the model is able to predict the crack growth retardation but the number of delay cycles is different sequence, from the test data. This error is due to the basic definition of crack-tip plasticity being the only cause of crack growth retardation in the modified Wheeler prediction model.

For flight spectra, the model predict well for Spectrum I (Wide body fuselage spectrum) and Spectrum III (Mega liner front fuselage spectrum). For Spectrum II (Mega liner aft fuselage spectrum) predictions are relatively poor. This mismatch is due to the different nature (frequent overloads are occurring closely) of Spectrum II from other spectra.

Finally, the crack closure model is used to predict the crack growth for the selective and flight spectra. Although, the model is able to show the delayed retardation at the application of overload and the number of delayed cycles matches the experimental data more than Yield zone model. but for the flight spectra, the predictions are quite far from the experimental data. This mismatch can be attributed to the over estimation of crack-tip plastic zone especially due to the estimation of secondary plastic zone.

In short, the yield zone model, predicted well for most of the spectra with limited load variations i.e. small peak-to-peak ratio and less arbitrary/distinct distribution of load cycles in spectrum.

References

[1] S. U. Khan, R. C. Alderliesten, J. Schijve, R. Benedictus, On the fatigue crack growth prediction under variable amplitude loading, in: D. G. Pavlou (Ed.), Computational and experimental analysis of damaged materials 2007, Transworld Research Network, Kerala, India., 2007, Ch. 4, pp. 77–105.

[2] H. M. Plokker, S. U. Khan, R. C. Alderliesten, R. Benedictus, Fatigue crack growth in fibre metal laminates under selective variable ampli-

tude loading, Fatigue & Fracture of Engineering Materials and Struc-tures 32 (2009) 233–248.

[3] S. U. Khan, R. C. Alderliesten, R. Benedictus, Linear damage accumu-lation for predicting fatigue in fmls under variable amplitude loading, AIAA Journal of Aircraft 46 (2009) 1706–1713.

[4] O. Wheeler, Spectrum loading and crack growth., Tech. rep., ASMR 72 MetX also G.D. Report FZM 5602 (1970).

[5] M. Finney, Sensitivity of fatigue crack growth prediction (using whee-ler retardation) to data representation, Journal of Testing and Evalua-tion 17 (1989) 74–81.

[6] B. K. C. Yuen, F. Taheri, Proposed modification to the wheeler re-tardation model for multiple overloading fatigue cycles, International Journal of Fatigue 28 (2006) 1803–1819.

[7] D. M. Corlby, P. F. Packman, On the influence of single and multiple peak overloads on fatigue crack propagation in 7075-t6511 aluminum, Engineering Fracture Mechanics 5 (1973) 479–497.

[8] K. S. Kim, S. C. Kim, C. S. Shim, P. J. Y., A study on the effect of overload ratio on fatigue crack growth, Key Engineering Material 261-263 (2004) 1159–1168.

[9] K. S. Kim, S. C. Kim, C. S. Shim, H. M. Cho, A study on evaluation of overload effects on fatigue crack growth, Key Engineering Material 261-263 (2004) 1169–1178.

[10] F. Taheri, D. Trask, N. Pegg, Experimental and analytical investigation of fatigue characteristics of 350wt steel under constant and variable amplitude loadings, Journal of Marine Structures 16 (2001) 69–91.

[11] P. A. Rushton, F. Taheri, Prediction of variable amplitude crack growth in 350wt steel using a modified wheeler approach, Journal of Marine Structures 16 (2003) 517–539.

[12] J. M. Finney, Modelling for fatigue crack growth prediction in aircraft, Fatigue Fracture Engineering Materials & Structures 8 (1985) 205–222.

[13] H. Alawi, Designing reliably for fatigue crack growth under random loading, Engineering Fracture Mechanics 37 (1990) 75–85.

[14] K. Dolinski, Fatigue crack growth with retardation under stationary stochastic loading, Engineering Fracture Mechanics 27 (1987) 279–290.

[15] B. Sheu, P. S. Song, S. Hwang, Shaping exponent in wheeler model under a single overload, Engineering Fracture Mechanics 51 (1995) 135–143.

[16] Z. Khan, A. Rauf, M. Younas, Prediction of fatigue crack propagation life in notched members under variable amplitude loading, Journal of Material Engineering Performance 6 (1997) 365–373.

[17] M. Hawkayard, B. E. Pawell, J. M. Stephenson, Fatigue crack growth from simulation flight cycles involving superimposed vibrations, International Journal of Fatigue 21 (1999) 559–568.

[18] P. S. Song, B. C. Sheu, L. Chang, A modified wheeler model to improve predictions of crack growth following a single overload, JSME Internation Journal Series A 44 (2001) 117–22.

[19] M. A. Wahab, R. G. R., J. H. Park, Experimental study on the influence of overload induced residual stress field on fatigue crack growth in aluminium alloy, Journal of Material and Processing Technology 153-154 (2004) 945–951.

[20] M. Skorupa, Load interaction effects during fatigue crack growth under variable amplitude loading-a literature review. part i: Empirical trends, Fatigue & Fracture of Engineering Materials and Structures, 21 (1998) 987–1006.

[21] J. Schijve, Fatigue of Structures and Materials, Kluwer, 2001.

[22] M. A. Meggiolaro, J. T. Pinho de Castro, Comparison of load interaction models in fatigue crack propagation., in: Proceedings of the XVI Brazilian Congress in Mechanical Engineering (COBEM), ABCM, Vol. 12, 2001, p. 247256.

[23] M. Sander, H. A. Richard, Fatigue crack growth under variable amplitude loading part ii: analytical and numerical investigations, Fatigue Fracture Engineering Materials & Structures 29 (2006) 303–319.

[24] M. Skorupa, Empirical trends and prediction models for fatigue crack growth under variable amplitude loading, Tech. Rep. ECN-R-96-007, Netherlands Energy Research Foundation ECN, The Netherlands. (1996).

[25] P. C. Paris, M. P. Gomez, W. E. Anderson, A rational analytic theory of fatigue, The trend in Engineering 13 (1) (1961) 9–14.

[26] R. Alderliesten, Fatigue crack propagation and delamination growth in glare, Ph.D. thesis, Delft University of Technology, Delft (2005).

[27] R. C. Alderliesten, Analytical prediction model for fatigue crack pro-
pagation and delamination growth in glare, International Journal of
Fatigue 29 (2007) 628–646.

[28] A. U. de Koning, H. H. van der Linden, Prediction of fatigue crack
growth rates under variable amplitude loading using a simple crack
closure model, Tech. Rep. NLR MP 81023U, National Aerospace La-
boratory NLR, Amsterdam. The Netherlands (1981).

Chapter 7

PREDICTIONS:POST-STRETCHED LAMINATES

Occurrences in this domain are beyond the reach of exact prediction because of the variety of factors in operation, not because of any lack of order in nature.

Albert Einstein
(1879-1955)

Post-stretching is a potential method to change the unfavorable residual stress system in Fibre metal laminates (FMLs). During post-stretching of the material, the metal layers will be strained into the plastic region of the stress-strain curve, while the fibre layers remain elastic. After unloading, the residual stress system due to curing will be reduced or even reversed dependent on the amount of stretching. Classical laminate theory is further extended to calculate the stress redistribution after stretching the uni-directional laminates (ARALL and GLARE). This chapter present the method to calculate the residual internal stress distribution in the fibre direction. For the validation of the post-stretching formulations, fatigue crack growth tests performed on GLARE1-2/1, 3/2, 4/3, 5/4-0.3 have been compared with post-stretched prediction model.

ibre Metal Laminates *(FMLs)* are cured at elevated temperatures. At the curing temperature there are no internal stresses present. But during the cooling process the thermal contraction of the aluminium layers will be greater than the thermal contraction of the fibre layers as result of the difference in thermal expansion coefficients. This results in an un-favourable stress distribution of metal with tensile and fibre with compressive stresses.

Figure 2.1 shows that cooling down results in a tensile stress in the aluminium layers, which depends on the lay-up. This stress is unfavorable considering fatigue loading. The stress allows an increased crack opening and so enlarges the stress intensity factor variation at the crack tip.

Residual stress

		-100	0	100 Mpa
as cured	20°C -55°C	Fibers	Metals	
0.4% post-stretched	20°C -55°C	Metals	Fibers	

Compression ⟵   ⟶ **Tension**
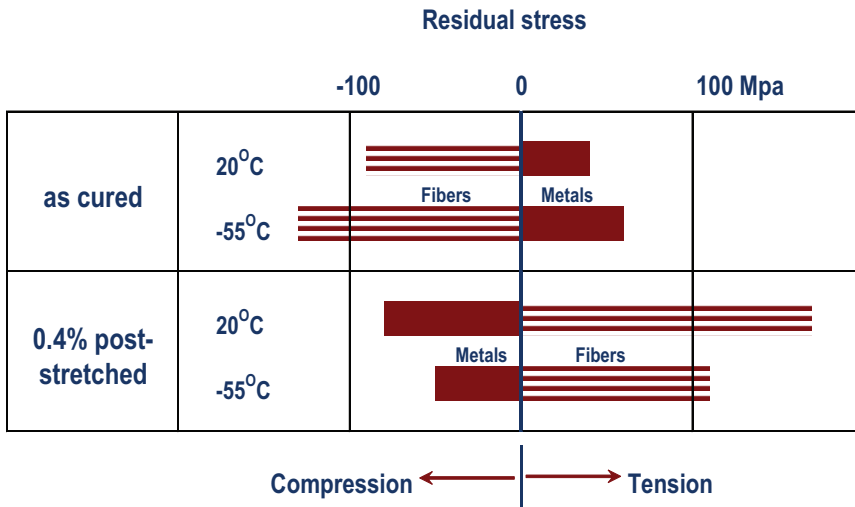
Figure 7.1: Residual stresses in the aluminium and fibre layers of *ARALL* in the as cured conditions and after post-stretching for room temperature and −55°C [1]

Post-stretching of cured fibre-metal laminates is sometimes performed to overcome potential negative effects of these residual tensile stress in the metal layers. The residual tensile stress in the aluminium layers can be reversed into a compressive stress by yielding the laminate to a small (positive) percentage. It has proven to have a beneficial effect on the fatigue properties. Post-stretching can be seen as a means to alter the internal stress distribution in the laminates to obtain desirable properties. The post-stretching mechanism is illustrated in figure 2.2.

The material state directly after the curing cycle is called the as-cured state.

For laminates containing the fatigue sensitive 7xxx aluminium, this state results in relatively poor fatigue properties compared to laminates containing 2024-T3 aluminium. The tensile stress can be altered by a small amount of yielding ($< 0.5\%$). The state after the stretching process is called post-stretched or pre-strained state of the material.
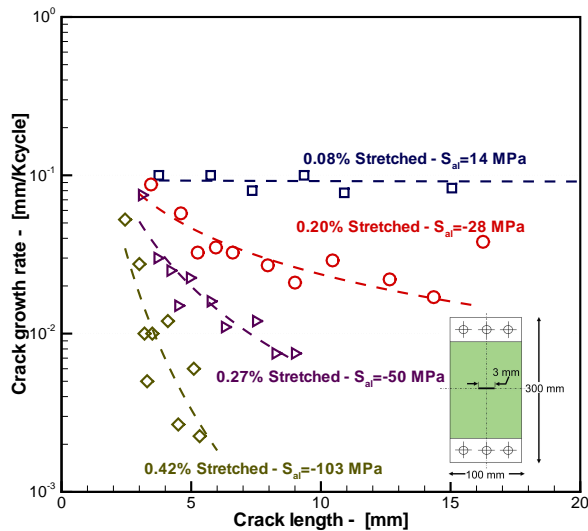
Figure 7.2: Effect of post-stretching level on the crack growth behaviour of GLARE1-3/2-0.3 at 150 MPa and R=0.05. [2]

An illustration of the residual stresses in the aluminium and fibre layers of *ARALL* is given in figure 7.1 for room temperature and $-55°$C. The residual stresses of the as-cured laminate increase for decreasing temperatures which is clearly visible in figures 2.1 and 7.1. Post-stretching of 0.4% reverses the residual stresses, resulting in compressive stresses in the aluminium layers and tensile stresses in the fibre layers.

Post-stretching results in improved fatigue initiation and crack growth properties. This can be attributed to three main reasons: First, due to the downward shift of stress cycle i.e., reduction of mean stress S_{mean}. Second, the tensile residual stresses in the prepreg reduce the extent of micro buckling failure of fibres (specially in case of aramid fibres), providing improved crack bridging. Third, the compressive residual stresses in aluminium have a crack closing effect and result in crack growth retardation in metal layers. Figure 7.2 shows the effect of the post-stretching percentage on fatigue crack growth for GLARE1-3/2-0.3 at S_{max} =150 MPa and R=0.05. The crack growth rate is highly influenced by the post-stretching percentage. Figure 7.3 com-
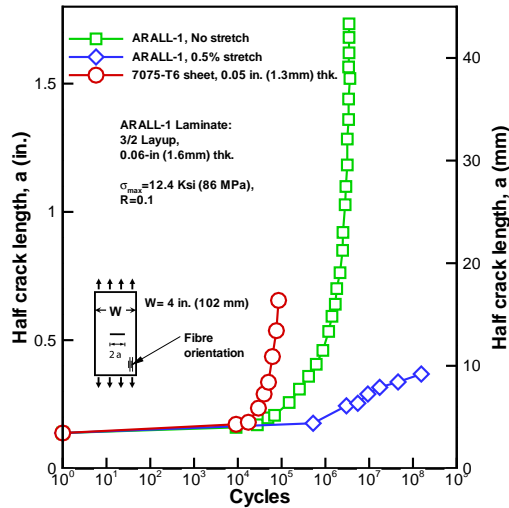
Figure 7.3: Fatigue crack growth of stretched and un-stretched ARALL-1 Laminate and 7075-T6 sheet. ARALL-1 Laminate: 3/2 lay-up; 1.6mm (0.06 in.) thick. 7075-T6 sheet: 1.3mm (0.05 in.) thick. σ_{max}=85.5 MPa (12.4 ksi), R=0.1 [3]

pares the crack growth of stretched, non-stretched ARALL and aluminium 7075-T6.

Post-stretching the laminate at higher percentages will result in plastic deformation that reduces the compressive yield strength of the laminate, due to the so-called Bauschinger effect [4–6].

7.1   Mathematical Modeling of Post-Stretching

The classical laminate theory (CLT) does not account for the laminates that have been cured at a temperature different from the design operating temperature. Homan [7] modified the *CLT* by incorporating the thermal and curing stress components. Honselaar [8] has incorporated a formulation in the CLT to calculate the residual internal stress in metal layer after post-stretching, while he used the Marissen model [9] for fatigue crack growth predictions. In this chapter, the Honselaar technique is used to calculate the residual internal stress in metallic layers but it is implemented in Alderliesten model [10, 11].

For fatigue crack growth prediction for post-stretched laminates, a post-
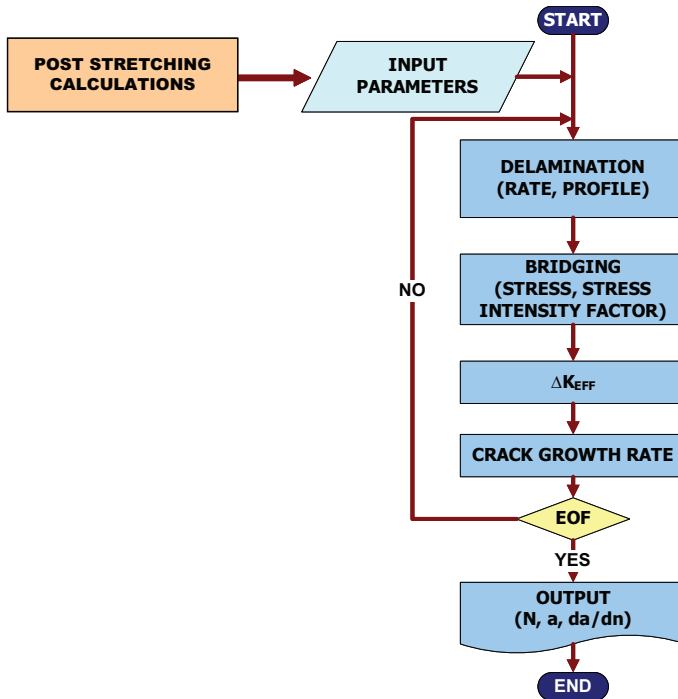
Figure 7.4: Flow diagram for the crack growth prediction model

stretching subroutine is added to the analytical model of Alderliesten [10, 11]. The flow diagram of the prediction model is shown in figure 7.4. The input parameters are the post-stretched stress state (output of post-stretching subroutine), input parameters i.e., material parameters, crack geometry, Paris constants for crack and delamination growth and initial delamination shape. Outputs are crack length, crack growth rate, number of cycles.

7.2   Test Specifications

Test data presented in [12] is used for the validation of the calculation procedure explained in the section 7.1. Fatigue crack growth tests have been performed on center-cracked tension *(CCT)* specimens, for which the geometry is illustrated in figure 7.5. The starter notches were made by drilling a hole of 1.5 mm diameter with two saw cuts, directing perpendicular to the loading direction. The total length of the starter notch $(2a_0)$ was approximately 3 mm.
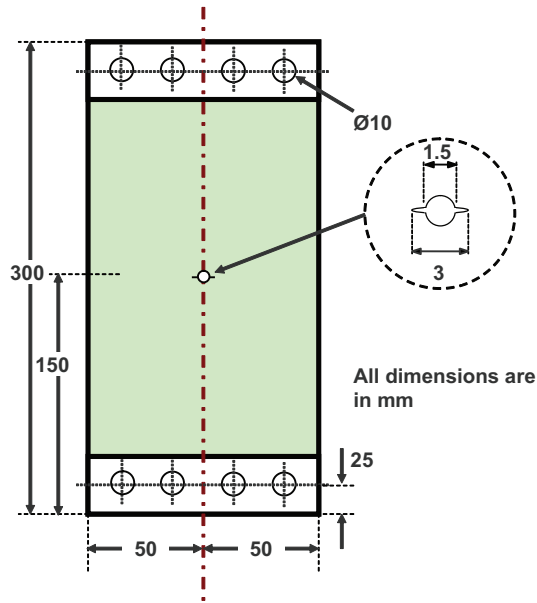
Figure 7.5: Test specimen dimensions

The tests were conducted in lab air at room temperature on a closed loop mechanical and computer controlled servo-hydraulic material testing system (MTS) with a load capacity of 6 metric tons. Constant amplitude sinusoidal shaped cycles were applied at frequency of 10 Hz. The crack length was visually inspected with a microscope (magnification 15X). The tests were stopped at a crack length of a=20 mm or at a number of 500,000 fatigue cycles. The half crack length of the left and right crack was recorded every 20,000 cycles for the first 100,000 cycles and later for every 50,000 cycles. Final crack growth curves were generated with an average between left and right half crack length. Details of these tests have been given in Table 7.1.

7.3   Results and Discussion

Figure 7.6-(a) exhibits the comparison of test results with the predictions for GLARE1-2/1-0.3 with S_{max}=150 MPa and R = 0.05. The comparison is done for the 0.065% and 0.27% post-streching. For both post-stretching percentages the fatigue crack growth predicitons are fairly close to the test data. But in case of high post-streching precentages, i.e., 0.30 and 0.42, shown in figure 7.6-(b) and (a), predictions are not accurate enough. However, for

Table 7.1: GLARE1 test matrix for validation of calculations

Maximum applied stress S_{max}	Stress ratio R	Post-stretching %	Lay-up
120	0.1	0.065,0.30,0.45	2/1
		0,0.20,0.32,0.45	3/2
		0,0.20,0.40	4/3
		0,0.14,0.33	5/4
150	0.1	0.065,0.27	2/1
		0.08,0.2,0.27,0.42	3/2
		0.13,0.30	5/4

the low post-stretching percentages and smaller crack lengths, the prediction model is able to capture the trends. The difference between the predictions and test results in case of highly post-stretched laminates can be explained using dK/da, which has been introduced by Schijve [13]. The strongly negative dK/da value for the highly post-stretched materials (e.g.as shown in figure 7.6-(a)), will reduce the crack growth rate and will lead to the crack arrest. For negative dK/da, even in the case of CA loading, previous load cycles can act similar to peak loads for the following cycles and reduce the crack growth. This can be one of the reason of reduction in crack growth rate. Schijve [14] has explained this decreasing $K(a)$ function using crack edge loading.

The accuracy of prediction is also influenced by the layup. Comparing figure 7.6-(a), (b) and (a) it is observed that by increasing the number of metallic-fibre interfaces, the error increases between the prediction and test results. Similar trend is observed in the case of S_{max}=120 MPa, shown in figure 7.7-(a), (b), (a) and (b). This observation can be explained by looking at the post-stretching process. During post-stretching process, aluminium layers are plastically deformed. Due to yielding and subsequent strain hardening the yield strength changes, which has an effect on the crack growth behavior [15–17]. This is not accounted for in the model. In addition, one could expect that the post-stretching procedure affects the interface between aluminium and fibre. The aluminium yields and elongates, while the fibres do not and the adhesive in-between has to remain compatible. This could also effect the fatigue delamination resistance. Despite the fact that number of fibre-metal interfaces are considered in the model but the change in behaviour at the interfaces is not accounted for in the model. This also explains the initial correlation between the test and prediction. Furthermore, during the calculation only the elastic Poisson ratio is used which as-a-matter-of-fact can contribute to the error in the predictions and tests. On top of all that, the accuracy of post-stretching procedure can not be neglected. Obtai-
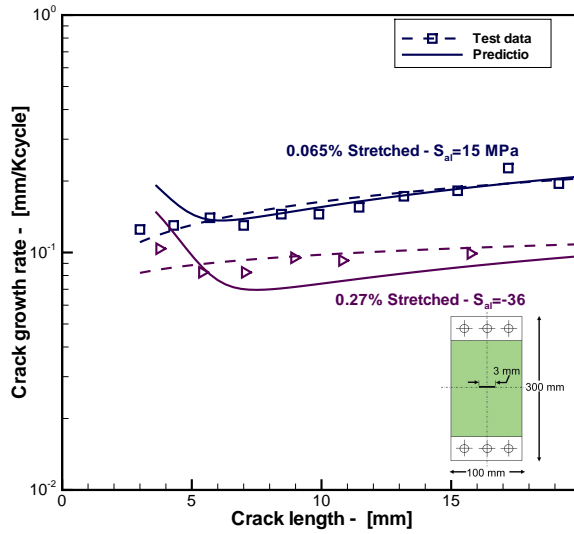
(a)
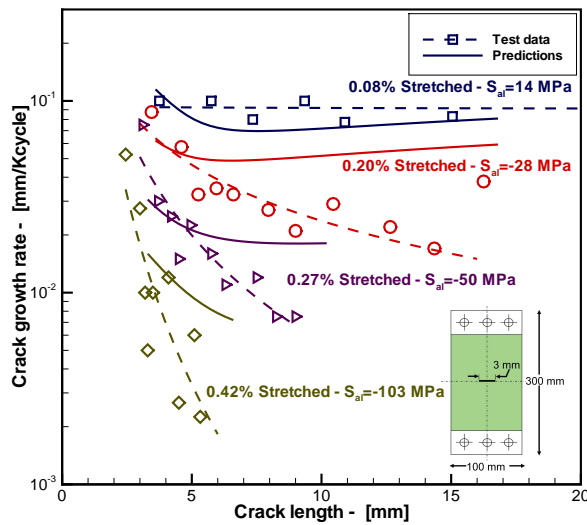
(b)

Figure 7.6: Comparison of test result and fatigue crack growth prediction for (a) GLARE1-2/1-0.3, $S_{max}=150\,\mathrm{MPa}$, R=0.05; (b) GLARE1-3/2-0.3, $S_{max}=150\,\mathrm{MPa}$, R=0.05

ning a required percentage of post-stretching within very small tolerances is not easy, but has significantly effect the stress distribution and subsequent

(a)

Figure 7.6: Comparison of test result and fatigue crack growth prediction for (a) GLARE1-5/4-0.3, $S_{max} = 150\text{MPa}$, $R = 0.05$

crack growth behavior.

Finally, high accuracy can never be expected for highly post-stretched laminates. The K values calculated with the model are the result of much higher (in absolute sense) positive K values due to external loading and negative K values resulting from post-stretching, have smaller relative error. However, when the absolute magnitude of these K values is added up, a large relative error can be expected. Nevertheless, the strongly decreasing predicted curves (shown in figures 7.6-(b), 7.7-(a) and 7.7-(b)), demonstrate the quality of the model.

The main focus of this chapter is post-stretching and the method to calculate the stress redistribution. From the comparison of test results and predictions, it can be concluded that the calculation of stress redistribution seems to work. The difference in prediction and test data is only related to crack growth and delamination as explained. To enhance the crack growth prediction, further investigation of these aspects is required. For example, the crack growth resistance could be determined for plastically stretched bare aluminium. In addition, delamination tests as reported in [10] could be repeated on post-stretched laminates.

(a)

(b)

Figure 7.7: Comparison of test result and fatigue crack growth prediction for (a). GLARE1-2/1-0.3, $S_{max} = 120\,MPa$, R = 0.05; (b) GLARE1-3/2-0.3, $S_{max} = 120\,MPa$, R = 0.05

(a)

(b)
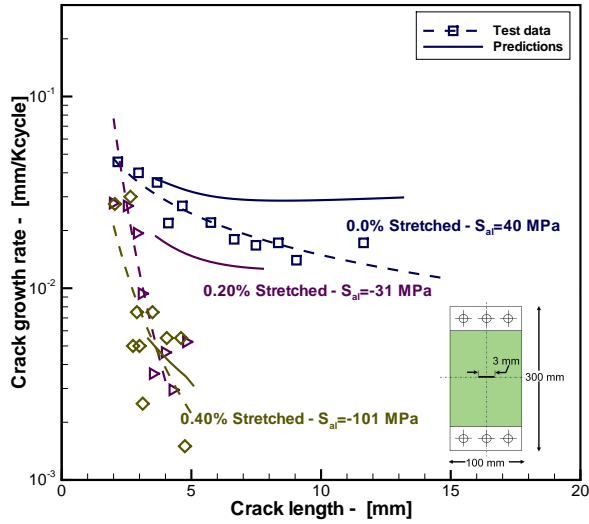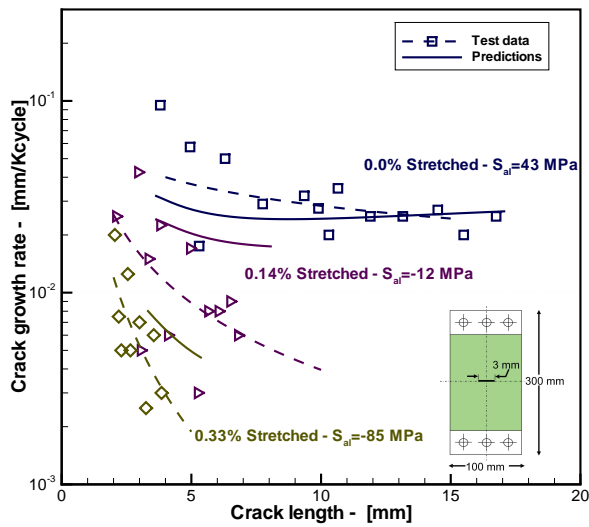
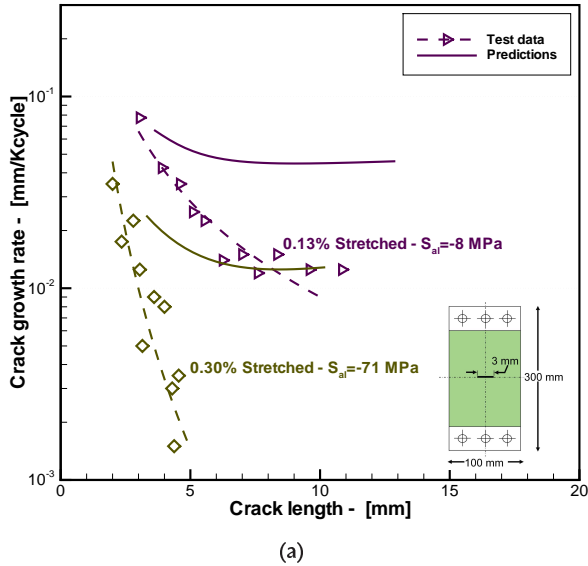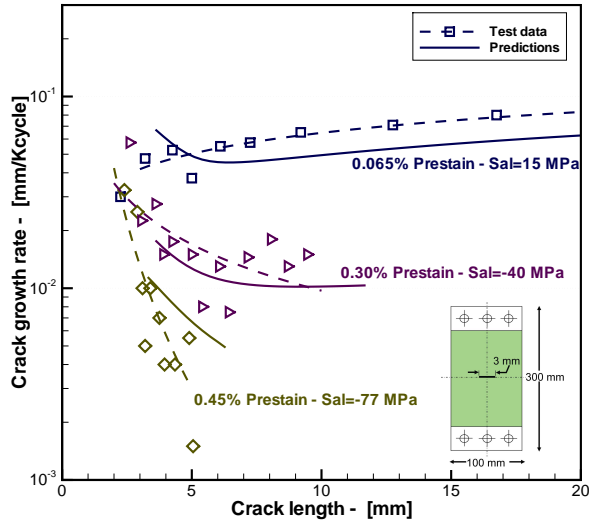**Figure 7.7:** Comparison of test result and fatigue crack growth prediction for (a). GLARE1-4/3-0.3, S_{max}=120MPa, R=0.05; (b) GLARE1-5/4-0.3, S_{max}=120MPa, R=0.05
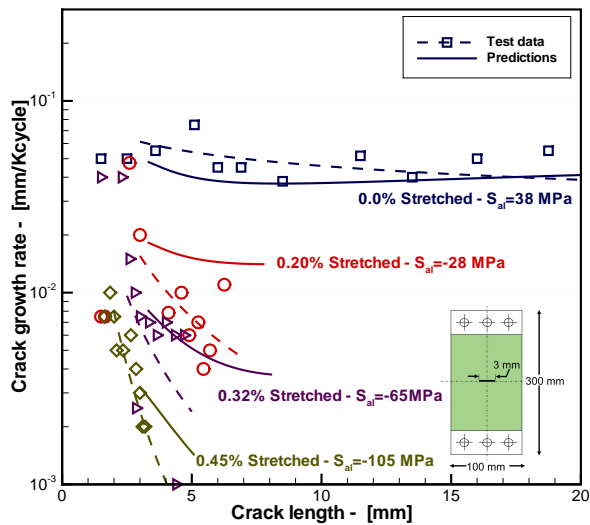
7.4 Summary

During curing of *FMLs* metallic layers have tensile stresses while the fibres have compressive stress. Post-stretching is the method to alter this unfa-

vourable internal stress distribution to favourable. Post-stretching results in compressive stress in metallic layers and tensile stress in fibre layers showing improvement of fatigue characteristics of *FMLs*.

In this chapter a method is presented to calculate the internal stress distribution in unidirectional *FMLs* after post-stretching. This modified classical laminate theory is implemented in already existing fatigue crack growth prediction model. A good correlation, between the test results and predictions, is obtained for the low post-stretching values. However, for high post-stretched laminates, the trends are predicted.

References

[1] G. H. J. J. Roebroeks, Towards glare, the development of a fatigue insensitive and damage tolerant aircraft material, Ph.D. thesis, Delft University of Technology, Delft (1991).

[2] R. C. Alderliesten, H. J. M. Woerden, Load history effects during fatigue crack propagation in glare, in: M. Guillaume (Ed.), Fatigue of Aeronautical structures as an Engineering Challenge, Vol. I, 2003, pp. 509–530.

[3] R. J. Bucci, L. N. Mueller, L. B. Vogelesang, J. W. Gunnink, Arall laminate, in: A. K. Vasudevan, R. D. Doherty (Eds.), Aluminium Alloys - Contemporary research and applications, Vol. 31 of Treatise on materials science and technology, Academic Press, Inc., 1989, Ch. 10, pp. 295–320.

[4] L. B. Vogelesang, R. Marissen, J. Schijve, Aircraft fatigue in the eighties, in: Proceedings of the 11th ICAF Symposium, Noordwijkerhout, Netherlands, 1981, p. 3.4/1.

[5] L. B. Vogelesang, J. W. Gunnink, Arall, a material for the next generation of aircraft - a state of the art, Tech. Rep. LR-400, Dept. of Aerospace Engineering, Delft University of Technology, Netherlands. (August 1983).

[6] A. Mendelson, Plasticity : Theory and Application, The Macmillan Company, USA., 1968.

[7] J. J. Homan, Fatigue initiation in fibre metal laminates, International Journal of Fatigue 28 (2006) 366–374.

[8] C. Honselaar, The residual internal stress distrubution in arall, Master's thesis, Delft University of Technology, Delft (1986).

[9] R. Marissen, Fatigue crack growth in arall - a hybrid aluminium-aramid composite material, Tech. rep., Delft University of Technology, Delft,LR-574 (1988).

[10] R. Alderliesten, Fatigue crack propagation and delamination growth in glare, Ph.D. thesis, Delft University of Technology, Delft (2005).

[11] R. C. Alderliesten, Analytical prediction model for fatigue crack propagation and delamination growth in glare, International Journal of Fatigue 29 (2007) 628–646.

[12] C. S. Pegels, A study on the residual stress of glare 1, Master's thesis, Delft University of Technology, Delft (August 1995).

[13] J. Schijve, F. A. Jacobs, P. J. Tromp, Fatigue crack growth in aluminium alloy sheet material specimens under flight simulation loading. effects of design stress level and loading frequency., Tech. Rep. NLR-TR 72019U, NLR-Amsterdam, The Netherlands (1972).

[14] J. Schijve, Fatigue of Structures and Materials, Kluwer, 2001.

[15] K. Schulte, R. Marissen, K.-H. Trautmann, H. Nowack, A contribution to the evaluation of sequence effects under variable amplitude loading by applying defined predeformations, in: G. Sih, E. Sommer, W. Dahl (Eds.), Application of Fracture Mechanics to Materials and Structures, Martinus Nijhoff Publisher, 1984, pp. 777–785.

[16] J. Schijve, The effect of pre-strain on fatigue crack growth and crack closure, Engineering Fracture Mechanics 8 (1976) 575–581.

[17] T. Kang, H. Liu, The effect of pre-stress cycles on fatigue crack growth - an analysis of the crack growth mechanism, Engineering Fracture Mechanics 6 (1974) 631–638.

Chapter 8

CONCLUSION

With a suddenness that startled them all, the wizard Gandalf sprang to his feet. He was laughing! "I have it!" he cried. "Of course, of course! Absurdly simple, like most riddles when you see the answer."

From The Fellowship, part 1 of the trilogy,
The Lord of the Rings
by J. R. R. Tolkien (Tolkien, 1954)

The investigation presented in this thesis is concerned with the fatigue crack growth behaviour of the aluminium layers in GLARE with the corresponding delamination growth behaviour at the aluminium/fibre interfaces under variable amplitude fatigue loading. The fatigue crack geometry considered is the through crack configuration with cracks in all aluminium layers having the same length equal to the visible crack length in the outer aluminium layers (this assumption is validated in chapter 5) .

The already developed fatigue crack and delamination growth model for constant amplitude has been extended to include variable amplitude loading. This variable amplitude prediction model has been implemented in a numerical programme, which has been verified with the results of an extensive test program presented in chapter 6

The model is based on the following assumptions:

- The damage mechanisms can be described with the concepts of Linear Elastic Fracture Mechanics.

- The crack growth rate can be related to the stress intensity factor with an empirical Paris equation.

- Plane stress conditions are applicable to the crack growth in metal layers.

- Plane strain conditions are applicable to the delamination growth at the interfaces.

- The delamination growth can be related to the strain energy release rate with an empirical Paris equation.

- The stress intensity factor at the crack tip can be determined by super-imposing the stress intensity factor for the far field opening stress and the stress intensity for the crack closing bridging stress.

- The interaction effects caused by the overload and *VA* loading is redu-ced by the intact fibres bridging the crack opening.

From the current investigation, several conclusions can be drawn with res-pect to the crack growth behaviour of GLARE and the crack growth prediction model. The conclusions are summarised hereafter.

8.1   Phenomena under Variable Amplitude Loading

During this research, fatigue crack growth and delamination growth were studied under variable amplitude loading. Although the mechanisms are coupled, they have been investigated independently prior to the study of combined growth mechanisms. The detailed conclusions about these phe-nomena are:

8.1.1   Delamination growth

The delamination growth behaviour in *GLARE* has been investigated with delamination experiments using double cracked lap-shear specimens, va-rious load sequences and load spectra. It has been observed in the block load sequence tests that the average delamination growth rate is independent of

the applied load sequence. In addition, no influence of different delamination growth measurement techniques has been observed on the growth rate in particular at the transition from low to high loads block.

Full flight spectrum tests have been performed, because it was thought that the block load sequence tests might not be sufficiently accurate to capture potential interaction effects. Correlation of the observed growth with linear damage accumulation prediction clearly showed that the delamination growth acceleration or retardation, due to overloads or load variations, under mode II delamination growth in *GLARE* are absent.

However, the Rain-flow counting technique must be used to load spectra with intermediate small cycles in the large cycles to calculate the delamination growth rate. Predictions correlated very well with the test results for the flight spectrum as well as the programmed block loading spectra, after applying this technique. This highlights the conclusion that delamination growth is mainly dependent on the high monotonic loads and load amplitudes.

ARALL and *GLARE* laminates have different delamination characteristics. Interaction effects were reported by Marissen in case of *ARALL*. On the other hand, *GLARE* specimens, when tested using the same load spectra, did not show any interaction effect. Further investigation on *ARALL* and *GLARE* showed that fibre-adhesive bonding, peel strength and multiple delamination paths have insignificant influence on the resulting delamination growth rate. Here, the topography of the fibres is considered to be the major reason to cause different delamination behaviour between *ARALL* and *GLARE*.

While looking at the delaminated surfaces in GLARE using *SEM*, no markings were observed at the fibre side, but at the resin/metal side striations (markings) due to delamination growth were observed. In case of block load sequences (LO-HI and HI-LO), no interaction effects were observed considering the striations and their spacing. For the periodic load sequences striations were observed and their spacings could be related to the maximum applied stress S_{max}.

8.1.2   Delamination shapes

The load variations slightly change the delamination shape in a *CCT* specimen. This change in delamination shape predominantly relates to the crack growth retardation in metal layers after application of the overload. However, this mechanism is insufficient to completely describe the transition of the delamination after the application of an overload. The transition can fully be understood, if in addition, the local post-stretching mechanism near the crack tip is considered.

The effect of this transition in delamination shape on subsequent fatigue crack growth has been related to the change in stress intensity. This investigation has evidently shown that the transition in delamination shape has no evident effect on the change in stress intensity factor and finally on the subsequent fatigue crack growth.

In other words, for accurately predicting the fatigue crack growth after an overload, it will be sufficient to attribute the transition of delamination shape solely to the crack retardation in metal layers, thus ignoring the post-stretching mechanism.

8.1.3   Crack-tip plasticity

Plastic zones created during the fatigue crack growth tests are predicted using the Irwin plastic zone relation, and are measured in the tests using Digital Image Correlation *(DIC)*. In case of monolithic metal and metal laminates, a big difference is observed between the predicted and measured sizes. Contrary, a small difference is observed between the predicted and measured plastic zone size in GLARE. The plastic zone size calculated and as measured for *GLARE* is almost constant at any crack length, which corresponds to the constant K_{tip} observed for *GLARE*.

8.1.4   Shear-lip formation

Shear-lip formation has been studied for monolithic metal, metal laminates and *FMLs*.

Monolithic metals have shown the typical shear-lip profile with the early tensile mode followed by a transition mode and finally the shear mode. For metal laminates (without fibres) the mode transition happens quite late during the fatigue crack growth life, but the transition length is smaller as compared to monolithic metals.

In *FMLs*, the crack propagates mainly in the tensile mode. Crack surfaces showed a quite clear tensile mode and no transition from tensile to shear mode.

8.2   Prediction Model

8.2.1   Linear Damage Accumulation

A Linear Damage Accumulation based model has been introduced and eva-
luated with experimental results. It has been shown that the model does
not predict the crack growth well when distinct load sequences occur in the
applied spectrum. However, for load variations with small interaction ef-
fects and for full aircraft load spectra with randomly distributed load cycles,
the model correlated fairly well with experimental results.

8.2.2   Modified Yield Zone Model

The fatigue crack growth behavior in *FMLs* has been further investigated
using a simple interaction model. The experimental data for different selec-
tive variable amplitude loading and flight spectra correlates reasonably with
the Yield Zone model predictions.

8.2.3   Crack-closure model

A crack closure model was used to predict the crack growth for the selec-
tive load sequences and flight load spectra. The model is able to show the
delayed retardation after the application of overloads and the number of
delayed cycles correlated better with the experimental data than the Yield
zone model. However, for the flight load spectra, the predictions are quite
far from the experimental data. The under prediction of fatigue crack growth
under flight spectra can be attributed to the over estimation of crack-tip
plastic zone especially due to the secondary plastic zone.

8.3   Future Work

Delamination growth under variable amplitude loading needs to be further
investigated, especially on a microscopic level at the fibre and metal inter-
face. At macroscopic level no plasticity is observed in the resin layer, as
detailed in this thesis. However, questions that may require further funda-
mental research are: how the delamination resistance be influenced by the
elastic plastic behaviour of resin (and this plasticity at the delamination tip)?
and How the thickness of resin would influence the results presented in this
thesis?

The next step in understanding fatigue in *FMLs* is the transition of mode-I (tensile) to mode-I and II (shear). Current research briefly touched upon this topic but compared the 2 mm Al monolithic metal with the laminates having cumulative 2 mm metal thickness. The logical next step would be to understand the effect of thickness of metal layers on the moment of transition and transition length. The follow-up questions can be whether the transition has any influence on the crack growth resistance, and whether the postponing the transition in inner sheets has a greater effect on the crack resistance. How does the stress state can be explained for the laminates with thick metal layers by using the understanding developed with the thin metal layers?

The next step in the modeling phase would be to understand the mismatch of crack closure model prediction with the test results for the flight spectra. This can be done by detailed study of different spectra and further validation of De Koning primary and secondary plastic zone assumption for *FMLs*.

Finally, it would be a logical step to integrate the *VA* loading model with the crack growth prediction model of laminates with variable thickness of metal layers (i.e., work of Greg Wilson), which can result in fatigue crack growth model for arbitrary *FMLs* under arbitrary loads. However, this integration can be quite challenging due to the effect of different metal layer's thickness on the crack growth, delamination shape and growth phenomena.

A

Energy Release Rate Equations

For delamination over a distance b, the elastic energies of the sheets and the fibre layers change due to a change of the stress in those layers after delamination. The external energy changes as well due to a displacement of the external load P. Figure A.1 shows the situation before and after some delamination.

The total energy balance is given

$$\frac{d}{db}W = \frac{d}{db}\left(F - \Delta U\right) \tag{A.1}$$
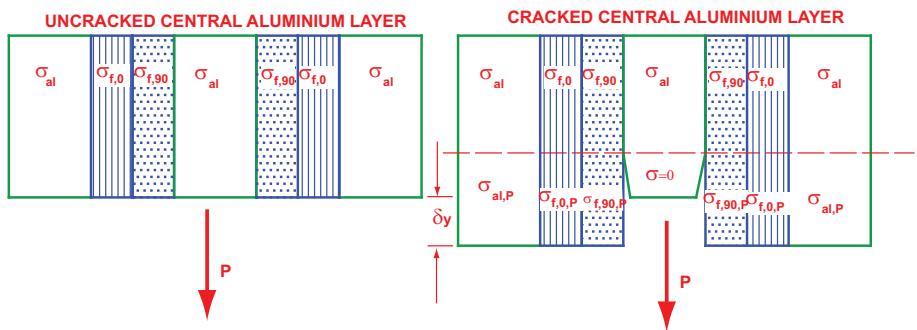
Figure A.1: The change of stress levels after delamination

where ΔU is the increase in elastic energy within the laminate due to delamination extension of length b, F is the work applied to the system during the displacement δy of the external force P, and W is the energy available per increment of crack extension.

As for the energy

$$F = P\delta y \qquad \Rightarrow \qquad P(b\Delta\varepsilon^*) \qquad (A.2)$$

where $\Delta\varepsilon^*$ is the strain difference between the delaminated and non-delaminated area of the laminate and can be calculated using

$$\Delta\varepsilon^* = \left(\frac{\sigma_{al,P} - \sigma_{al}}{E_{al}} \right) \qquad (A.3)$$

where $\sigma_{al,p}$ is the stress in the delaminated area, σ_{al} is the stress in the non-delaminated area of the laminate and E_{al} is the Young's modulus of aluminium. Applied load P is

$$P = \sigma_{al}n_{al}t_{al} + \sigma_{f,0}n_{f,0}t_{f,0} + \sigma_{f,90}n_{f,90}t_{f,90} \qquad (A.4)$$

From equations A.2 to A.4, it follows that

$$F = \sigma_{lam}t_{lam}\left[b\frac{\sigma_{al,P} - \sigma_{al}}{E_{al}} \right] \qquad (A.5)$$

where σ_{lam} is laminate stress and t_{lam} is the laminate thickness.

If U_1 is the increase of elastic energy in the delaminated laminate and U_2 the decrease of elastic energy in the non-delaminated laminate the total change (increase) of the elastic energy during delamination over distance b is

$$\Delta U = U_1 - U_2 \qquad (A.6)$$

The elastic energy of a uni-axially loaded body is given by

$$U_x = \frac{1}{2}\frac{\sigma^2}{E_x}volume$$

The strain energy in non-delaminated laminate is given by

$$U_2 = \frac{b}{2}\left[\frac{\sigma_{al}^2}{E_{al}}n_{al}t_{al} + \frac{\sigma_{f,0}^2}{E_{f,0}}n_{f,0}t_{f,0} \right.$$
$$\left. + \frac{\sigma_{f,90}^2}{E_{f,90}}n_{f,90}t_{f,90} \right] \qquad (A.7)$$

And for the delaminated laminate it is written as

$$U_1 = \frac{b}{2} \left[\frac{\sigma_{al,P}^2}{E_{al}} (n_{al} - n_{cr}) t_{al} + \frac{\sigma_{f,0,P}^2}{E_{f,0}} n_{f,0} t_{f,0} \right. $$
$$\left. + \frac{\sigma_{f,90,P}^2}{E_{f,90}} n_{f,90} t_{f,90} \right] \tag{A.8}$$

In these equations E is the Young's modulus, n is the number of layers and t is the layer thickness. The subscripts al, $f,0$ and $f,90$ indicate respectively the aluminium, the prepreg with fibres in the loading direction and the prepreg layer with fibres perpendicular to the loading direction.

Lamina stresses can be expressed as functions of the total applied laminate stress σ_{lam} using parameters λ and γ.

$$\sigma_{al} = \lambda \sigma_{lam} \qquad\qquad \sigma_{al,P} = \gamma \sigma_{lam}$$

$$\sigma_{f,0} = \frac{E_{f,0}}{E_{al}} \lambda . \sigma_{lam} \qquad\qquad \sigma_{f,0,P} = \frac{E_{f,0}}{E_{al}} \gamma . \sigma_{lam}$$

$$\sigma_{f,90} = \frac{E_{f,90}}{E_{al}} \lambda . \sigma_{lam} \qquad\qquad \sigma_{f,90,P} = \frac{E_{f,90}}{E_{al}} \gamma . \sigma_{lam}$$

γ and λ are defined as

$$\gamma = \frac{t_{lam}}{(n_{al} - n_{cr}) t_{al} + \frac{E_{f,0}}{E_{al}} n_{f,0} t_{f,0} + \frac{E_{f,90}}{E_{al}} n_{f,90} t_{f,90}}$$

$$\lambda = \frac{t_{lam}}{n_{al} t_{al} + \frac{E_{f,0}}{E_{al}} n_{f,0} t_{f,0} + \frac{E_{f,90}}{E_{al}} n_{f,90} t_{f,90}}$$

where n_{cr} is the number of cracked aluminium layers. Equations A.5, A.7 and A.8 can be simplified by replacing γ and λ.

$$F = b \sigma_{lam}^2 [\gamma - \lambda] t_{lam} \tag{A.9}$$

$$U_1 = \frac{b \sigma_{lam}^2}{2} \left[\frac{\lambda^2}{E_{al}} (n_{al} - n_{cr}) t_{al} + \frac{\left(\frac{E_{f,0}}{E_{al}} \gamma\right)^2}{E_{f,0}} n_{f,0} t_{f,0} \right.$$
$$\left. + \frac{\left(\frac{E_{f,90}}{E_{al}} \gamma\right)^2}{E_{f,90}} n_{f,90} t_{f,90} \right] \tag{A.10}$$

$$U_2 = \frac{b \sigma_{lam}^2}{2} \left[\frac{\lambda^2}{E_{al}} n_{al} t_{al} + \frac{\left(\frac{E_{f,0}}{E_{al}} \lambda\right)^2}{E_{f,0}} n_{f,0} t_{f,0} \right.$$
$$\left. + \frac{\left(\frac{E_{f,90}}{E_{al}} \lambda\right)^2}{E_{f,90}} n_{f,90} t_{f,90} \right] \tag{A.11}$$

Substituting equations A.9, A.10 and A.11 in equation A.1, one can calculate G

$$\frac{d}{db}W = \frac{d}{db}\left[F - (U_1 - U_2)\right] = \frac{d}{db}\left(F - U_1 + U_2\right)$$

$$
\begin{aligned}
G = \frac{d}{db}W = \frac{d}{db}\Bigg[& \frac{b\sigma_{lam}^2}{2}\Bigg[2(\gamma - \lambda)t_{lam} \\
& - \frac{\lambda^2}{E_{al}}(n_{al} - n_{cr})t_{al} - \frac{\left(\frac{E_{f,0}}{E_{al}}\gamma\right)^2}{E_{f,0}}n_{f,0}t_{f,0} \\
& - \frac{\left(\frac{E_{f,90}}{E_{al}}\gamma\right)^2}{E_{f,90}}n_{f,90}t_{f,90}\frac{\lambda^2}{E_{al}}n_{al}t_{al} \\
& + \frac{\left(\frac{E_{f,0}}{E_{al}}\lambda\right)^2}{E_{f,0}}n_{f,0}t_{f,0} \\
& + \frac{\left(\frac{E_{f,90}}{E_{al}}\lambda\right)^2}{E_{f,90}}n_{f,90}t_{f,90}\Bigg]\Bigg]
\end{aligned}
\tag{A.12}
$$

Equation A.12 gives the total energy release rate for four fibre-aluminium interfaces. The energy release rate per fibre-aluminium interfaces is given by $G/4$, or it can be generalized by G/j, where j is the number of fibre-aluminium interfaces. The energy release rate for delamination, per fibre-aluminium interface G_d can be, then, simplified as

$$
\begin{aligned}
G_d = \frac{\sigma_{lam}^2}{2jE_{al}}\Bigg[& \frac{\lambda^2}{E_{al}}(n_{al} - n_{cr})t_{al} - \lambda^2 n_{al}t_{al} + \\
& \frac{E_{f,0}}{E_{al}}n_{f,0}t_{f,0}(\gamma^2 - \lambda^2) + \\
& \frac{E_{f,90}}{E_{al}}n_{f,90}t_{f,90}(\gamma^2 - \lambda^2)\Bigg]
\end{aligned}
\tag{A.13}
$$

B

Post-Stretched Classical Laminate Theory

The three-dimensional thermoelastic anisotropic stress-strain relations are

$$\varepsilon_i = S_{ij}\sigma_j + \varepsilon_{i,pl} + \alpha_i \Delta T \, i, j = 1, 2, ..., 6 \tag{B.1}$$

Wherein the total strains, ε_i, are the sum of the mechanical strains, $S_{ij}\sigma_j$, pre-strains, $\varepsilon_{i,pl}$ and the six free thermal strains, $\alpha_i \Delta T$, for a temperature change ΔT. The three dimensional stress-strain relations are obtained by inversion

$$\sigma_i = C_{ij}\left[\varepsilon_i - \varepsilon_{i,pl} - \alpha_i \Delta T\right] i, j = 1, 2, ..., 6 \tag{B.2}$$

In both Equations B.1 and B.2, the six α_i are the coefficients of thermal deformation (expansion or contraction and distortion, i.e., shear), and ΔT is the temperature difference. In Equation B.2, the terms $C_{ij}\alpha_i\Delta T$ are the thermal residual stresses if the total laminate strain is zero.

For a plane stress state in an orthotropic lamina in the principal material coordinates yields

$$\begin{bmatrix} \sigma_1 \\ \sigma_2 \\ \tau_{12} \end{bmatrix} = \begin{bmatrix} Q_{11} & Q_{12} & 0 \\ Q_{12} & Q_{22} & 0 \\ 0 & 0 & Q_{66} \end{bmatrix} \begin{bmatrix} \varepsilon_1 - \varepsilon_{1,pl} - \alpha_1 T \\ \varepsilon_2 - \varepsilon_{2,pl} - \alpha_2 T \\ \gamma_{12} \end{bmatrix} \tag{B.3}$$

		UD Glass Prepreg	7475–T761
E_{11}	$[\text{MPa}]$	54000	72000
E_{22}	$[\text{MPa}]$	9410	72000
G_{12}	$[\text{MPa}]$	5550	26400
μ_{12}		0.33	0.33
μ_{21}		0.0575	0.33
α_{11}	$[10^{-6}C^{-1}]$	6.1	24
α_{22}	$[10^{-6}C^{-1}]$	26.2	24

Table B.1: Material Properties [1]

Where

$$Q_{11} = \frac{E_1}{1-\mu_{12}\mu_{21}} Q_{22} = \frac{E_2}{1-\mu_{12}\mu_{21}}$$

$$Q_{12} = \frac{\mu_{12}E_2}{1-\mu_{12}\mu_{21}}$$

$$Q_{66} = G_{12}$$

Values of all these material parameters for *GLARE* are given in Table B.1. Note that the coefficients of thermal expansion affect only extensional strains, not the shear strain. Equation B.3 can be written as

$$\begin{bmatrix} \sigma_1 \\ \sigma_2 \\ \tau_{12} \end{bmatrix} = [Q] \begin{bmatrix} \varepsilon_1 - \varepsilon_{1,pl} - \alpha_1\Delta T \\ \varepsilon_2 - \varepsilon_{2,pl} - \alpha_2\Delta T \\ \gamma_{12} \end{bmatrix}$$

For transformation of the properties from the principal material coordinates to laminate coordinate, transformation matrix, M is used

$$M = \begin{bmatrix} \cos^2\theta & \sin^2\theta & 2\cdot\cos\theta\cdot\sin\theta \\ \sin^2\theta & \cos^2\theta & -2\cdot\cos\theta\cdot\sin\theta \\ -\cos\theta\cdot\sin\theta & \cos\theta\cdot\sin\theta & \cos^2\theta-\sin^2\theta \end{bmatrix}$$

Where θ is the angle from x-axis to the 1-axis (see figure B.1).

The transformation matrix is applied using the transformation relation with superscript T denoting the matrix transpose.

$$[\bar{Q}] = [M]^{-1}[Q][M]^{-T}$$

The stresses in the laminate coordinates for the Kth layer obtained by the transformation of coordinates (Figure. B.1) are
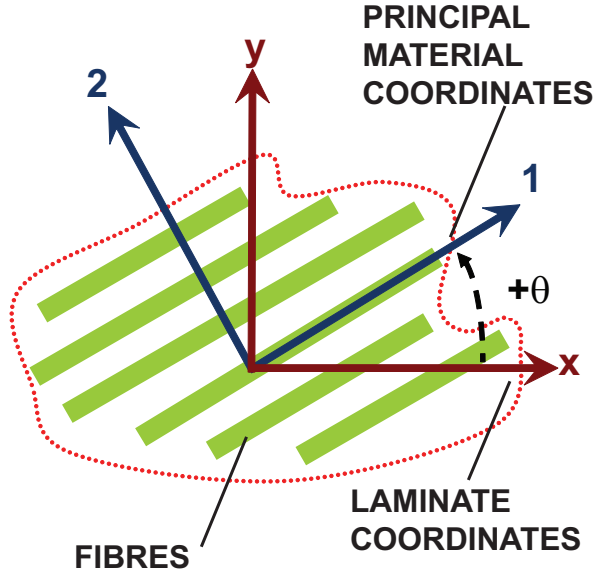
Figure B.1: Positive rotation of principal material axes from arbitrary x-y axes

$$
\begin{bmatrix} \sigma_x \\ \sigma_y \\ \tau_{xy} \end{bmatrix} = [\bar{Q}] \begin{bmatrix} \varepsilon_x - \varepsilon_{x,pl} - \alpha_x \Delta T \\ \varepsilon_y - \varepsilon_{y,pl} - \alpha_y \Delta T \\ \gamma_{xy} \end{bmatrix}
\tag{B.4}
$$

The strains for the kth layer at a distance z from the middle of the laminate, as shown in figure B.2, are

$$
\begin{bmatrix} \varepsilon_x \\ \varepsilon_y \\ \gamma_{xy} \end{bmatrix}_k = \begin{bmatrix} \varepsilon_x \\ \varepsilon_y \\ \gamma_{xy} \end{bmatrix}_0 + z \begin{bmatrix} k_x \\ k_y \\ k_{xy} \end{bmatrix}_0 + \begin{bmatrix} \varepsilon_{x,pl} \\ \varepsilon_{y,pl} \\ 0 \end{bmatrix}_0
\tag{B.5}
$$

Where ε_{i_0} are the middle surface strains, k_{i_0} are the middle surface curvatures and ε_{i,pl_0} are the middle surface plastic strains of the laminate.

When the linear variation of strain through the thickness, equation B.5, is substituted into equation B.4 and the resulting expressions for the layer stresses are integrated through the thickness, the force resultants for uni-directional *FMLs* (the principal material coordinates 1,2 of the layers coincides with the laminate coordinates x,y i.e., $\theta = 0$), are
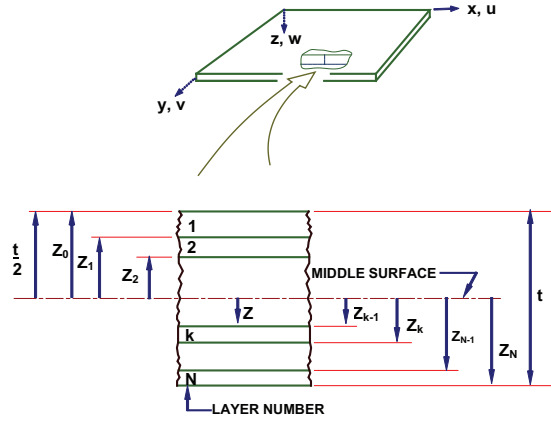
Figure B.2: Geometry of an n-layered laminate

$$
\begin{bmatrix} N_1 \\ N_2 \\ N_{12} \end{bmatrix} = \begin{bmatrix} A_{11} & A_{12} & A_{16} \\ A_{12} & A_{22} & A_{26} \\ A_{16} & A_{26} & A_{66} \end{bmatrix} \begin{bmatrix} \varepsilon_1 + \varepsilon_{1,pl} \\ \varepsilon_2 + \varepsilon_{2,pl} \\ \gamma_{12} \end{bmatrix}_0 +
$$

$$
\begin{bmatrix} B_{11} & B_{12} & B_{16} \\ B_{12} & B_{22} & B_{26} \\ B_{16} & B_{26} & B_{66} \end{bmatrix} \begin{bmatrix} k_1 \\ k_2 \\ k_{12} \end{bmatrix}_0 - \begin{bmatrix} N_1^T \\ N_2^T \\ N_{12}^T \end{bmatrix} \qquad (B.6)
$$

$$
\begin{bmatrix} M_1 \\ M_2 \\ M_{12} \end{bmatrix} = \begin{bmatrix} B_{11} & B_{12} & B_{16} \\ B_{12} & B_{22} & B_{26} \\ B_{16} & B_{26} & B_{66} \end{bmatrix} \begin{bmatrix} \varepsilon_1 + \varepsilon_{1,pl} \\ \varepsilon_2 + \varepsilon_{2,pl} \\ \gamma_{12} \end{bmatrix}_0 +
$$

$$
\begin{bmatrix} D_{11} & D_{12} & D_{16} \\ D_{12} & D_{22} & D_{26} \\ D_{16} & D_{26} & D_{66} \end{bmatrix} \begin{bmatrix} k_1 \\ k_2 \\ k_{12} \end{bmatrix}_0 - \begin{bmatrix} M_1^T \\ M_2^T \\ M_{12}^T \end{bmatrix} \qquad (B.7)
$$

Where:

$$
A_{ij} = \sum_{k=1}^{n} \left(\bar{Q}_{ij} \right)_k \left(Z_k - Z_{k-1} \right)
$$

$$
B_{ij} = \frac{1}{2} \sum_{k=1}^{n} \left(\bar{Q}_{ij} \right)_k \left(Z_k^2 - Z_{k-1}^2 \right) \qquad (B.8)
$$

$$
D_{ij} = \frac{1}{3} \sum_{k=1}^{n} \left(\bar{Q}_{ij} \right)_k \left(Z_k^3 - Z_{k-1}^3 \right)
$$

$$\begin{bmatrix} N_1^T \\ N_2^T \\ N_{12}^T \end{bmatrix} = \zeta + \frac{E_{al,1}t_{al}n_{al}}{1-\mu_{al,1}} \begin{bmatrix} 1 \\ 1 \\ 0 \end{bmatrix} \tag{B.9}$$

$$\zeta = \Delta T \cdot \frac{t_f}{(1-\mu_{f,12} \cdot \mu_{f,21})} \cdot \begin{bmatrix} E_{f,1}\alpha_{f,1} + \mu_{f,12}E_{f,2}\alpha_{f,2} \\ E_{f,2}\alpha_{f,2} + \mu_{f,12}E_{f,1}\alpha_{f,2} \\ 0 \end{bmatrix}$$

$$\Delta T = T_{RT} - T_{cure}$$

In equation B.6, B.7 and B.8 , the A_{ij} are extensional stiffnesses, the B_{ij} are bending-extension coupling stiffnesses and D_{ij} are bending stiffnesses. N_i^T is the force due to thermal expansion and N_i is the force due to external loading.

In case of symmetric and balanced laminates B_{ij} matrix will be zero. The elimination of B_{ij} matrix has two important practical benefits. First, such laminates are usually much easier to analyze than laminates with bending-extension coupling. Second, symmetric laminates do not have a tendency of bending or twisting from the inevitable thermally induced contractions that occur during cooling following the curing process. However, in case of a cross-ply laminate (laminate with every fibre layer oriented at either 0° or 90°) the components $A_{16}, A_{26}, B_{16}, B_{26}, D_{16}$ and D_{26} are all zero. These laminate categories are discussed in detail in [2, 3]. It is important to mention that presence of bending and twisting in laminate will result in $B_{ij} \neq 0$.

Since uni-directional *FMLs* i.e., *GLARE1* are symmetric and balanced, putting the B_{ij} matrix to zero and substituting equation B.6 in equation B.3 yields the stresses in the principle directions of the layers due to external loading, thermal loading and pre-strain. This yields for the aluminium layers

$$\begin{bmatrix} \sigma_1 \\ \sigma_2 \\ \tau_{12} \end{bmatrix}_{al} = \begin{bmatrix} Q_{11} & Q_{12} & 0 \\ Q_{12} & Q_{22} & 0 \\ 0 & 0 & Q_{66} \end{bmatrix}_{al} \eta_{al} \tag{B.10}$$

$$\eta_{al} = \begin{bmatrix} \varepsilon_{1,pl} \\ \varepsilon_{2,pl} \\ 0 \end{bmatrix}_{lam} + \begin{bmatrix} A_{11} & A_{12} & 0 \\ A_{12} & A_{22} & 0 \\ 0 & 0 & A_{66} \end{bmatrix}^{-1} \cdot N -$$

$$\begin{bmatrix} 1 \\ 1 \\ 0 \end{bmatrix} \alpha_{al}\Delta T - \begin{bmatrix} \varepsilon_{1,pl} \\ \varepsilon_{2,pl} \\ 0 \end{bmatrix}_{al}$$

And for the fibre layers:

$$\begin{bmatrix} \sigma_1 \\ \sigma_2 \\ \tau_{12} \end{bmatrix}_{f} = \begin{bmatrix} Q_{11} & Q_{12} & 0 \\ Q_{12} & Q_{22} & 0 \\ 0 & 0 & Q_{66} \end{bmatrix}_{f} \eta_{f} \tag{B.11}$$

$$\eta_f = \begin{bmatrix} \varepsilon_{1,pl} \\ \varepsilon_{2,pl} \\ 0 \end{bmatrix}_{lam} + \begin{bmatrix} A_{11} & A_{12} & 0 \\ A_{12} & A_{22} & 0 \\ 0 & 0 & A_{66} \end{bmatrix}^{-1} \cdot N - \begin{bmatrix} 1 \\ 1 \\ 0 \end{bmatrix} \alpha_f \Delta T$$

Where

$$N = N_i + N_i^T$$

Plastic Strain of the Aluminium Layers

In order to couple the deformations due to the post-stretching of the layers and the laminate, an extra equilibrium equation is necessary (external forces equal to 0):

$$\begin{bmatrix} \sigma_1 \\ \sigma_2 \\ \tau_{12} \end{bmatrix}_{al} t_{al} + \begin{bmatrix} \sigma_1 \\ \sigma_2 \\ \sigma_3 \end{bmatrix}_f t_f = \begin{bmatrix} 0 \\ 0 \\ 0 \end{bmatrix} \tag{B.12}$$

According to the von-Mises criterion, yielding occurs when:

$$\sigma_e = \sqrt{\frac{1}{2}\left((\sigma_1 - \sigma_2)^2 + (\sigma_2 - \sigma_3)^2 + (\sigma_3 - \sigma_1)^2\right)} = \sigma_{0.2} \tag{B.13}$$

At the yielding, the stresses in the aluminium layers satisfy equation B.8 with both $\varepsilon_{i,pl_{lam}}$ and $\varepsilon_{i,pl_{al}}$ equal to 0:

$$\begin{bmatrix} \sigma_1 \\ \sigma_2 \end{bmatrix}_{al} = \begin{bmatrix} Q_{11} & Q_{12} \\ Q_{12} & Q_{22} \end{bmatrix}_{al} \cdot$$

$$\left(\begin{bmatrix} A_{11} & A_{12} \\ A_{12} & A_{22} \end{bmatrix}^{-1} N - \begin{bmatrix} 1 \\ 1 \end{bmatrix} \alpha_{al} \Delta T_{postr} \right) \tag{B.14}$$

Where matrix N is calculated with ΔT during the post-stretching process : $\Delta T_{postr} = T_{postr} - T_{cure}$. With these stresses the deviator stresses [4] are calculated as:

$$S_{T1} = 2/3\sigma_1 - 1/3(\sigma_2 - \sigma_3)$$

$$S_{T2} = 2/3\sigma_2 - 1/3(\sigma_3 - \sigma_1)$$

$$S_{T3} = 2/3\sigma_3 - 1/3(\sigma_1 - \sigma_2)$$

In $FMLs$ $\sigma_3 = 0$ because of the plane stress condition. The plastic strain distribution is defined by the deviator stresses:

$$\left[\begin{array}{c} \varepsilon_{1,pl} \\ \varepsilon_{2,pl} \\ \varepsilon_{3,pl} \end{array}\right]_{al} = \left[\begin{array}{c} S_{T1} \\ S_{T2} \\ S_{T3} \end{array}\right] \Delta\lambda$$

Where

$$\Delta\lambda = \frac{\varepsilon_{1,pl_{lam}}}{t_{al}((C_{11}S_{11al} + C_{12}S_{12al})S_{T1} + (C_{11}S_{12al} + C_{12}S_{22al})S_{T2})}$$

The stress-strain distribution results obtained with the von-Mises yield criterion, are sufficient accurate for aluminium with a low anisotropy of the yield stress. It should be kept in mind that this calculation method is not suitable to aluminium with a high anisotropy of yield stress. The reason is that the von-Mises criterion does not account for the anisotropic yield stress of aluminium sheet material. To consider anisotropic behaviour, a complicated iterative calculation of the development of the internal stress and strain distribution during the post-stretching will be required.

B.1 Calculation of the Residual Internal Stress Distribution

B.1.1 Non-Stretched $FMLs$

For non-stretched $FMLs$, both $\varepsilon_{1,pl_{lam}}$ and $\varepsilon_{3,pl_{al}}$ are equal to zero. The residual internal stress distribution then satisfies equation B.10 and B.11 with $N_i = 0$.

B.1.2 $FMLs$ Stretched in One Principle Material Direction

For $FMLs$ stretched in only direction 1, $\varepsilon_{1,pl_{lam}}$ is known. During the yield process, N_2 is equal to 0. This means that N_1 at the moment of yield can be solved from equation B.13 and B.14. $\varepsilon_{2,pl_{lam}}$ can be calculated using:

$$\varepsilon_{1,pl_{lam}} \frac{(C_{11}S_{11al} + C_{12}S_{12al})S_{T1} + (C_{12}S_{12al} + C_{22}S_{22al})S_{T2}}{(C_{11}S_{11al} + C_{12}S_{12al})S_{T1} + (C_{11}S_{12al} + C_{12}S_{22al})S_{T2}}$$

The residual internal stress distribution can now be calculated with equation B.10 and B.11, where $N_i = 0$.

References

[1] C. Honselaar, The residual internal stress distrubution in arall (1986).

[2] M. Hyer, Stress Analysis of Fiber-Reinforced Composite Materials, McGraw-Hill, 1998.

[3] R. M. Jones, Mechanics of composite materials, 2nd Edition, Taylor & Francis, USA., 1999.

[4] A. Mendelson, Plasticity : Theory and Application, The Macmillan Company, USA., 1968.

Appendix C

Model Validation

C.1 ARALL

C.1.1 TWIST and MiniTWIST

The TWIST (Transport WIng STandard) flight-simulation load history was the first standardized flight-simulation history developed in 1973 [1]. The load spectrum was obtained as an average of several civil transport aircrafts wing load spectra.In one block 4000 flights of 10 different types (A to J shown in table C.1) occur in a random number selection. The severity of spectrum vary from light (type J, nice weather) to highly severe (Type A, severe storm).

MiniTWIST [2] was generated because experiments with TWIST were rather time consuming due to the large average number of 100 cycles per flight. MiniTWIST was derived from TWIST by omitting small amplitude cycles from the load spectrum, shown in figure C.1. The average number of cycles per flight was thus reduced to 15 which is a drastic reduction in spectrum as well as the testing time.

C.1.2 EXPERIMENTAL PROGRAM

Specimen Geometry

The specimens were made with the loading direction in parallel to the rolling direction. The cutting edges of the specimens were removed by contour

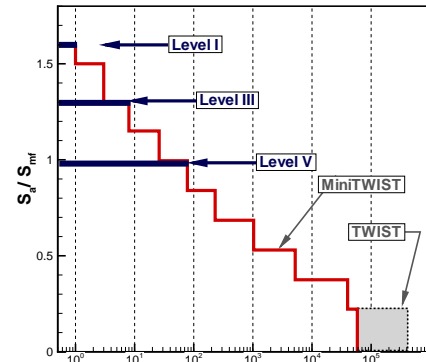| Flight type	Number of flights in one block
A	1
B	1
C	3
D	9
E	24
F	60
G	181
H	420
I	1,090
J	2,211

Table C.1: TWIST flight-simulation load spectrum flights detail [1]

Figure C.1: MiniTWIST load spectrum, 3 truncation levels used

milling to the dimensions shown in figure C.2. The holes were drilled using an NC machine in order to obtain a good and uniform hole edge quality.
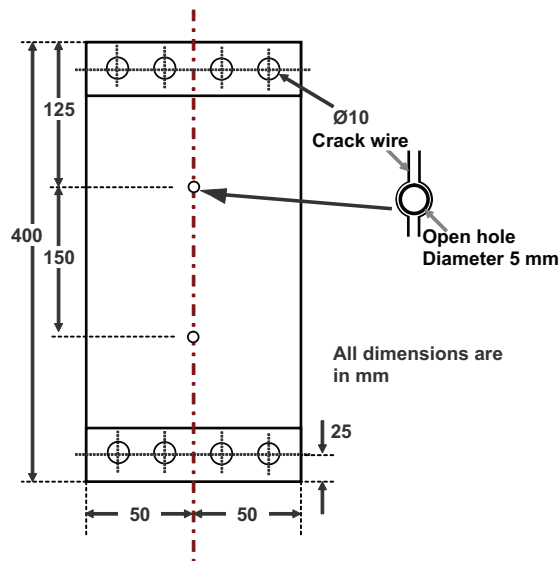

Figure C.2: Specimen geometry

S_{mf} MPa	Material	Truncation level $(S_{a,max}/S_{mf})$					
		I(1.6)		II(1.3)		III(0.995)	
		S_{ground}/S_{mf}					
		-0.5	-0.1	-0.5	-0.1	-0.5	-0.1
81.6	ARALL2			x			not
86.0	ARALL2	x	x	x	x	x	used
81.6	ARALL3	x	x	x	x	x	
86.0	ARALL3	x	x	x	x	x	
86.0	GLARE1	x	x	x	x	x	
95.0	GLARE1				x		
86.0	GLARE2	x	x	x	x	x	
95.0	GLARE2				x		

Table C.2: Test Matrix

C.1.3   Results & Discussion

The comparison of test results with the predictions using the Yield zone model (presented in 6.2) shows that the predictions are sufficiently accurate for GLARE 2 (figure C.3(a)). This highlights the fact that all the metal related phenomena like crack growth retardation and plastic-zone exist in *FMLs* under flight-simulation loading but to a small extent. These phenomena can be investigated using a simple interaction model. However, for *ARALL 2* (figure C.3(b)) the predictions are not very accurate. The difference is due to the fibre failure, corresponding delamination is shown in figure C.4(a). The current model is not capable of predicting the crack growth in the presence of fibre failure. Post-stretching is used to avoid the fibre failure and improve the fatigue properties. Therefore, a better correlation between test data and predictions is obtained for *ARALL 3* (figure C.3(a)) which shows the effect of post-stretching.

Figure C.3(a) shows the comparison of predictions and test results for *GLARE 2* under 86 MPa and 95 MPa. The tests were stopped at a small crack length, when crack growth rate was still decreasing due to the start of fibre bridging phenomenon. This trend was captured by the prediction model. However, more information about the accuracy of predicting the full curve could have been provided if the tests had been continued till the crack growth rate gets to larger crack lengths.
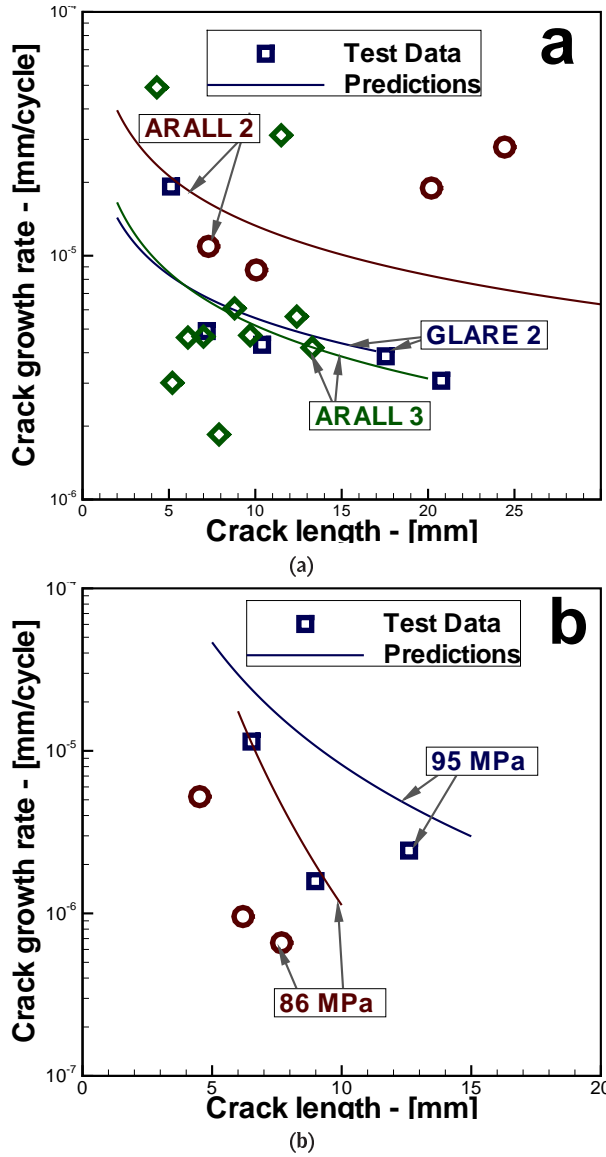
(a)

(b)

Figure C.3: Comparison of crack growth prediction and test data for *ARALL* for $S_{gr}/S_{mf} = -0.5, S_{a,max}/S_{mf} = 0.995$ ((a)) and *GLARE* for $S_{mf} = 86$ and 95 MPa ((b))
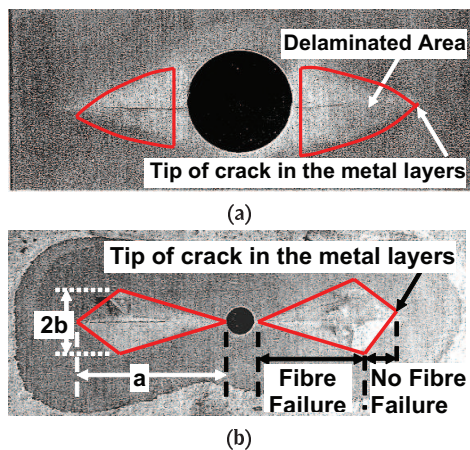
Figure C.4: Delamination shape of *GLARE* ((a)) and *ARALL* ((b))

C.2 HSS-GLARE Crack growth results

For the model validation work, test results of HSS Glare were compared with the prediction done using Yield Zone Model under three different flight spectra mentioned in table 6.1.

References

[1] J. B. d. Jonge, D. Schutze, H. Lowak, J. Schijve, A standardized load sequence for flight-simulation tests on transport aircraft wing structures, Tech. Rep. NLR-TR-73029, National Aerospace Laboratory NLR, Amsterdam (1973).

[2] H. Lowak, J. B. De Jonge, J. Franz, D. Schutze, Mini-twist, a shortened version of twist, Tech. Rep. NLR-MP 79018, National Aerospace Laboratory NLR, Amsterdam (1979).
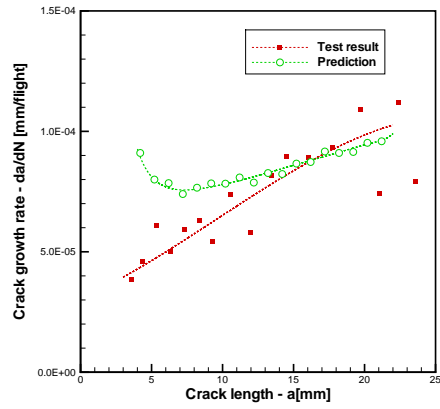
(a)
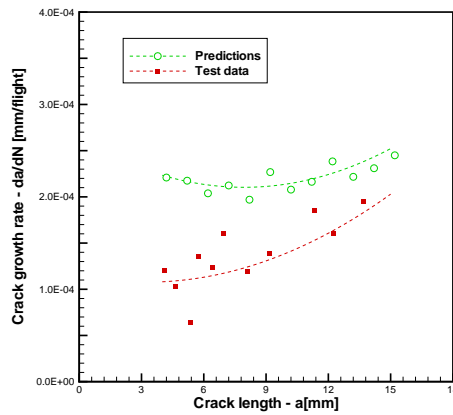
(b)
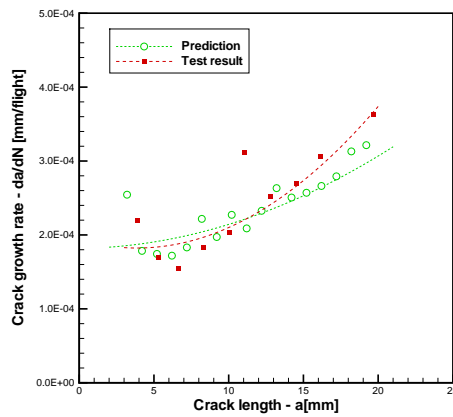
(c)

Figure C.5: Correlation between experimental HSS Glare and Yield Zone prediction for flight spectra: (a). Spectrum I, (b).Spectrum II, (c).Spectrum III,

Plastic Zone and Delmination Shape Experiments

D.1   specimen

Three types of *CCT* specimens, as shown in Figure D.1, were used for the delamination shape and plastic zone size investigation. These specimens were manufactured with cumulative metal thickness of 2 mm. The specimen used for delamination shape investigation were manufactured with 5 metal layers of 0.4 mm thickness and 4 composite cross-ply fibre layers with a nominal thickness of 0.266 mm (i.e., Glare3-5/4-0.4). Beside Glare specimen, monolithic metal specimen of 2 mm thickness and laminated metal specimens manufactured with 5 metal layers of 0.4 mm thickness were used. The width of these specimen was 140 mm. The starter notches were made by drilling a hole of 3 mm diameter with two saw cuts oriented perpendicular to the loading direction. The length of the starter notch ($2a_0$) was also approximately 5 mm.

D.2   Testing Setup

Digital Image correlation *DIC* was used as the delamination shape observation technique for the Glare test program, detailed in table D.1. For all
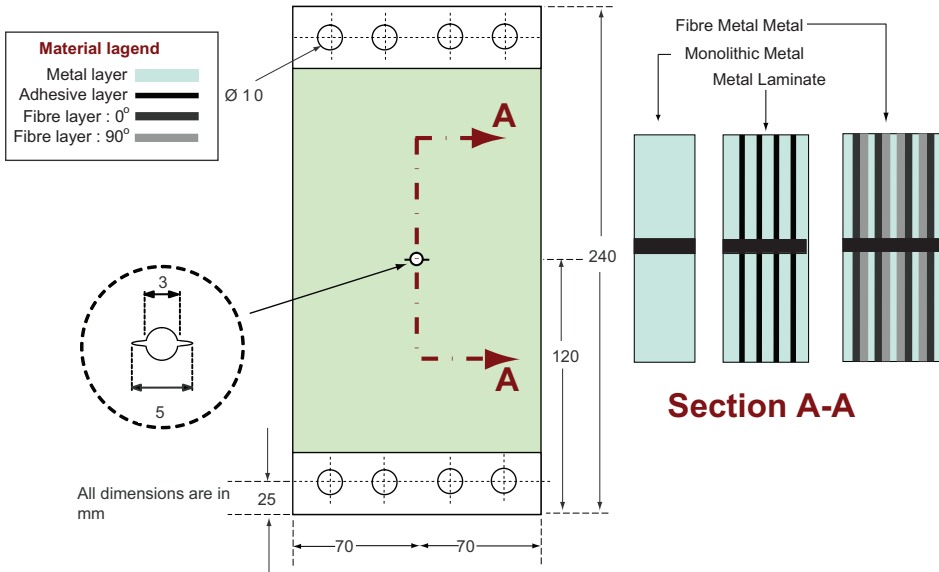
Figure D.1: Geometry of test specimen and cross section of materials used for DIC
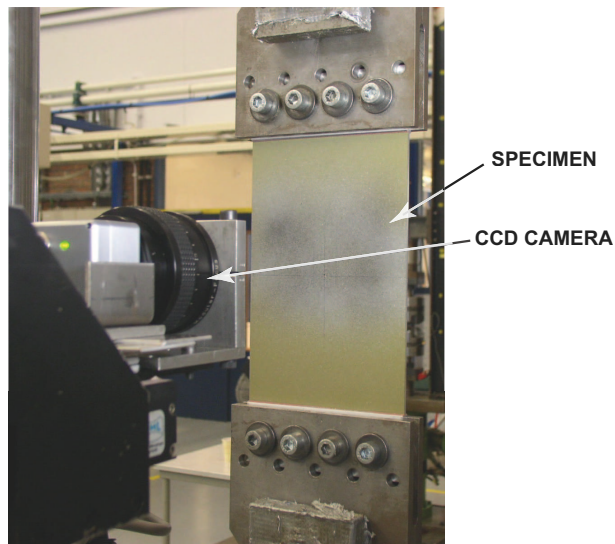
Figure D.2: Testing setup

three materials, plastic zone size was measured using the *DIC*. The test se-

tup is shown in figure D.2. These tests were performed using a computer controlled servo-hydraulic testing system with a load capacity of 25 metric tons.

D.3   Test Matrix

The set of specimens have been tested using a *CA* baseline spectrum with a maximum stress S_{max} = 100 MPa and a stress ratio R = 0.1. The single overload spectrum has an overload S_{OL} = 145 MPa at a_{OL}=10 mm. The multiple overload spectrum has three overloads i.e. S_{OL1} = 145 MPa; S_{OL2} = 130 MPa and S_{OL3} = 115 MPa at a_{OL}=9, 12 and 15 mm respectively. Block load spectra are constituted of two stress levels $S_{max,LO}$ = 100 MPa and $S_{max,HI}$ = 140 MPa.

Detail of the test program is given in table D.1 for Glare specimens, while for monolithic metal the details are given in table D.2 and laminated metal test matrix is given in table D.3.
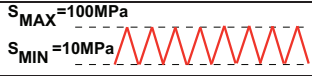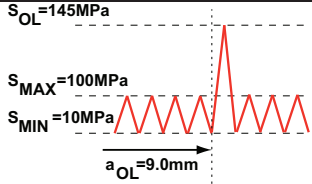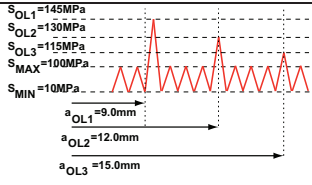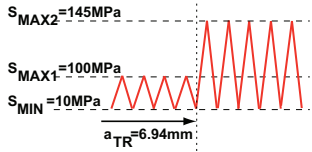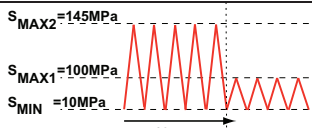
	Load variation	CA cycles		Load variation
		Maximum stress [MPa]	Stress ratio	[MPa]
B1	Constant amplitude $S_{MAX}=100MPa$ $S_{MIN}=10MPa$	100	0.1	
B2	Single overload $S_{OL}=145MPa$ $S_{MAX}=100MPa$ $S_{MIN}=10MPa$ $a_{OL}=9.0mm$	100	0.1	145
B3	Multiple overload $S_{OL1}=145MPa$ $S_{OL2}=130MPa$ $S_{OL3}=115MPa$ $S_{MAX}=100MPa$ $S_{MIN}=10MPa$ $a_{OL1}=9.0mm$ $a_{OL2}=12.0mm$ $a_{OL3}=15.0mm$	100	0.1	145,130,115
B4	Block loading-LO-HI $S_{MAX2}=145MPa$ $S_{MAX1}=100MPa$ $S_{MIN}=10MPa$ $a_{TR}=6.94mm$	100	0.1	145
B5	Block loading-HI-LO $S_{MAX2}=145MPa$ $S_{MAX1}=100MPa$ $S_{MIN}=10MPa$ $a_{TR}=12.7mm$	145	0.1	100

Table D.1: Fatigue crack growth test matrix – GLARE3-5/4-0.4 specimen
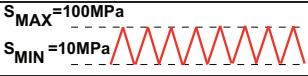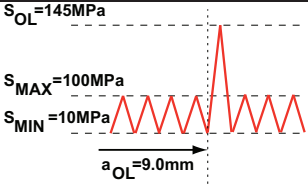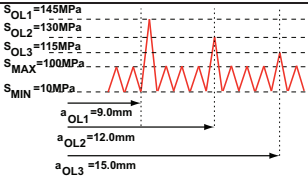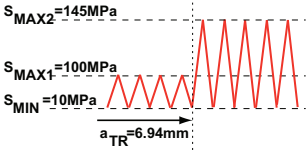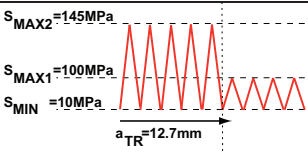
| | Load variation | | CA cycles | | Load variation |
			Maximum stress [MPa]	Stress ratio	[MPa]
C1	Constant amplitude	S_{MAX}=100MPa S_{MIN}=10MPa	100	0.1	
C2	Single overload	S_{OL}=145MPa S_{MAX}=100MPa S_{MIN}=10MPa a_{OL}=9.0mm	100	0.1	145
C3	Multiple overload	S_{OL1}=145MPa S_{OL2}=130MPa S_{OL3}=115MPa S_{MAX}=100MPa S_{MIN}=10MPa a_{OL1}=9.0mm a_{OL2}=12.0mm a_{OL3}=15.0mm	100	0.1	145,130,115
C4	Block loading-LO-HI	S_{MAX2}=145MPa S_{MAX1}=100MPa S_{MIN}=10MPa a_{TR}=6.94mm	100	0.1	145
C5	Block loading-HI-LO	S_{MAX2}=145MPa S_{MAX1}=100MPa S_{MIN}=10MPa a_{TR}=12.7mm	145	0.1	100

Table D.2: Fatigue crack growth test matrix – Monolithic metal specimen
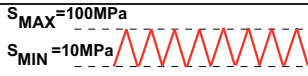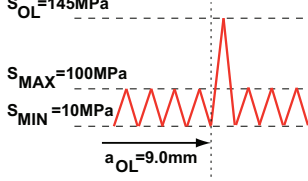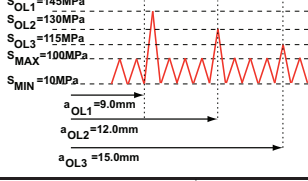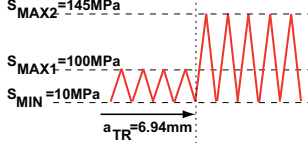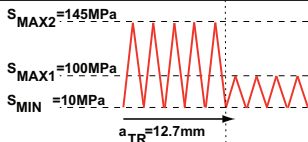
	Load variation		CA cycles		Load variation
			Maximum stress [MPa]	Stress ratio	[MPa]
D1	Constant amplitude	S_{MAX}=100MPa S_{MIN}=10MPa	100	0.1	
D2	Single overload	S_{OL}=145MPa S_{MAX}=100MPa S_{MIN}=10MPa a_{OL}=9.0mm	100	0.1	145
D3	Multiple overload	S_{OL1}=145MPa S_{OL2}=130MPa S_{OL3}=115MPa S_{MAX}=100MPa S_{MIN}=10MPa a_{OL1}=9.0mm a_{OL2}=12.0mm a_{OL3}=15.0mm	100	0.1	145,130,115
D4	Block loading–LO–HI	S_{MAX2}=145MPa S_{MAX1}=100MPa S_{MIN}=10MPa a_{TR}=6.94mm	100	0.1	145
D5	Block loading–HI–LO	S_{MAX2}=145MPa S_{MAX1}=100MPa S_{MIN}=10MPa a_{TR}=12.7mm	145	0.1	100

Table D.3: Fatigue crack growth test matrix – Laminated Aluminium Sheets specimen

Summary

FATIGUE CRACK & DELAMINATION GROWTH IN FIBRE METAL LAMINATES
under Variable Amplitude Loading

This thesis presents the investigation into the fatigue propagation and delamination growth of Fibre Metal Laminates under variable amplitude loading. As explained in the first chapter, the motivation of the research is twofold: first, to obtain a clear understanding and detailed characterization of the failure mechanisms in GLARE under variable amplitude loading (selective and flight load spectra). Second is to obtain an accurate prediction model for fatigue crack propagation in GLARE accounting for fibre bridging, delamination and influence of plasticity.

The major concept in this thesis is that the stress intensity at the crack tip in the metal layers of a Fibre Metal Laminates *FML* is the factor determining the extension of that crack under cyclic loading. This implies that the stress intensity factor can be described with Linear Elastic Fracture Mechanics, including the contribution of the fibre layers and the with the crack growth associated delamination behaviour. The investigation presented in this thesis, covers the theoretical analysis of the crack growth phenomena and experiments to support and validate the developed prediction model. This investigation has been restricted to through-the-thickness cracks with the same crack length in all metal layers.

In the second chapter, the various GLARE grades and lay-ups are defined together with a description of the manufacturing process, quality assurance

171

procedures and fatigue crack growth phenomena. The aspects introduced are the fatigue crack growth in the aluminium layers, controlled by the stress intensity factor at the crack tip, and the delamination of the aluminium and prepreg layers, which occurs in the wake of the propagating crack. The crack opening is constrained by the bridging fibre layers, while the stress redistribution to these fibre layers determines the delamination growth. In addition, this chapter discusses the effects of variable amplitude loading in metals, together with the models developed so far to predict fatigue crack growth.

The influence of variable amplitude loading on the delamination growth (i.e. a major phenomenon contributing to the slow fatigue crack growth in $FMLs$) is discussed in chapter 3. An extensive test programme is presented in this chapter utilizing double and multiple block loads, and flight load spectra to validate the hypothesis that delamination in $FMLs$ is independent of retardation effects under variable amplitude loading. Furthermore, the use of scanning electronic microscopy is presented to study the delamination growth striations on the disbonded fracture surfaces.

Chapter 4 presents the effect of variable amplitude loading on delamination shapes. These delamination shapes influence the bridging stresses and the crack tip stress intensity factor. The change in the delamination shape due to variable amplitude loading is understood, and the hypothesis on the reason of this change in delamination shapes has been validated. The use of Digital Image Correlation *(DIC)* is presented to observe delamination shapes and crack tip plastic zones in-situ fatigue testing. Although a change in delamination shape can be observed, its effect on the bridging stress profile is observed to be negligible.

Crack tip plasticity and shear-lip formation both were investigated, as presented in chapter 5. Difference in shear-lip morphology was observed in monolithic metals, adhesively bonded metal laminates and $FMLs$. Monolithic metals revealed typical shear-lip profiles with the early tensile mode followed by a transition mode and finally the transverse shear mode. For metal laminates (without fibres), the mode transition happened quite late during fatigue crack growth, but the transition length was smaller than those of monolithic metals. In $FMLs$ the shear lip profiles were rather difficult to see with the naked eye or optical microscope. However, the straight appearance of the crack when observed from the specimen side, implied a flat cracked fracture surface without shear lips. Plastic zone sizes are compared in the same chapter. In case of monolithic metals and metal laminates, a big difference is observed between the predicted plastic zone sizes (using Irwins relation) and the sizes measured with DIC. However, comparing these sizes for $FMLs$ revealed only a small difference. In $FMLs$, the plastic zone sizes are observed to be independent of the crack length which corresponds to the

constant crack tip stress intensity factors.

Chapter 6 presents the development and validation of three different types of prediction models. These models include a linear damage accumulation (non-retardation) model, a yield zone model and a crack closure model. The predictions using these models correlated with experimentally observed crack growth behaviour.

Chapter 7 outlines the sub-routine added to the prediction model for post-stretched laminates. This routine has been validated with the data from post-stretched GLARE 1 and ARALL from the literature.

Chapter 8 summarizes the conclusions of the investigation. It can be concluded that with the proposed prediction model, the mechanism of crack propagation and delamination growth in GLARE is fully described and understood. The prediction model has been validated with experimental crack growth data, and is considered accurate. In its implemented form, the model has the potential to be extended to other material-, geometrical- and test parameters.

Samenvatting

FATIGUE CRACK & DELAMINATION GROWTH IN FIBRE METAL LAMINATES
under Variable Amplitude Loading

D it proefschrift presenteert het onderzoek naar vermoeiingss-cheurgroei en -delaminatiegroei van vezelmetaallaminaten o-nder variabele amplitude belastingen. Zoals in het eerste hoofdstuk uitgelegd, is de motivatie voor dit onderzoek twee-ledig: In de eerste plaats, het verkrijgen van een duidelijk begrip en gede-tailleerde karakterisering van de faalmechanismen in GLARE onder variabele amplitude belastingen (selectieve en vliegbelastingspectra). Ten tweede, het verkrijgen van een nauwkeurig voorspellingsmodel voor vermoeiingsscheur-groei in GLARE met inbegrip van vezeloverbrugging, delaminatie en invloe-den van plasticiteit.

The belangrijkste concept in dit proefschrift is dat de spanningsintensiteit aan de scheurtip in the metaallagen van een *FML* de bepalende factor is voor de scheuruitbreiding onder cyclische belastingen. Dit houdt in dat de span-ningsintensiteit factor beschreven kan worden met linear elastische breuk-mechanica, inclusief de bijdrage van de vezellagen en de met de scheurgroei geassocieerde delaminatiegroei. Het onderzoek in dit proefschrift gepre-senteerd omvat the theoretische analyse van de scheurgroei fenomenen, en de experimenten ter ondersteuning en validatie van het ontwikkelde voor-spellingsmodel. Dit onderzoek is gelimiteerd tot scheuren door de dikte met gelijke lengte in alle metaallagen.

In het tweede hoofdstuk worden the verschillende GLARE configuraties en gedefinieerd, tezamen met een beschrijving van het productieproces, the kwaliteitsbewaking en de vermoeiingsscheurgroei fenomenen. De gentro-duceerde aspecten zijn de vermoeiingsscheurgroei in de aluminium lagen, gecontroleerd bij de spanningsintensiteit factor aan de scheurtip, en de de-laminatiegroei tussen de aluminium en prepreg lagen, welke achter de scheur-tip plaatsvindt. De scheuropening is gelimiteerd door de overbruggende vezellagen, terwijl de herverdeling van spanningen naar deze lagen de de-laminatiegroei bepaald. Bovendien bespreekt dit hoofdstuk de effecten van variabele amplitude vermoeiing in metalen, samen met de modellen tot nu toe ontwikkelt voor het voorspellen van scheurgroei.

De invloed van variabele amplitude belasting op delaminatiegroei (een be-langrijp fenomeen dat bijdraagt aan de langzame scheurgroei in *FMLs*) is be-discussieerd in hoofdstuk 3. Een uitgebreid test programma is gepresenteerd in dit hoofdstuk dat gebruik maakt van dubbele en meervoudige Block be-lastingen, en vleugel belastingspectra, om de hypothese te valideren dat de-laminatie in FMLs onafhankelijk is van retardatie effecten. Bovendien is het gebruik van elektronenmicroscoop gepresenteerd om de delaminatiegroei striations te bestuderen op de gedelamineerde breukvlakken.

Hoofdstuk 4 presenteert het effect van variabele amplitude belastingen op delaminatie vormen. Deze delaminatievormen benvloeden de overbrug-gingsspanningen en de scheurtip spanningsintensiteit factor. De verander-ing in de delaminatievorm als gevolg van variabele amplitude belastingen is begrepen, en de hypothese betreffende de reden van deze verandering in delaminatievormen is gevalideerd. Het gebruik van Digitale Beeld Corre-latie *(DIC)* is gepresenteerd om delaminatievormen en plastische zones tij-dens de testen te observeren. Hoewel een verandering van delaminatievorm waargenomen kon worden, bleek het effect daarvan op de overbruggingss-panning verwaarloosbaar.

Scheurtip plasticiteit en scheurlip vorming zijn beide onderzocht, zoals in hoofdstuk 5 gepresenteerd. Verschil in scheurlip morfologie is waargenomen in monolithisch metaal, gelijmde metaallaminaten en FMLs. Monolithisch metaal liet typische scheurlip profielen zien met een in aanvang trekmodus, gevolgd door een transitie modus, en uiteindelijk een transversale afschuif-modus. Voor metaallaminaten (zonder vezels), trad de transitie laat op tij-dens de vermoeiingsscheurgroei, maar de lengte van de transitie was kleiner dan die voor monolithische metalen. In *FMLs* bleken de scheurlip profielen tamelijk moeilijk waarneembaar met het blote oog of met optische micro-scopen. Echter, het rechte voorkomen van de scheur wanneer geobserveerd van de proefstukzijkant, betekent een vlak breukvlak zonder scheurlippen. De grootte van plastische zones zijn vergeleken in ditzelfde hoofdstuk. In geval van monolithische metalen en metaal laminaten, een groot verschil

werd waargenomen tussen de voorspelde plastische zone grootte (gebruik-makend van Irwins vergelijking) en de grootte gemeten met *DIC*. Maar wanneer deze groottes vergeleken werden voor FMLs, dan bleek dit verschil klein te zijn. De delaminatie groottes geobserveerd in FMLs bleken onafhankelijk te zijn van de scheurlente, wat correspondeert met een constante scheurtip spanningsintensiteit factor.

Hoofdstuk 6 presenteert de ontwikkeling en validatie van drie verschillende typen voorspellingsmodellen. Deze modellen betreffen een lineair schadeaccumulatie model (zonder scheurretardatie), een plastische zone model, en een scheursluiting model. De voorspellingen met behulp van deze modellen correleerden met experimenteel waargenomen scheurgroei gedrag.

Hoofdstuk 7 schetst de subroutine die toegevoegd is aan het model voor voorgestrekte laminaten. Deze routine is gevalideerd met data van voorgestrekt GLARE1 en ARALL uit de literatuur.

Hoofdstuk 8 vat de conclusies van dit onderzoek samen. Er kan geconcludeerd worden dat met het voorgestelde voorspellingsmodel, het mechanisme van scheurgroei en delaminatiegroei in GLARE volledig is beschreven en begrepen. Het voorspellingsmodel is gevalideerd met experimentele scheurgroei data, en wordt beschouwd nauwkeurig te zijn. In de wijze waarop het geïmplementeerd is, heeft het model potentie om uitgebreid te worden voor andere materiaal- geometrische- en testparameters.
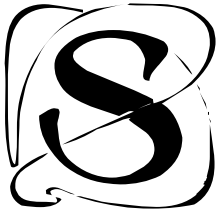
harif was born on the 6th of April, 1979 in Bannu, Pakistan. With due course of time, he got into a habit of changing his coordinates. His first move was to Islamabad in his early childhood. He finished his schooling and pre-university at Islamabad. It was about time to move again. This time the destination was Peshawar for Mechanical Engineering in 1997. Graduated with BSc. Mechanical Engineering in 2001 he further moved to Karachi for a job in mechanical design company. Finding lot of time in hand beside his job he joined Institute of Business Administration (IBA) for MBA-MIS. The habit of moving haunted once again in June 2004 and this time the destination was ENSAE-SUPAERO, Toulouse, France for MSc. Aerospace Engineering. Another move to Faurecia Innerruim System GmbH in Hagenbach, Germany in August 2005. He defended his M.Sc. thesis and graduated in January 2006. Next move was towards Delft The Netherlands in June 2006. This time for PhD at Faculty of Aerospace Engineering. During his PhD he has presented his research for a number of conferences and published in peer reviewed Journals.

Publications

Contribution To Book

- **Khan, S.U.**, Alderliesten, R.C., Schijve, J., and Benedictus, R. *On the fatigue crack growth prediction under variable amplitude loading.* Computational & Experimental Analysis of Damage Materials, pp. 77-105 (Edited by D.G. Pavlou), Transworld Research Network, Kerala, (2007).

Conference Proceedings

- **Khan, S.U.**, Alderliesten, R. C., Benedictus, R. *Delamination in fibre reinforced metal laminates under Variable amplitude loading.* Proceedings of SAMPE Europe SEICO 08 Conference, Paris, (2008).

- **Khan, S.U.**, Alderliesten, R. C., Benedictus, R. *LDA's Applicability for Predicting Fatigue Crack Growth in FML's Under VA Loading.* Proceedings of 49th AIAA Structures, Structural Dynamics, and Materials Conference, (Paper Number: AIAA-2008-2017), Schaumburg, Illinois, USA,(2008)

- **Khan, S.U.**, Alderliesten, R. C., Benedictus, R. *Fatigue crack growth in fibre reinforced metal laminated under variable amplitude loading.* Proceedings of the 26th Congress of International Council of the Aeronautical Sciences-ICAS 2008, Anchorage, Alaska, USA, (2008).

- **Khan, S.U.**, Alderliesten, R. C., Schijve, J., Benedictus, R. *Fatigue Performance Of Fibre Metal Laminates Under Flight Loading Spectra.* 2nd Second International Conference on Material and Component Performance under Variable Amplitude Loading, 23-26 March, Darmstadt, (2009).

- **Khan, S.U.**, Alderliesten, R. C., Benedictus, R. *Fatigue crack growth in fibre metal laminated under variable amplitude loading.* Accepted for International Committee on Aeronautical Fatigue (ICAF) 2009. Rotterdam, The Netherlands, (2009)

- **Khan, S.U.**, Alderliesten, R. C., Schijve, J., Benedictus, R. *Fibre Metal Laminates and Variable Amplitude Loading.* 12th International Conference of Fracture, 12-17 July, Ottawa, Canada, (2009).

- Alderliesten, R. C., Rans, C. D., **Khan, S.U.**, Benedictus, R. *Understanding the Fatigue Behavior of FML Structures and Materials under Complex Variable Amplitude Loading,* The 2009 Aircraft Structural Integrity Program Conference (ASIP2009), 1-3 December, Jacksonville, Florida, USA, (2009).

Journal Publications

- **Khan, S.U.**, Alderliesten, R.C., Benedictus, R. *Post-Stretching Induced Stress Redistribution In Fibre Metal Laminates For Increased Fatigue Crack Growth Resistance.* Composite Science and Technology, 69(3-4), pp. 396-405, (2009).

- Plokker, H.M., **Khan, S.U.**, Alderliesten, R.C., Benedictus, R. *Fatigue crack growth in Fibre Metal Laminates under Selective Variable Amplitude Loading.* Fatigue and Fracture of Engineering Materials and Structures, 32(3), pp. 233-248, (2009).

- **Khan, S.U.**, Alderliesten, R. C., Benedictus, R. *Linear Damage Accumulation for Predicting Fatigue in FMLs under Variable Amplitude Loading.* AIAA Journal of Aircraft,46(5),pp. 1706-1713, (2009).

- **Khan, S.U.**, Alderliesten, R. C., Benedictus, R. *Delamination growth in Fibre Metal Lamintes under Variable Amplitude Loading.* Composite Science and Technology,69(15-16), pp. 2604-2615, (2009).

- **Khan, S.U.**, Alderliesten, R. C., Rans, C. D. Benedictus, R. *A Modified Wheeler Model to Capture The Limited Interaction Effects in Fibre Metal Laminates under Variable Amplitude Loading.* Engineering Fracture Mechanics, 77(9), pp.1400-1416, (2010).

- **Khan, S.U.**, Alderliesten, R. C., Benedictus, R. *Delamination Shape in Fibre Metal Laminates under Variable Amplitude Loading*. International Journal of Fatigue, 33(9), pp. 1292-1303, (2011).

Planned Journal Publications

- **Khan, S.U.**, Alderliesten, R. C., Benedictus, R. *Crack tip Plasticity in Fibre Metal Laminates under Variable Amplitude Loading*. Will be submitted to Mechanics of Materials.

- **Khan, S.U.**, Alderliesten, R.C., Benedictus, R. *Crack growth prediction in Fibre Metal Laminates using Crack Closure Model under Variable Amplitude Loading*. Will be submitted to International Journal of Fatigue.

- **Khan, S.U.**, Alderliesten, R. C., Benedictus, R. *Fatigue crack growth in Fibre Metal Laminates, Crack growth and Delamination growth*. Will be submitted to Engineering Fracture Mechanics.

Acknowledgments

*"Very gratifying," said Professor Albus Dumbledore mildly. " We
all like appreciation for our own hard work, of course . . ."*

*From Harry Potter and the Half-Blood Prince
by J.K. Rowling (Rowling, 2005)*

The four years spent at TU Delft were full of surprises each filled with a new challenge. Those years felt like sitting on a Sine Wave, one day you are at the positive peek of it with all achieved but the very next day takes you to the negative one and it seems like a never ending journey. But finally this chapter of my life is coming to an end. It was indeed a wonderful experience meeting and working with many people from different cultures and backgrounds. All of them helped me to develop various skills and friendships which I will cherish for the rest of my life. Although, I am the author of this thesis but in fact this would not have been possible without the support and guidance of many individuals whom I wish to acknowledge.

Thanks to **Almighty Allah**, the merciful and the passionate, for providing me the opportunity to step in the excellent world of science. Through this journey, I have been supported and supervised by many people to whom I would like to express my deepest gratitude.

First of all, I owe my most sincere gratitude to my promoter **Rinze** for providing me with a wonderful opportunity to carry out this research. I feel

really lucky to work with Glare and Fatigue at Faculty of Aerospace Engineering Delft University of Technology. **Rinze**, it was you who has invited me to twice to Delft for discussions with you, Jos Sinke, René and Johanas. You were very much inspired by my presentations and offered me this interesting and challenging opportunity funded by Airbus. From the start till end you had been so confident about me. Your comments *"This is great work!"* always played magic after every meeting. I have been able to finish the research not only with interesting results but also with a number of publications in high impact factor peer reviewed Journals.

I have to admit that having **René** as my daily supervisor and co-promoter is the best thing that has ever happened to me. **René** is always available and ready for discussions. Things became quite interesting when he said in the beginning of second year: *"Just let me know what and how you want to do it and then I will challenge you"*. And that is what he has been doing; challenging me at each step, ranging from the test programs until the publications. I am highly obliged and want to say, Thank you very much **René** for giving me this outstanding PhD opportunity. I really appreciate your believe in me. I can not forget the day when you mentioned during my third year review that you are not worried about me finishing my PhD.

The most inspiring person I have met during my PhD at TU Delft is **Prof. Schijve**. He is always so enthusiastic about the research and innovative ideas for fatigue and crack growth. During discussions, he would always come up with interesting questions. **Prof. Schijve** is always the first one to read and review my paper with keen interest. I really acknowledge and honor his efforts from a young researcher point of view. He is indeed an asset to the group.

I still remember meeting **Thomas Beumlar** for the first time during his visit to Delft with Fred Pellenkoft. In the first informal introduction in 2006, **Thomas** asked me *"So the model is ready now?"*. **Thomas** always believed in me regarding the research, outcome and quarterly reports. I am extremely thankful to **Thomas** for always supporting my research but asking critical questions. Thank you **Thomas** for arranging the funding from Airbus for my Glare research for the whole duration.

Rinze mentioned during my first interview that in case of any issue or trouble talk to **Gemma**. Starting from that day till now **Gemma** helped me in managing everything. **Gemma** we were really touched when we have received a flower bouquet and a get well soon wish card for my wife after returning from hospital,. I am thankful to **Gemma** for making things work during my stay at Delft. And **Gemma** Yes you are right! it was stupid of me not to backup my outlook files.

Using laboratory and testing facility for making or breaking specimen remained a major part of my research. Thanks to a number of people who

educated me about the fatigue testing machines. In the start **Berthil** and **Niels** helped me a lot with setting up the specimen and test. Running the variable amplitude and flight spectra during my delamination testing was quite challenging but thanks to **Berthil** it went well. During half way through my research **Bob** has joined the lab. I am extremely thankful to him for solving my troubles with fatigue machines, changing and rotating the clamps. First time, the guy who explained and showed me how to laminate Glare specimen was **Kees**. He was always helpful in any lab. related stuff. **Kees** has also helped me in making single and double cracked lap-shear specimens for the delamination growth tests. Whilst my quest for FM906 and HSS Glare, I have met **Rob** and I appreciate his help in searching for the data and Glass fibre rolls. **Rob** helped me in making the laminates for the delamination shape and plastic zone size test program. Although, I have never worked with **Hans** and **Michel** but it was always nice talking with them at 15h00 coffee breaks.

Amir, I must acknowledge your help and tips during my research. You were always there to guide me ranging from discussions on my research up to the filling of tax (Belasting) forms. It would be unjust not to mention that for my Journal's publications, **Amir**, you were the main inspiration. In addition, it was pleasure being your neighbor and joining the weekend parties.

My roommates, **Rik-Jan** and **Riccardo**. **Rik** was always critical about my work and his questions always made me think ahead. I felt like defending in front of him what I have been doing and what I will do. On the other hand, **Riccardo** is always there for his suggestions and advices. I have to appreciate the patience of my roommates during the time I started using digital image correlation, airbrush and speckle on the specimens.

Milan!, the guy who has spent most of this time either in the dark room with the microscope *(SEM)* making the pictures or in his room looking at those pictures. I was really inspired by his discoveries using *SEM* and I appreciate his help when I started using SEM. Beside the microscope, **Milan** is always enthusiastic about photography discussion.

Calvin! thank you very much for your tips regarding the conference's presentations and reviewing my first Journal paper as advised by the reviewers. The discussion about SLRs and photography was always fun with you and good luck in managing 365 snaps.

I also like to acknowledge the rest of PhD community which includes **Ligeia, Pascal, Gianni, Greg W., Greg R., Cory, Gustavo and Patrecio**. I really enjoy working with you guys and especially the informal PhD meet-ups. I have to admit that now when I am visiting the faculty, I miss meeting and talking to the familiar PhD researchers except **Greg R.**.

Harrie and **Kiomara** you had not only been wonderful neighbors but also

family friends in a foreign country. Your help in tough times, participation in happy moments, hospitality all the way through and love for my son Zulfiqar; all this and much more makes me feel indebted.

I would like to acknowledge all of my Pakistani friends who were indirectly involved in the achievement of my target and never let me feel alone in Delft. My special thanks to **Zubair & Family** for arranging Pizza parties, **Zeeshan & Family** for his tips as being the most senior Pakistani PhD student, **Atif & Family** for weekend gatherings, live cricket matches and on top of all, a nice sense of humor, **Burhan & Family** for their such a welcoming attitude and hospitality,**Jawad & Family** for their enjoyable company and un-wanted habit of changing locations almost every year,**Omer & Family, Haroon & Family, Farhan & Family**, Pakistani friends from the Aerospace Faculty **Shafqat, Rafi, Akram, Mahzar, Hafiz Saleem and Iftikhar**.

After a long time without Pushtu, in 2007 I have got a chance to polish my Pushtu language by talking to my Pukhtoon friends. Deera Deera Meharbani **Laiq, Mehfooz, Faisal, Fakhar, Seyab and Humanyoon Khana**.

John– **Alan Pascoe** and **Robert Gouwen**, I really acknowledge your help for translating the propositions to Dutch.

Of course no acknowledgments would be complete without giving thanks to **my parents**. Both have instilled many admirable qualities in me and given me a good foundation to meet life. Theyve taught me about hard work and self-respect, about persistence and about how to be independent. Mom, especially, was a great role model of resilience, strength and character. Both have always expressed how proud they are of me and how much do they love me. I too am proud of them and love them very much. I am grateful to both of them for the smart genes they passed on to me.

I like to say thanks to an elegant lady, my **Mom**-**in law** for her prayers for my success plus her so lively nature. It is always fun to talk to her. I really appreciate that she always find time to send the best selection of poetry books and CDs to me. Even while writing these lines I am listening to the latest update to my music collection, thanks to her.

I like to thanks to my brothers **Nasir Bhai**, **Rahat** and sisters **Mahjabeen** and **Mussarat** for praying for my research and its successful completion.

For my family from Germany **Rafey, Saadat, Mujtaba and Muneeza**, I have to say "Danke schön" as it is nice to have a family living close and **Saadat** thanks God that you are not in my defense committee else it would be an ever lasting argument.

I can well imagine that my son, **Zulfiqar** you have to finish a number of Lego projects on your own as I was busy finishing my research. I can see that you were missing me but never let me get the feeling that I have been missed. I

also have pleasure of showing **Zulfiqar** our fatigue testing lab. and aerospace hall at the faculty. He was really keen and interested in looking at all the aircraft and helicopters with great interest. He would always come up with the difficult questions starting from the word "Why".

Last but certainly not the least, I must acknowledge with tremendous and deep thanks my wife, **Uzma**. Through her love, patience, support and unwavering belief in me, I have been able to complete this long dissertation journey. She is my biggest fan and supporter. She has patiently endured many, many long hours alone while I worked on my dissertation. At the same time, she has also given me so many happy and beautiful memories throughout this journey. We have laughed and cried, traveled and played, built and settled, and planned and discussed our lives. I could not have completed this journey without **Uzma** by my side. She went through every excruciating step and mood change with me, as well as read my study as many times as I, yet somehow made everything less burdensome. Her wit has kept me smiling and her sarcasm has given me a different view of the world helping me keep things in perspective. **Uzma** has been central to my completion of this study as she has given me confidence and motivated me in so many ways. Through her eyes I have seen myself as a capable, intelligent man who could do anything once he makes up his mind. There are no words that can express my gratitude and appreciation for all you have done and been for me. As I ramble, I still have not found the words that describe or express how I feel for this woman and what her presence in my life has meant. She loves me like no one else has and has changed me for the better. Thank you with all my heart and soul. I love you and am forever indebted to you for giving me life, your love, and your heart. Your complete and unconditional love carries me through always.
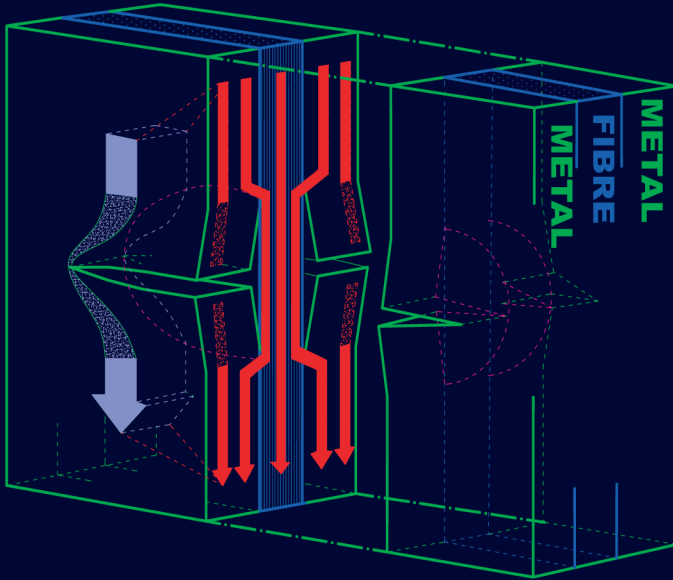
Sharif

Delft,
November 2012
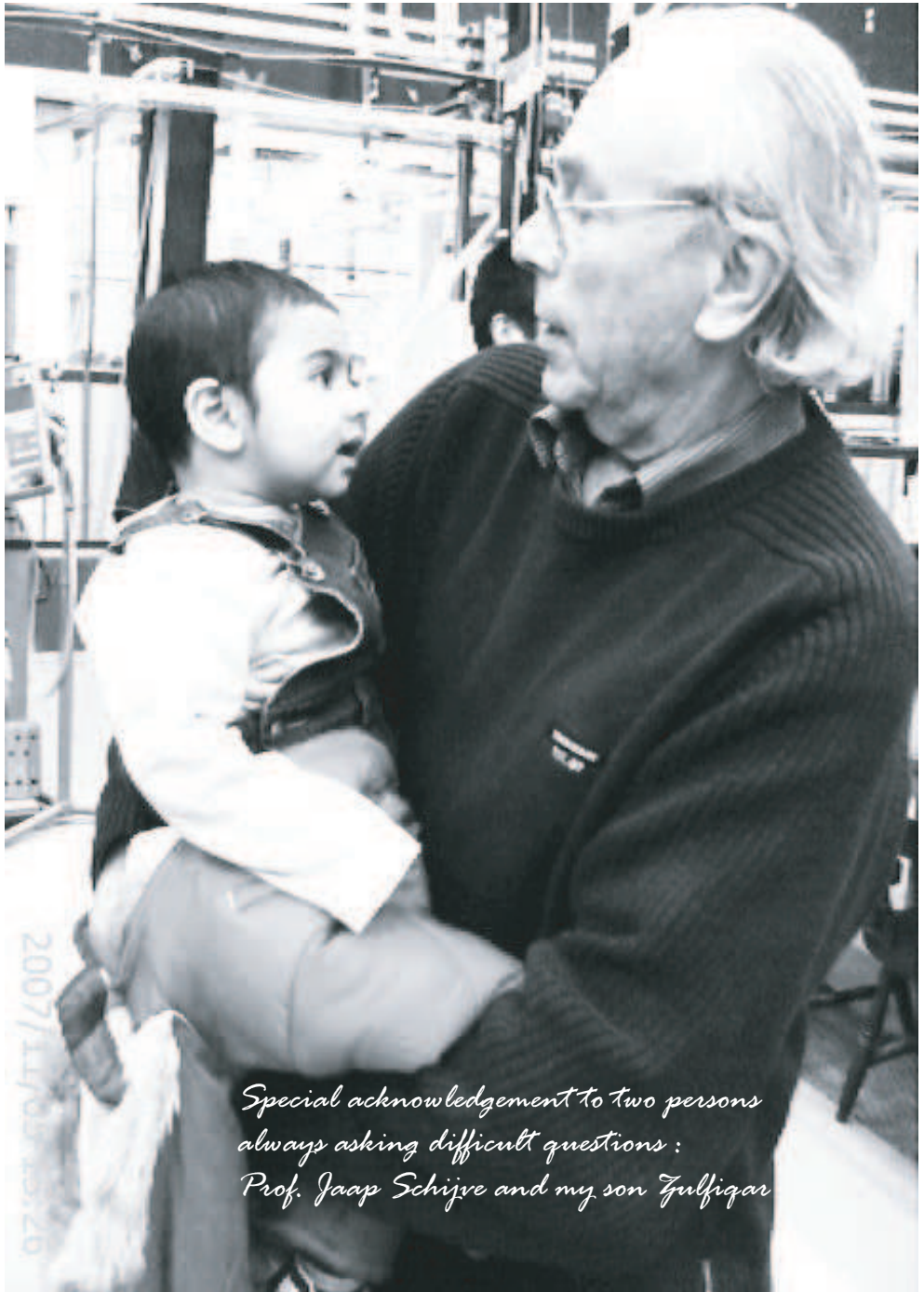
*Special acknowledgement to two persons
always asking difficult questions :
Prof. Jaap Schijve and my son Zulfiqar*

A big Thanks to René who never missed an oppertunity to discuss my research

Fibre Metal laminates (FMLs) consist of alternating layers of unidirectional impregnated fibres and thin metallic sheets adhesively bonded together. FMLs are hybrid materials combining mechanical and damage tolerance properties of the individual constituents. These materials have been developed primarily for aircraft structures as a substitute to high strength aluminium alloys. In FMLs, fatigue crack propagation can be divided into two main mechanisms: crack propagation in metal layers and delamination at the metal-fibre interface. In reality, both of these mechanisms form a balanced and so-called coupled process.

The main focus of this research was to investigate the fatigue behavior of FMLs under variable amplitude (VA) loading. Both fatigue mechanisms were first investigated separately under VA loading, adressing subsequently their interaction. Finally a crack growth model has been developed based on the developed understanding of these mechanisms.

Delft
University of
Technology

9 789088 915550